DYSBIOSIS-ASSOCIATED CHANGES IN HOST METABOLISM PRODUCE LACTATE TO SUPPORT ENTEROBACTERIAL EXPANSION DURING INFLAMMATION

APPROVED BY SUPERVISORY COMMITTEE

_____

David R. Hendrixson, Ph.D.

_____

Vanessa Sperandio, Ph.D.

_____

Ezra Burstein, M.D.

_____

Sebastian E. Winter, Ph.D.

DEDICATION

To my parents, for always putting my education first.

DYSBIOSIS-ASSOCIATED CHANGES IN HOST METABOLISM PRODUCE LACTATE TO SUPPORT ENTEROBACTERIAL EXPANSION DURING INFLAMMATION

by

CAROLINE CATHERINE GILLIS

DISSERTATION

Presented to the Faculty of the Graduate School of Biomedical Sciences

The University of Texas Southwestern Medical Center at Dallas

In Partial Fulfillment of the Requirements

For the Degree of

DOCTOR OF PHILOSOPHY

The University of Texas Southwestern Medical Center at Dallas

Dallas, Texas

May, 2019

DYSBIOSIS-ASSOCIATED CHANGES IN HOST METABOLISM PRODUCE LACTATE TO SUPPORT ENTEROBACTERIAL EXPANSION DURING INFLAMMATION

Caroline Catherine Gillis, Ph.D.

The University of Texas Southwestern Medical Center at Dallas, 2019

Supervising Professor: Sebastian E. Winter, Ph.D.

The lumen of the gastrointestinal tract is heavily colonized by microbes, termed the gut microbiota. Under normal conditions, fermentative anaerobes constitute the majority of the gut microbiota. However, during inflammation there is a change in the nutritional environment of the gut that enables the outgrowth of facultative aerobic Enterobacteriaceae through respiratory metabolism.

Salmonella enterica serovar Typhimurium (*S.* Tm) is a pathogenic member of the Enterobacteriaceae family that benefits from inflammation. We found that *S.* Tm uses lactate as a nutrient during infection, which maximizes colonization of the gut. During *S.* Tm infection, a profound change in the microbial community of the gut occurs. In particular, butyrate-producing Clostridia species are depleted. Butyrate is the preferred substrate for β-oxidation by intestinal

epithelial cells (IEC). In the absence of butyrate, IEC perform a fermentative metabolism that produces lactate as a waste product. Lactate is then used in conjunction with oxygen as a terminal electron acceptor to support growth of *S.* Tm in the murine gut lumen.

We next investigated the regulation of lactate utilization in *S.* Tm. We found that the lactate utilization genes (*lldPRD*), were inducible by electron acceptors and L-lactate. The transcriptional response to L-lactate was coordinated by the regulatory protein LldR, which maximized colonization of the murine gut. Under anaerobic conditions, *lldPRD* expression was repressed by the two-component system ArcAB.

Commensal members of the Enterobacteriaceae family also expand during non-infectious colitis. We investigated whether lactate was also produced during non-infectious colitis and if commensal Enterobacteriaceae could use this nutrient. Butyrate was depleted and lactate was abundant in a murine model of colitis. Metagenomic sequencing demonstrated that lactate dehydrogenase genes were more abundant in the microbiome of inflamed mice than control mice. We next began to characterize putative lactate dehydrogenases in *E. coli*. We identified several putative lactate dehydrogenases, however, their role in *E. coli* fitness requires further study.

In conclusion, we identified an important host-derived nutrient that promotes *S.* Tm fitness during infection and may serve as a nutrient for commensal Enterobacteriaceae during non-infectious colitis. This illustrates the importance of nutrient acquisition for Enterobacteriaceae during inflammatory colonization of the gut.

TABLE OF CONTENTS

PRIOR PUBLICATIONS

Gillis CC, Winter MG, Chanin RB, Zhu W, Spiga L, Winter SE. Host-derived metabolites modulate transcription of *Salmonella* genes involved in L-lactate utilization during gut colonization. **Infection & Immunity**. 2019. doi: 10.1128/IAI.00773-18. PMID: 30617205

Gillis CC, Hughes ER, Spiga L, Winter MG, Zhu W, Furtado de Carvalho T, Chanin RB, Behrendt CL, Hooper LV, Santos RL, Winter SE. Dysbiosis-associated change in host metabolism generates lactate to support Salmonella growth. **Cell Host & Microbe**. 2018 Jan 10;23(1):54-64.e6. doi: 10.1016/j.chom.2017.11.006. PMID: 29276172

Zhu W*, Winter MG*, Byndloss MX, Spiga L, Duerkop BA, Hughes ER, Buttner L, De Lima Romao E, Behrendt CL, Lopez CA, Sifuentes-Dominguez L, Huff-Hardy K, Wilson RP, **Gillis CC**, Tukel C, Koh AY, Burstein E, Hooper LV, Baumler AJ[#], Winter SE[#]. Precision editing of the gut microbiota ameliorates colitis. **Nature.** 2018 Jan 11;553(7687):208-211. doi: 10.1038/nature25172. *Authors contributed equally. [#] Corresponding authors.

Spiga L*, Winter MG*, Furtado de Carvalho T, Zhu W, Hughes ER, **Gillis CC**, Behrendt CL, Kim J, Chessa D, Andrews-Polymenis H, Beiting DP, Santos RL, Hooper LV, Winter SE. An oxidative central metabolism enables Salmonella to utilize microbiota-derived succinate. **Cell Host & Microbe**. 2017 Sep 13;22(3):291-301.e6. doi: 10.1016/j.chom.2017.07.018. PMID: 28844888 *Authors contributed equally.

Hughes ER*, Winter MG*, Duerkop BA, Spiga L, Furtado de Carvalho T, Zhu W, **Gillis CC**, Büttner L. Smoot MP, Behrendt CL, Cherry S, Santos RL, Hooper LV, Winter SE. Microbial respiration and formate oxidation as metabolic signatures of inflammation-associated dysbiosis. **Cell Host & Microbe**. 2017 Feb 8;21(2):208-219. doi: 10.1016/j.chom.2017.01.005. PMID: 28182951 *Authors contributed equally.

LIST OF FIGURES

LIST OF TABLES

LIST OF APPENDICES

LIST OF ABBREVIATIONS

AAMs	Alternatively activated macrophages
AE lesions	Attaching and effacing lesions
AIEC	Adherent invasive *E. coli*
ANOSIM	Analysis of similiarities
ATP	Adenosine triphosphate
CAMs	Classically activated macrophages
Carb	Carbenicillin
CD	Crohn's disease
CE	Collision energy
CFU	Colony forming units
Cm	Chloramphenicol
DSS	Dextran sulfate sodium
EHEC	Enterohemorrhagic *E. coli*
GC/MS	Gas chromatography mass spectrometry
GC/MS/MS	Tandem gas chromatography mass spectrometry
IBD	Inflammatory bowel disease
IEC	Intestinal epithelial cells
iNOS	Inducible nitric oxide synthase
Kan	Kanamycin
LB	Lysogeny broth
LEE	Locus of enterocyte effacement
M cells	Microfold cells

MRM	Multiple reaction monitoring
NAD+	Nicotinamide adenine dinucleotide, oxidized form
NADH	Nicotinamide adenine dinucleotide, reduced form
NADPH	Nicotinamide adenine dinucleotide phosphate, reduced form
NCE	No carbon E medium
ONPG	*O*-nitrophenyl-β-D-galactoside
PMN	Polymorphonuclear leukocyte
PPAR	Peroxisome proliferator-activated receptor
RPM	Revolutions per minute
S. Tm	*Salmonella enterica* serovar Typhimurium
SCV	*Salmonella* containing vacuole
SDS	Sodium dodecyl sulfate
SO	Sodium oxamate
SPI	*Salmonella* pathogenicity island
T3SS	Type 3 secretion system
Tregs	Regulatory T cells
UC	Ulcerative colitis
WT	Wild-type
X-gal	5-bromo-4-chloro-3-indolyl-β-D-galactopyranoside
X-phos	5-Bromo-4-chloro-3-indolyl phosphate
μL	Microliter
μM	Micromolar
μm	Micron

CHAPTER ONE

INTRODUCTION AND LITERATURE REVIEW

The gut microbiota

The microbiota during homeostatic conditions

The distal portion of the mammalian gastrointestinal tract is densely colonized by microbes. This consortium of microbes is collectively termed the gut microbiota. The microbiota of this region of the gastrointestinal tract is dominated by the phyla Bacteroidetes and Firmicutes in both humans [1] and mice [2]. These phyla encompass mostly obligate anaerobic species of bacteria. These microbes confer a number of benefits to the host, including providing nutrients [3], education of the immune system (reviewed in [4]), and colonization resistance to enteric pathogens [5].

Polysaccharide degradation by the gut microbiota

One of the key processes mediated by the gut microbiota is the fermentation of complex polysaccharides (fiber) [6, 7]. Complex polysaccharides contain glycosidic linkages that require specialized enzymes to be broken down. The Carbohydrate-Active EnZymes (CAZy) database broadly categorizes these enzymes into glycoside hydrolases, carbohydrate esterases, and polysaccharide lyases [8]. The human genome encodes only 8 glycoside hydrolases that are related to digestion, which enable digestion of starch, maltose, lactose, sucrose, trehalose, and isomaltose [9]. There are nine additional glycoside hydrolases that are putatively related to digestion [9]. As a result, many complex polysaccharides in the diet are not degraded during digestion of food by the host and are abundant in the distal gut.

In contrast to the mammalian host, many gut symbionts are well-adapted to breaking down complex polysaccharides. The human symbiont *Bacteroides thetaiotaomicron* has been used as a model organism to study polysaccharide utilization by the gut microbiota [10]. Genomic analysis by Xu *et al.* uncovered that the *B. thetaiotaomicron* genome encodes 226 glycoside hydrolases, 15 polysaccharide lyases, and 209 paralogs of the SusC/SusD starch utilization system [11]. This suggests that *B. thetaiotaomicron* is able to utilize a wide variety of polysaccharides. Recent studies of *B. thetaiotaomicron* showed that the bacterium can utilize complex dietary polysaccharides when available [12, 13]. In the absence of dietary polysaccharides, *B. thetaiotaomicron* will instead forage from host glycans, including from mucus [12, 14]. Interestingly, *B. thetaiotaomicron* is able to degrade rhamnogalacturonan II, a very complex polymer with 21 distinct glycosidic linkages [13]. All but one of these glycosidic linkages requires a unique enzyme to be broken down [15]. The example of *B. thetaiotaomicron* illustrates the diversity of polysaccharide utilization enzymes required for fitness in gut symbionts.

Other members of the gut microbiota take a more specialized approach to polysaccharide degradation, such as *B. ovatus,* which can degrade many types of plant-derived polysaccharides but not host-derived mucin *O*-glycans [13]. Additionally, members of the other major phylum of the gut microbiota, the Firmicutes, also ferment complex polysaccharides [7, 16]. Through a combination of primary fermentation and syntrophic relationships, the gut microbiota successfully degrades complex polysaccharides into fermentation end products [17] (reviewed in [18]). Among the most abundant fermentation end products are the short chain fatty acids acetate, propionate, and butyrate [19]. Short chain fatty acids play many important roles in maintaining homeostasis,

including harvesting energy from non-digestible polysaccharides that can then be provided to the host (reviewed in [20]).

A recent computational study by Eilam and colleagues found that the ability of a bacterial species to degrade the complex polysaccharides within the host diet was predictive for abundance within the microbiota [21]. This supports the idea that one of the major drivers of gut microbiota composition is the relative abundance of complex polysaccharides available for degradation. Furthermore, a mechanistic study performed by Sonnenburg *et al.* demonstrated the importance of specific polysaccharide availability during competitive colonization experiments of gnotobiotic mice with two Bacteroides strains, *B. thetaiotaomicron* and *B. caccae. B. caccae* is able to utilize the complex polysaccharide inulin, whereas *B. thetaiotaomicron* grows poorly on inulin *in vitro.* When gnotobiotic mice co-colonized with both species were fed an inulin-based chow, the abundance of *B. caccae* in the gut increased significantly. However, when the genetic loci for inulin utilization were inserted into the *B. thetaiotaomicron* genome, the fitness advantage for *B. caccae* during inulin supplementation was abolished [22]. The ability of the members of the phylum Bacteroidetes and Firmicutes to ferment complex polysaccharides is an essential component to occupying this niche in the distal gut. The picture emerging from these studies is that nutrient acquisition by microbes is a major determinant of the composition of the microbiota.

Dysbiosis

Dysbiosis during human diseases

In contrast to the Bacteroidetes and Firmicutes species that make up the bulk of the microbiota, members of the Enterobacteriaceae family (Phylum Proteobacteria, Class γ-Proteobacteria) make up a very small proportion of the microbiota under homeostatic conditions

[1]. However, during inflammatory settings, a shift in the composition of the gut microbiota, termed dysbiosis, can occur. In many diseases, this dysbiosis is characterized by an outgrowth of Enterobacteriaceae. For example, this type of dysbiosis has been observed in patients with Inflammatory Bowel Disease (IBD) [23-26]. IBD is a set of diseases, Crohn's disease (CD) and Ulcerative Colitis (UC), which are characterized by severe inflammation of the gastrointestinal tract. The etiology of IBD likely contains genetic, environmental, and microbial components; however, the exact mechanisms that cause IBD are not completely elucidated (reviewed in [27]). Interestingly, other inflammatory diseases are also characterized by Enterobacterial outgrowth, including HIV-associated enteropathy [28]. This suggests a connection between intestinal inflammation and Enterobacterial expansion in the gastrointestinal tract.

Dysbiosis in animal models of intestinal inflammation

Studies in murine models of colitis have recapitulated the expansion of Enterobacteriaceae during intestinal inflammation. One commonly used murine model of colitis is treatment with Dextran Sulfate Sodium (DSS). DSS induces the host immune response and recapitulates many aspects of UC [29]. Okayasu and colleagues observed a significant increase in the amount of Enterobacteriaceae in the stool of mice treated with DSS [29]. Similarly, Lupp *et al.* found that treatment of mice with DSS resulted in an outgrowth of non-pathogenic *E. coli* [30].

Further experiments have been carried out in mice that are genetically susceptible to colitis. One such model are mice with genetic ablation of *Il10,* which can develop spontaneous enterocolitis [31]. Lupp and colleagues also found that experimentally-introduced non-pathogenic *E. coli* grows to a high abundance in *Il10*-deficient mice without the need for any DSS treatment [30]. Another genetic model of spontaneous intestinal inflammation is the *Tbet -/-* x *Rag2 -/-*

(TRUC) mouse model. These mice develop severe intestinal inflammation [32]. The microbiota of TRUC mice harbors the enterobacterial species *Klebsiella pneumoniae* and *Proteus mirabilis* [33]. In summary, there is an association between non-homeostatic levels of Enterobacteriaceae in the microbiota and intestinal inflammation in both human patients and animal models.

Nutrient acquisition by Enterobacteriaceae during inflammation

At first glance, the increased levels of Enterobacteriaceae observed during intestinal inflammation appear incongruent with the idea that nutrient availability and bacterial metabolism are major determinants of microbiota composition. In contrast to commensal Bacteroidetes and Firmicutes, Enterobacteriaceae do not possess a large repertoire of complex polysaccharide degradation machinery. For example, the CAZy database lists predicted 50 glycoside hydrolases in the strain *E. coli* K-12 MG1665, only a fraction of which are predicted to be related to degradation of diet-derived polysaccharides [9]. The human gastrointestinal *E. coli* strains Nissle 1917 and NRG 857C, a commensal probiotic strain and an Adherent-Invasive *E. coli* (AIEC) strain, respectively, contain similar numbers and categories of predicted glycoside hydrolases [9].

In contrast to most fermentative gut commensals, Enterobacteriaceae possess diverse electron transport systems and are capable of both aerobic and anaerobic respiration (reviewed in [34]). The outgrowth of Enterobacteriaceae during intestinal inflammation therefore suggests that there is a change in the metabolic environment of the gastrointestinal tract that favors the outgrowth of respiratory Enterobacteriaceae at the expense of the fermentative members of the microbiota.

Consistent with this idea, the electron acceptor nitrate (NO_3^-) arises during intestinal inflammation. During IBD flares in humans, there is increased activity of inducible nitric oxide

synthase (iNOS) and increased nitric oxide (NO•) in the gut [35-37]. NO• can combine with superoxide ($\bullet O_2^{2-}$) created by host NADPH oxidases to produce peroxynitrite ($ONOO^-$) and then nitrate (reviewed in [38]). During intestinal inflammation, there is an accumulation of nitrate within the mucus layer of mice treated with DSS. Nitrate levels are significantly reduced when DSS-treated mice also received an iNOS inhibitor [39]. *E. coli* uses this electron acceptor to perform nitrate respiration (reviewed in [34]). Nitrate respiration greatly enhances the fitness of *E. coli* during colonization of the inflamed gut in both murine and bovine ileal loop models of intestinal inflammation [39]. Our lab also recently identified oxidation of microbially-derived formate and aerobic respiration as important metabolic pathways that allow *E. coli* and other enterobacterial species to expand during inflammation [40].

Both the formate dehydrogenases and nitrate reductases that support *E. coli* outgrowth share a common cofactor. This cofactor, termed the molybdopterin cofactor (MoCo), contains a molybdenum in its active site. Tungsten can be incorporated into the active site of molybdoenzymes due to the similarities in chemistry between tungsten and molybdenum coordination complexes (reviewed in [41]). Administration of tungstate, a water-soluble sodium salt of tungsten, renders *E. coli* MoCo inactive and unable to assist in nitrate reduction effectively [42]. This suggests that administration of tungstate could abolish the fitness advantage of formate utilization and nitrate respiration *in vivo.* To test this hypothesis, our lab administered tungstate in the drinking water of DSS-treated mice. Tungstate treatment selectively inhibited the outgrowth of Enterobacteriaceae. This effect was limited to the enterobacterial population and did not affect the other members of the microbiota, presumably because they are not reliant on molybdenum-dependent enzymes for their metabolism during inflammation [43].

In summary, the host inflammatory response modifies the gastrointestinal lumen into an environment where Enterobacteriaceae are able to thrive. In the inflamed gut, Enterobacteriaceae-accessible electron donors (e.g. formate) and electron acceptors (e.g. nitrate) become available for use in respiration. Respiration allows Enterobacteriaceae to produce more energy than the fermentative microbiota and therefore dominate the gastrointestinal tract.

Salmonella enterica serovar Typhimurium infection as a model system to study Enterobacterial metabolism during inflammation

Interestingly, infection with many pathogenic Enterobacteriaceae also results in a severe dysbiosis. Lupp *et al.* found that during infection of mice with the murine pathogen *Citrobacter rodentium,* there was a significant reduction in the number of microbes present in the infected colon, which correlated with maximum colonization by the pathogen as well as maximum inflammation-induced pathology [30]. From an evolutionary perspective, pathogens have evolved to disrupt the mechanisms that maintain homeostasis within the host. In the case of enteric pathogens, this also includes disruption of host-microbiota relationships. This evolutionary paradigm supports the idea that enteric pathogen infection could serve as a model system to identify metabolic mechanisms of enterobacterial expansion during gut inflammation. *Salmonella enterica* serovar Typhimurium (*S.* Tm) is one such enterobacterial pathogen that induces dysbiosis [5, 44, 45]. Additionally, *S.* Tm is one of the most well-studied enteric pathogens, is genetically tractable, and has well characterized *in vivo* models of infection. *S.* Tm infection is therefore an excellent model system for understanding the complex relationship between the host, the microbiota, and enteric pathogens.

***S.* Tm virulence factors and pathogenesis**

S. Tm causes acute, self-limiting gastroenteritis in immune-competent individuals. After ingestion of contaminated food or water, *S.* Tm transits through the upper digestive tract and is able to survive the acidic pH of the stomach [46]. In the gastrointestinal lumen, *S.* Tm uses its flagella to reach the intestinal epithelium prior to invasion [47].

Type 3 Secretion System 1 and invasion of the epithelium

In murine models of infection, invasion largely takes place through microfold cells (M cells). M cells are specialized cells in the gut-associated lymphoid tissue of Peyer's Patches. These cells sample antigens in the gastrointestinal lumen and transport them across the epithelium to antigen presenting cells [48]. *S.* Tm can also invade intestinal epithelial cells (IEC) in cell culture and in bovine models of infection [49, 50]. The genes required for invasion of the epithelium are encoded in *Salmonella* Pathogenicity Island 1 (SPI-1), which is thought to have been acquired by horizontal gene transfer [51]. SPI-1 encodes a Type 3 Secretion System (T3SS), termed T3SS-1. T3SSs are so-called "molecular syringes" that penetrate host cell membranes and inject effector molecules in the host cell cytoplasm [52]. Deployment of T3SS-1 effectors induces membrane ruffling and rearrangement of the actin cytoskeleton of the host cell. This results in the internalization of the bacterium (reviewed in [53]).

Type 3 Secretion System 2 and intracellular replication

S. Tm utilizes a second T3SS (T3SS-2) to promote intracellular survival inside of professional phagocytes, such as dendritic cells and macrophages. T3SS-2 is encoded in SPI-2, which was likely acquired by horizontal gene transfer [54]. T3SS-2 effectors prevent maturation of the phagosome and modify it into a compartment that supports bacterial replication, termed the *Salmonella* containing vacuole (SCV) (reviewed in [55]). The combination of *S.* Tm's virulence

factors results in a strong immune response from the host. Both T3SS-1 and T3SS-2 are required for a maximal inflammatory response in both murine and bovine models of infection [56, 57]. Interestingly, Hapfelmeier and colleagues found there is also a T3SS-1-independent mechanism for induction of inflammation by *S.* Tm through internalization of the pathogen during antigen sampling by CX3CR1+ dendritic cells early in infection [58, 59].

The neutrophilic response to S. Tm *infection*

In both humans and animal models, a hallmark of infection is the recruitment of neutrophils to the gut, including into the lumen [50, 57, 60]. Neutrophils kill *S.* Tm within the tissue, which keeps infection largely confined to the gastrointestinal tract [61]. However, significant tissue damage and pathology does occur as a result of the host inflammatory response [50].

Transmission of S. Tm *requires virulence-dependent colonization of the distal gut.*

The dysbiosis induced by *S.* Tm infection is dependent on the virulence factors T3SS-1 and T3SS-2 [5, 44, 45]. This is consistent with the idea that *S.* Tm uses the host inflammatory response to occupy the niche of the distal gut during infection. Additionally, robust colonization of the distal gut is required for transmission via the fecal-oral route in animal models. Using a chronic model of infection, Lawley and colleagues found that mice that were very highly colonized ($>10^8$ CFU/g in the feces), so called "supershedders," are able to successfully transmit *S.* Tm to other mice via the fecal-oral route. Transmission is also dependent on T3SS-1 and T3SS-2 [62]. In summary, *S.* Tm depends on the virulence factors T3SS-1 and T3SS-2 to induce the host immune response, successfully colonize the distal gut through disruption of the microbiota, and subsequently transmit to new hosts through feces.

Mechanisms of nutrient acquisition by *S.* Tm

During *S.* Tm infection, several electron acceptors become available in the gut lumen. One such electron acceptor is tetrathionate ($S_4O_6^{2-}$) [63]. During normal metabolism, the microbiota produces hydrogen sulfide (H_2S) as a byproduct [64]. As hydrogen sulfide is harmful [65], the intestinal epithelium detoxifies hydrogen sulfate to thiosulfate ($S_2O_3^{2-}$) [66, 67]. During *S.* Tm-induced inflammation, the reactive species produced by phagocyte NADPH oxidase reacts with thiosulfate to produce tetrathionate. *S.* Tm is then able to use tetrathionate respiration to outcompete the microbiota and successfully colonize the gut [63, 68, 69].

S. Tm is also able to utilize nitrate as a terminal electron acceptor using the periplasmic nitrate reductase NapABC, maximizing fitness in the inflamed gut [70]. Interestingly, the *S.* Tm strain SL1344 contains the lysogenized phage SopEΦ, which encodes the T3SS-1 effector gene *sopE*. SopE increases the severity of intestinal inflammation and results in increased nitrate production during infection. This enables *S.* Tm to undergo nitrate respiration, which is more energetically favorable than tetrathionate respiration [71].

In addition to the increased accessibility of electron acceptors, inflammation increases the availability of carbon sources as well as electron donors for respiration. Recent work by Faber and colleagues identified that the oxidation of sugars mediated by the host immune response produces the sugar-acids galactarate and glucarate. Catabolism of these sugar acids facilitates *S.* Tm colonization in a post-antibiotic expansion model of salmonellosis [72].

The presence of the alternative electron acceptors nitrate and tetrathionate enables *S.* Tm to run a complete, oxidative TCA cycle under anaerobic conditions [73]. Under anaerobic conditions without any alternative electron acceptors, Enterobacteriaceae utilize a branched TCA cycle, with an oxidative and reductive branch. The genes required for a complete TCA cycle are

repressed under anaerobic conditions [73-75]. Redox equivalents are regenerated using reduction of fumarate to succinate (fumarate respiration), with succinate being excreted as a waste product. However, in the presence of the alternative electron acceptors tetrathionate and nitrate, repression of complete TCA cycle enzymes is relieved [73]. Thus, the presence of these electron acceptors allows for *S.* Tm to run a full, oxidative TCA cycle [73]. This in turn enables the regeneration of redox equivalents and enhanced ATP production through the electron transport chain (reviewed in [76]).

Interestingly, there are several nutrients that become accessible to *S.* Tm through respiration. One example of this is ethanolamine, which is derived from cell membranes. Ethanolamine levels do not change after the induction of inflammation during infection. However, tetrathionate respiration that occurs during inflammation enables *S.* Tm to take advantage of this nutrient and outgrow in the distal gut [77]. Similarly, respiration enables the utilization of fructose-asparagine [78], microbiota-derived 1,2-propanediol [79], and succinate [73]. In summary, a complete, oxidative TCA cycle maximizes energy production and facilitates colonization of the inflamed gut by *S.* Tm [73].

Changes in host metabolism during intestinal inflammation

Butyrate production by commensal Clostridia during homeostasis and inflammation

Butyrate, like other short chain fatty acids produced by the microbiota, has many roles in maintaining homeostasis in the host. Butyrate is primarily produced by members of Clostridia Clusters IV and XIVa [80-83]. During intestinal inflammation, the resulting dysbiosis is characterized by a depletion of Clostridia species from the microbiota and therefore a depletion of

butyrate from the gastrointestinal tract [84, 85]. Clostridia appear to be particularly sensitive to neutrophil elastase that is produced during the neutrophilic response to *S.* Tm infection [86].

Butyrate and IEC metabolism

Butyrate is the preferred substrate for β-oxidation by intestinal epithelial cells (IEC) [87]. This allows the host to harvest energy from the microbial fermentation of complex polysaccharides (reviewed in [20]). Germ-free mice, which are microbiologically sterile, have altered IEC metabolism. Donohoe and colleagues found that the colons of germ-free animals had dramatically lower levels of ATP and a decreased $NADH/NAD^+$ ratio compared to conventional animals, indicating that the absence of gut microbes dramatically alters cellular metabolism in the colon and diminishes energy production. The same study also found that IEC from germ-free mice had increased activation of 5'-adenosine monophosphate-activated protein kinase, a sensor of low ATP levels, and had entered autophagy. However, these markers of metabolic distress were markedly improved when germ-free mice were colonized with butyrate-producing strains or when IEC were treated *ex vivo* with butyrate [88]. Another study by Donohoe *et al.* found that glucose metabolism is altered in germ-free IEC, which produce dramatically more lactate than IEC from conventional mice [89].

Similar changes in host metabolism were observed in mice that were treated with DSS. DSS administration causes dysbiosis and a depletion of butyrate-producing organisms from the gastrointestinal tract [84]. Ahmad *et al.* found that IEC from mice treated with DSS exhibited impaired metabolism and increased lactate production, consistent with the idea that butyrate deprivation alters IEC metabolism [90].

β-oxidation of butyrate also consumes oxygen from the tissue, which helps to maintain the "physiological hypoxia" of the gut lumen [91] and protects the strict anaerobes that inhabit the lumen. However, during inflammatory conditions such as *S.* Tm infection, Clostridia are depleted from the microbiota, resulting in butyrate starvation conditions for IEC. In the absence of microbially-derived butyrate, oxygen from host tissues can leak into the lumen of the gut [84, 85, 91]. Utilization of this oxygen for aerobic respiration facilitates colonization of the gastrointestinal tract by *S.* Tm [85]and *E. coli* [84].

Butyrate modulates host gene expression and signaling in IEC through PPARγ

The transcription factor peroxisome proliferator-activated receptor gamma (PPARγ) is a transcription factor that mediates cellular metabolism, in particular metabolism of fatty acids [92]. PPARγ is highly expressed in terminally differentiated IEC of the colon of humans and rodents [93]. Treatment of Caco-2 cells *in vitro* with butyrate can selectively upregulate PPARγ, but not other PPAR family members [94]. Furthermore, butyrate can activate PPARγ signaling [92], although it is not clear if butyrate binds directly to PPARγ. The loss of PPARγ signaling leads to an IEC metabolism that is based on anaerobic glycolysis [95]. Additionally, PPARγ signaling in IEC is protective against experimentally induced colitis [96]. In summary, butyrate is a microbial product that exerts profound effects on the host intestinal epithelium through activation of PPARγ signaling.

Butyrate and regulatory T-cells

In addition to the effect of PPARγ signaling in IEC, this pathway also plays an important role in the differentiation of regulatory T-cells (Tregs). Tregs modulate the host inflammatory response and are essential for the resolution of intestinal inflammation. Germ-free mice have fewer

Tregs in the colonic tissue, but not in other body sites such as the spleen and small intestine [97]. Interestingly, germ-free mice have similar levels of so-called natural Tregs that are differentiated in the thymus, but not of inducible (also known as peripheral) Tregs that differentiate after migration to the colon [98]. Butyrate can also alter gene expression by blocking deacetylation of histones [99, 100]. Butyrate is known to induce the differentiation of Tregs in the colon through its histone deacetylase inhibitor activity [101]. Butyrate can also act indirectly through dendritic cells and macrophages to induce Treg differentiation in the colon [102]. Other short-chain fatty acids such as propionate can also play a role in Treg function and work in concert with butyrate to limit the intestinal immune response [103]. Taken together, this body of work suggests that manipulation of PPARγ signaling by butyrate is a way in which the microbiota is able to modulate host metabolism and immunity.

Impact of changes in PPARγ signaling on bacterial metabolism

Until recently, the effect of butyrate starvation and subsequent changes in host metabolism on the microbiota remained unexplored. A seminal paper by Byndloss *et al.* identified PPARγ signaling as an important pathway for maintaining microbiota composition. During antibiotic-mediated depletion of butyrate-producing bacteria from the gut, the lack of activation of epithelial PPARγ signaling resulted in an increased concentration of nitrate in the gastrointestinal tract due to increased expression of iNOS. Additionally, leakage of oxygen from the host into the lumen of the gastrointestinal tract allows *E. coli* to undergo aerobic respiration. However, administration of tributyrin (a source of butyrate), butyrate-producing bacterial strains, or the PPARγ agonist rosiglitazone reduced the advantage of aerobic respiration for *E. coli* after antibiotic treatment. Tregs also play an important role in limiting the availability of oxygen in the gut lumen [84]. In

summary, butyrate exerts a significant effect on the host, which supports an environment that favors a homeostatic microbiota composition and limits the outgrowth of Enterobacteriaceae.

Regulation of nutrient acquisition in *S.* Tm

During infection with *S.* Tm, the metabolic landscape of the gut lumen changes dramatically [104]. As a consequence, *S.* Tm requires dynamic gene regulation systems to respond to changes in nutrient availability. For example, to sense increases in nitrate concentrations during infection, *S.* Tm relies upon the NarPQ two-component system [70]. NarQ, a sensor kinase, senses nitrate and subsequently phosphorylates NarP, the response regulator, although some cross-talk between NarPQ and the other nitrate sensing system, NarXL, exists in *E. coli* [105]. NarPQ promotes the transcription of the *napABC* genes needed for nitrate respiration [70, 106]. This emphasizes the importance of sensing new nutrients that arise over the course of infection and appropriately changing gene expression to maximize energy production during infection.

Study Rationale

While recent work has delineated several mechanisms by which *S.* Tm and *E. coli* gain a competitive advantage over the microbiota during inflammation, the carbon and energy sources utilized by these organisms remain incompletely described. In this study, we used *S.* Tm infection as a model system in which gut dysbiosis occurs and the metabolic landscape changes in favor of enterobacterial outgrowth. This experimental approach allowed us to identify lactate as a novel nutrient that *S.* Tm exploits during infection. We then expanded our studies to examine how lactate utilization is regulated in *S.* Tm as well as to investigate lactate production by the host during non-infectious colitis and its potential exploitation by *E. coli.* Investigation into the nutrients used

during enteric pathogen infection provides valuable insight into the mechanisms that pathogens use to disrupt host-microbiota interactions, as well as to identify potential drug targets for enteric pathogen infections and dysbiosis-associated diseases.

CHAPTER TWO*

MATERIALS AND METHODS

Mouse lines

Conventional Swiss Webster and C57BL/6 mice were bred in-house in barrier, specific-pathogen-free facilities at UT Southwestern. Mice were mixed and randomized 3 days prior to the beginning of each experiment. Male and female mice aged 6-8 weeks were used for all experiments and no differences between male and female mice were identified. Germ-free mice were reared in germ-free facilities at UT Southwestern and fed sterile food and water. All mice were on a 12-hour light/dark cycle and received food (Envigo 2919, Teklad Global 16% Protein Diet, irradiated) and water *ad libitum*. Mice that were euthanized early due to health concerns and mice that were insufficiently colonized (<10 colonies in 100 μL of undiluted sample; competitive infections only) were excluded from analysis. All mouse experiments were performed in accordance with the Institutional Animal Care and Use Committee at UT Southwestern.

Bacterial strains

All strains used in this study are listed in Table 1. All *S.* Tm and *E. coli* strains were cultured in LB broth (10 g/L tryptone, 5 g/L yeast extract, 10 g/L sodium chloride) or on LB plates (LB broth, 15 g/L agar) and incubated at 37 °C. Nalidixic acid (Nal), carbenicillin (Carb), Kanamycin (Kan), and Chloramphenicol (Cm) were added to LB broth and LB agar plates at a concentration of 50 mg/L, 100 mg/L, 100 mg/L, and 15 mg/L, respectively, as needed. *Clostridium symbiosum*

was grown on thioglycollate plates for 2 days at 37 °C under anaerobic conditions and in pre-reduced chopped meat media for 3 days at 37 °C under anaerobic conditions. To distinguish between *S.* Tm strains, the chromogenic substrate 5-Bromo-4-chloro-3-indolyl phosphate (X-phos) was used to detect the activity of the acidic phosphotase PhoN. To distinguish between *E. coli* NRG 857C strains, the chromogenic substrate 5-bromo-4-chloro-3-indolyl-β-D-galactopyranoside (X-gal) was used to detect the activity of the β-galactosidase LacZ. All plasmids and primers for mutagenesis used in this study are listed in Table 2 and Table 3, respectively. All suicide plasmids were constructed using the Gibson Assembly Cloning kit.

Mutagenesis in *S.* Tm

To generate plasmids pCG1, pCG2, pCG89*,* CG124, pCG200, pCG226, pMW195, and pMW89*,* upstream and downstream regions of the gene were amplified using the Q5 Hot Start High Fidelity DNA Polymerase. PCR products were ligated into SphI-digested pRDH10 during the Gibson Assembly reaction. For pMW1, the upstream and downstream regions of *sseD* were amplified and cloned into digested pGP706 as described above. The *lldD* promoter region and coding regions were then cloned into SphI-digested pSW327 to generate pCG142. The insertion in all newly constructed plasmids except for pCG142 were sequenced. The cloning strain for all plasmids was DH5α λ*pir*. For the construction of CG6, CG8, CG89, CG124, MW285, CG200, CG226, MW118, and MW119, suicide plasmids were grown in DH5α λ*pir* and extracted before transformation into S17-1 λ*pir*, which served as a donor strain for conjugation with *S.* Tm. Single crossover events were selected by using LB plates containing the appropriate antibiotics. Counterselection was performed to identify second crossover events using sucrose plates (5 % sucrose, 15 g/L agar, 8 g/L nutrient broth base). This results in the creation of a clean and unmarked

deletion. For the construction of CG142, pCG142 was conjugated into IR715 using S17-1 λ*pir*. A single crossover event was selected for using Carb containing plates followed by picking and patching onto Nal and X-phos plates. Integration into the *phoN* gene was identified by the white color of the colonies on X-phos plates. A P22 HT *int-105* phage lysate was then prepared from the exconjugates, which transduced the mutation into CG6. CG9 was generated by transducing Δ*lldD* using phage P22 HT *int-105* into CG8. *phoN*::Kan^r was similarly transduced into CG9 to generate CG110. pMW1 was conjugated into CG9 via S17 λ*pir* to generate MW292. Δ*ldhA* was transduced into CG9 to generate CG111. *phoN*::Kan^r was also transduced into CG89 to generate CG116. Δ*dld* and Δ*lldD* were sequentially transduced into SPN487 to generate CG12 and CG30. *phoN*::Cm^r was transduced into MW285 to generate MW287. To generate CG127 and CG131, Δ*lldD* and *phoN*::Kan^r were each transduced into CG124. To generate CG115, Δ*dld* and Δ*lldD* were sequentially transduced into FF283. To generate CG107, *phoN*::Kan^r was transduced into FF283. To generate pCG254, 379 nucleotides of the 3' end of the *lldD* coding sequence (including the stop codon) and 31 nucleotides immediately downstream of the stop codon were amplified and cloned into SmaI-digested pFUSE. pCG254 was conjugated into IR715, CG124, MW119, and MW118 as described above to generate the *lldD* transcriptional fusion in strains CG254, CG270, CG267, and CG268, respectively.

Mutagenesis in *E. coli*

To generate the suicide plasmids, pCG168, pCG190, and pCG169, the upstream and downstream regions of the gene of interest were amplified and cloned into SphI-digested pGP706. To construct CG168, CG190, and CG169, mutagenesis was performed as described in *S.* Tm prior to the final conjugation of the suicide plasmid into *E. coli* NRG 857C. Counterselection and mutant

screening were performed as described in *S.* Tm. To construct CG185 and CG184, pCG169 and pCG190, respectively, were conjugated into CG168. To construct CG188, pCG190 was conjugated into CG169. To construct CG189, pCG190 was conjugated into CG185.

_S._ Tm infections in conventional Swiss Webster mice

Six- to eight-week-old male and female Swiss Webster mice were gavaged with 1 x 10^9 CFU of *S.* Tm strains. For competition experiments, mice were administered 5 x 10^8 CFU of each strain. After 8 days of infection, mice were sacrificed, and colonic content, cecal content, and tissue were collected. Colonic and cecal contents were placed into sterile Phosphate Buffered Saline (PBS; pH = 7.4) and were serially diluted on selective agar plates to determine CFU/g of each *S.* Tm strain. For the Δ*lldD* and WT competition time course experiment, mice were also sacrificed on day 4 and day 6 after infection and samples were taken as described for the 8-day infection. Competitive indices were calculated by dividing the CFU/g of wild-type *S.* Tm recovered over the CFU/g of mutant *S.* Tm recovered, which was then divided by the same ratio in the inoculum. In the lactate-free diet experiment, mice received lactate-free food for all 8 days of the experiment. For single infection experiments, groups of Swiss Webster mice received 1 x 10^9 CFU of either WT *S.* Tm or the isogenic Δ*lldD* Δ*dld* mutant. Eight days after infection, cecal content was collected and plated to determine the CFU/g of each strain. To evaluate the contribution of the host lactate dehydrogenase, groups of *S.* Tm infected mice were treated with 0.5 % sodium oxamate, or mock (sterile water) in their drinking water for the duration of the 8-day experiment. The exact number of mice used in each group is indicated above each graph or in the figure legend.

_S._ Tm infections in C57BL/6 mice

Seven-week-old C57BL/6 male and female mice were intragastrically pre-treated with 20 mg of sterile streptomycin sulfate or neomycin trisulfate hydrate one day prior to infection. For all experiments, except for the sodium oxamate administration in the streptomycin-treated C57BL/6 model, mice were inoculated with 1 x 10^5 CFU of *S.* Tm strains. During competition experiments, mice were administered 5 x 10^4 CFU of each strain. After 5 days of infection, mice were euthanized, and samples were collected as described above. Rosiglitazone-treated, *S.* Tm-infected mice received 200 µL of 0.75 mg/mL rosiglitazone solution or vehicle control (50 % DMSO in PBS) by intraperitoneal injection for the last 3 days of the infection. Dextran sulfate sodium (DSS)-treated mice received sterile 2.7 % DSS in their drinking water for 4 days prior to infection with 1 x 10^5 CFU of *S.* Tm strains. After 5 days of infection, the competitive index in the cecal content was determined as described above. For sodium oxamate administration in the streptomycin-treated C57BL/6 model, mice were infected with 1 x 10^9 CFU of *S.* Tm strains (5 x 10^8 CFU of each competitor strain). These mice received 0.5 % sodium oxamate in their drinking water or mock (sterile water) beginning the day after infection and were sacrificed 4 days after infection. Sample collection was done as described for other experiments to determine the competitive index. For intraperitoneal infections with *S.* Tm, C57BL/6 mice were injected intraperitoneally with 1 x 10^4 CFU of *S.* Tm strains (5 x 10^3 CFU of each competitor strain). After 3 days, mice were sacrificed, and the spleen, liver, and mesenteric lymph nodes were collected for analysis. Organs were homogenized and plated on selective agar to determine the competitive index as described above.

For analysis of bacterial transcription, wild-type C57BL/6 mice were intragastrically treated with 20 mg of sterile streptomycin sulfate in water. One day later, mice were infected

intragastrically with 1 x 10^5 CFU of *S.* Tm strains. Mice were euthanized 5 days after infection. Cecal content and cecal tissue was flash-frozen in liquid nitrogen for RNA extraction and stored at -80 °C. The exact number of mice used in each group is indicated above each graph or in the figure legend.

Treatments in Streptomycin-treated C57BL/6 mice

Mice treated only with streptomycin received 20 mg of intragastric streptomycin sulfate and were sacrificed 1 to 5 days after treatment. Tributyrin treated mice received 5 % tributyrin fortified chow and 100 μL of undiluted sterile tributyrin by gavage every day after streptomycin treatment. Mice were sacrificed 3 days after streptomycin treatment. Rosiglitazone-treated mice received 200 μL of 0.75 mg/mL rosiglitazone solution or vehicle control by intraperitoneal injection for one day following streptomycin treatment. Cecal content and tissue were collected from these experiments for analysis 2 days after streptomycin treatment. The exact number of mice used in each group is indicated above each graph or in the figure legend.

***S.* Tm infections in germ-free Swiss Webster mice**

Germ-free Swiss Webster mice were gavaged with 1 x 10^5 CFU of *S.* Tm strains. During competition experiments, mice were administered 5 x 10^4 CFU of each strain. Germ-free mice pre-colonized with *C. symbiosum* were gavaged with 3 x 10^9 CFU of *C. symbiosum* three days prior to a 10-day infection with *S.* Tm. For sodium oxamate experiments, germ-free Swiss Webster mice received sterile 0.5 % sodium oxamate in their drinking water or mock treatment (sterile water) for two days. The exact number of mice used in each group is indicated above each graph or in the figure legend.

DSS treatment and *E. coli* infections

For GC/MS measurements of lactate and butyrate during DSS colitis, wild-type C57BL/6 mice were treated with 3.4 % DSS in their drinking water (sterile water for mock) for 8 days, then switched to sterile water for 1 day prior to necropsy. Samples of cecal content were taken for analysis by GC/MS as described below.

For *E. coli* infections during DSS colitis, wild-type C57BL6 mice were treated with 3 % DSS for 8 days, followed by 1 day of water prior to necropsy. Mice were infected with 1 x 10^9 CFU (5 x 10^8 CFU of each strain) of the indicated *E. coli* NRG 857C strains on day 4 of the experiment. Cecal content was collected in PBS to determine the competitive index as described above.

Gas Chromatography Mass Spectroscopy metabolic profiling and measurements of lactate and butyrate

Cecal contents were collected and placed into sterile PBS. Samples were vortexed for 2 minutes and centrifuged at 6,000 x g at 4 °C for 15 minutes. Supernatant was then aliquoted, and 50 μM each of deuterated lactate (sodium L-lactate-3,3,3-d_3) and butyrate (sodium butyrate-d_7) was added as the internal standard. Samples were then evaporated to dryness in a vacuum centrifuge and stored at -80 °C prior to analysis. Standards were prepared in the same way as samples, with set concentrations of deuterated and non-deuterated compounds. Samples were then resuspended in pyridine, sonicated for 1 minute, and incubated at 80 °C for 20 minutes. Samples were derivatized with *N*-*tert*-butyldimethylsilyl-*N*-methyltrifluoroacetamide with 1 % *tert*-Butyldimethylchlorosilane and incubated for 1 hour at 80 °C. Samples were then centrifuged at 16,000 x g for 1 minute to remove debris, and supernatant was transferred to autosampler vials. Analysis was performed using Shimadzu TQ8040 triple quadrupole GC/MS. The injection

temperature was 250 °C with a split ratio of 1:100 and a volume of 1 μL. An Rtx-5 SilMS fused silica capillary column was used with helium as the carrier gas (50 cm/s velocity). The oven temperature began at 50 °C for 2 minutes and rose to 100 °C in increments of 20 °C per minute, with a hold at 100 °C for 3 minutes. The oven temperature was then increased to a final temperature of 330 °C, rising in increments of 40 °C per minute with a final hold for 3 minutes. The ion source was used in electron ionization mode (70 V, 150 μA, 200 °C). Selected ion monitoring and multiple reaction monitoring (MRM) was used, with an event time of 50 ms. The following mass spectrometry parameters were used (the *m/z* used for quantification is italicized): lactate-d_3 (MRM, *264 > 236*, collision energy (CE) = 6 V; 264 > 189, CE = 8 V) and lactate (MRM, *261 > 233*, CE 6 V; 261 > 189, CE 8 V). For qualitative experiments, Q3 scans (ranging from 50-550 *m/z* to 1000 *m/z* per second) were performed and putative compounds identified by searching the NIST/EPA/NIH Mass Spectral Library (Standard Reference Database v14). To measure butyrate, Q3 scans were performed as described above. The target and reference ions for butyrate were *m/z* 145 and *m/z* 75>146. The target and reference ions for deuterated butyrate were *m/z* 152 and *m/z* 76>153, respectively. Recovery of each sample was calculated using the recovery of internal deuterated standards.

Preparation of cDNA and qPCR

cDNA was prepared using TaqMan reverse transcription reagents as described by the manufacturer. Briefly, the reaction mixture was prepared using 2.5 μL of 10 x RT-PCR buffer, 5.5 μL $MgCl_2$ (25 mM), 5 μL of dNTPs (2.5 mM each), 1.25 μL of random hexamers (50 μM), 1 μL RNase Inhibitor, 0.625 μL of reverse transcriptase, and 9.6 μL of template RNA. The RNA concentration and A_{260}/A_{280} ratio were evaluated. For bacterial RNA samples, a reaction with RT-

PCR buffer, water, and template RNA (no reverse transcriptase) was performed to quantify contamination with DNA. Samples with more than 5 % DNA contamination were excluded from analysis. The reverse transcription reaction was performed using the following protocol: 10 minutes at 25 °C, 30 minutes at 48 °C, 5 minutes at 95 °C, and 4 °C indefinitely. cDNA and no-reverse transcription controls were stored at -20 °C prior to analysis.

qPCR was performed using SYBR Green with 2 μL of template DNA and 250 nM of each primer in a final reaction volume of 11 μL. Primer sequences are listed in Table 4. qPCR was performed using a QuantStudio 6 Flex instrument with the vendor-supplied, standard SYBR green qPCR protocol. Unless indicated otherwise, the ramp speed was 1.6 °C/s. The hold stage was at 50 °C for 2 min and 95 °C for 10 min. The amplification stage consisted of two steps, 95 °C for 15 s and 60 °C for 1 min, which were repeated for a total of 40 times. The melt curve was determined by increasing the temperature from 60 °C to 95 °C at a speed of 0.05 °C/s. A non-template control (water) was run in addition to samples. Two technical replicates per biological replicate were assayed. Melt curves for each reaction were evaluated prior to analysis. Data was analyzed using QuantStudio real-time PCR software V1.2. Baselines were determined using the Baseline Threshold algorithm. Data were further analyzed using the comparative C_T method for **Fig. 14, Fig. 15**, **Fig 18A-C,** and **Fig. 19** in Microsoft Excel [107]. PCR fragments containing known concentrations of the qPCR target were used to determine the limit of quantification (the C_T value for the lowest value in the linear dynamic range), the linear dynamic range, and the efficiency of the qPCR reaction for targets in *S.* Tm. Serial dilutions of plasmids containing the gene of interest were used to quantify absolute counts for targets *Mus musculus* and to perform quality control analysis for the qPCR assays [108].

Analysis of microbiota composition by qPCR

Cecal content was flash frozen in liquid nitrogen and stored at -80 °C. Bacterial DNA was then isolated using the PowerFecal DNA Isolation Kit. Microbiota composition was determined using SYBR Green-based qPCR as described above. Primer sequences are listed in Table 4. Serial dilutions of plasmids containing the gene of interest cloned into the TOPO cloning vector were also analyzed to generate a standard curve and calculate absolute counts of the gene of interest.

16S rDNA sequencing and analysis

Cecal content was collected, and the DNA was extracted from fecal samples using the MoBio PowerFecal kit per the recommendations of the manufacturer. The 16sV4 Region was amplified with the 515f-806R primer pair and barcoded prior to sequencing. The barcoded amplicons were purified and quantified on a 2200 TapeStation. The libraries were sequenced to generate 250 bp paired end reads using an Illumina Miseq system. A standard workflow for processing and quality assessment was applied to process the raw 16S sequence data [109]. The QIIME (Quantitative Insights into Microbial Ecology) open source software package (Version 1.91) [109] was employed to perform sequence alignment, operational taxonomic units (OTUs) picking against the Silva database (Version 128, released on 02/06/2017) [110], clustering, phylogenetic and taxonomic profiling, ANOSIM, and beta diversity analysis on the demultiplexed sequences. The analysis of beta diversity (principle coordinate analysis) was visualized using Emperor [111].

Cytokine mRNA quantification from intestinal tissue

Flash frozen tissue was homogenized using a Mini-BeadBeater, and RNA was extracted using the TRI Reagent manufacturer protocol. RNA preparations were also subjected to DNase I

treatment prior to use. cDNA was made using TaqMan reverse transcription reagents as described above. qPCR analysis of *Nos2*, *Cxcl1*, and *Tnf* was then conducted as described above, with *Gapdh* as the housekeeping gene.

β-galactosidase assays

5 mL of LB supplemented with various concentrations of L- or D-lactate were pre-incubated in the anaerobic chamber one day prior to inoculation. Overnight cultures were grown in the anaerobic chamber (**Fig. 16B-D**) or aerobically with shaking (**Fig. 16A** and **17A**). The pre-reduced media was inoculated with 100 μL of overnight culture and incubated in the anaerobic chamber (no electron acceptor conditions) or microaerobic chamber (1 % or 8 % oxygen conditions, as indicated) for 135 minutes (**Fig. 16A** and **17A**) or 5 hours (**Fig. 16B-D**). At the end of incubation, cultures were placed on ice for 20 minutes and β-galactosidase assays were performed based on the protocol described by Miller [112]. Briefly, the OD_{600} of the chilled cultures was taken. 100 μL or 500 μL of chilled culture was added to 900 μL or 500 μL of PBS with β-mercaptoethanol (2.7 μl/mL), respectively. Bacterial cells were lysed with 20 μL of 0.1 % SDS and 40 μL of chloroform, vortexed for 10 seconds, and incubated at room temperature for 5 minutes. 200 μL of 4 mg/mL *O*-nitrophenyl-β-D-galactoside (ONPG) was then added to the reaction. After sufficient yellow color had developed, the reaction was stopped with 500 μL of 1 M Na_2CO_3, and the time was recorded. The A_{420} and A_{550} were taken, and the Miller units were calculated according to the following equation (where t = time and v = volume):

$$\text{Relative Activity (Miller units)} = 1000 \times \frac{A_{420} - (1.75 \times A_{550})}{t \times v \times OD_{600}}$$

Histopathology analysis

Tissue was fixed in 10 % phosphate buffered formalin, followed by storage in 70 % ethanol. Samples were embedded in paraffin, cut into 5 μm sections and stained with hematoxylin and eosin. Blinded samples were then scored for signs of inflammation, including neutrophil and mononuclear cell infiltration, edema, epithelial damage, and exudate as listed in Table 5 [39].

Growth competitions in mucin broth

Sterile hog mucin (0.5 % [w/v]) was dissolved in No-carbon E (NCE) medium (0.2 g/L $MgSO_4$*7 H_2O, 3.9 g/L KH_2PO_4, 5.0 g/L anhydrous K_2HPO_4, and 3.5 g/L $NaNH_4HPO_4$*4 H_2O) [113, 114]. Sodium D,L-lactate, D-lactate, or L-lactate was added to designated samples. Sodium nitrate and potassium tetrathionate were added as indicated. Where indicated, sodium oxamate was added to mucin broth at a final concentration of 5 % [w/v]. 1.8 mL of mucin broth was inoculated with a 1:1 ratio of the indicated *S.* Tm or *E. coli* strains and incubated in an anaerobic chamber, in a microaerobic chamber, or aerobically in a shaking culture (250 RPM) for 18 hours. The CFU/mL of each indicator strain was determined by plating serial dilutions on indicator agar. Each experiment was performed with at least 4 independent biological replicates.

Quantification of mRNA during growth in mucin broth

Mucin broth was prepared as described above at a final concentration of 0.5 % [w/v] mucin. Other compounds were dissolved in water and filter-sterilized (0.2 μm) prior to adding to the complete mucin broth. Sodium L-lactate and sodium nitrate were added to the media as specified for a final concentration of 20 mM and 40 mM, respectively. All media was pre-incubated in an anaerobic chamber 1 day prior to inoculation. 5 mL of media were inoculated with 100 μL of overnight culture of the strains of interest. Cultures were grown for 3 hours in the anaerobic chamber (no electron acceptor condition and nitrate condition) or a microaerobic chamber as

indicated in each figure. RNA was extracted using the Aurum Total RNA Mini kit according to the manufacturer's protocol. RNA was then treated with the DNase I kit twice according to the manufacturer's instructions prior to analysis by RT-qPCR. RNA samples were stored at -80°C.

RNA extraction from cecal content for analysis of bacterial RNA

Cecal content was collected and flash-frozen in liquid nitrogen and stored at -80 °C. RNA was extracted with TRI reagent. Briefly, frozen samples were resuspended in 0.5 mL of TRI reagent and homogenized in a Mini-BeadBeater twice for 30 seconds. 0.1 mL of chloroform was then added to the tube, shaken, and incubated for 5 minutes at room temperature. The samples were then centrifuged at 12,000 x g for 15 minutes at 4 °C. 0.2 mL of aqueous phase supernatant was transferred to a new tube. RNA was precipitated by adding 0.25 mL of isopropanol followed by incubation at room temperature for 10 minutes. Samples were then centrifuged at 12,000 x g for 8 minutes at 25 °C to pellet the RNA. The pellet was then washed with 0.5 mL of 75 % ethanol and centrifuged at 12,000 x g for 5 minutes at 25 °C. The pellet was then air-dried and resuspended in DNase/RNase free water. RNA preparations were then treated twice with DNase I prior to use. cDNA preparation and qPCR were performed as described above.

Metagenomics

Wild-type C57BL/6 mice were treated with 3 % DSS (or sterile water for mock) for 8 days, followed by 1 day of sterile water as described above. Cecal content was collected and DNA was extracted. Metagenomic analysis was performed as described by Hughes *et al.* [40].

Quantification and statistical analysis

Data analysis was performed in Microsoft Excel and GraphPad Prism v7.0. Histopathology scores and PMN counts were analyzed using the non-parametric Mann-Whitney *U*-test. All other

data was transformed by the natural logarithm before inferential and descriptive statistical analysis. The normality of the log-transformed data was assessed using the D'Agostino-Pearson normality test for large groups (>8 samples) and the Shapiro-Wilk normality test for smaller groups (<8 samples). No predicted statistical outliers were removed since the presence or absence of these potential statistical outliers did not affect the overall interpretation. Mice that were euthanized early due to health concerns and mice that were insufficiently colonized (<10 colonies in 100 μL of undiluted sample; competitive infections only) were excluded from analysis. A two-tailed, paired Student's *t*-test was used to determine statistical differences between wild-type and mutant bacterial populations within the same animal (competitive infection experiments). A two-tailed, unpaired Student's *t*-test was applied to the log-transformed data to determine statistical difference between groups of mice. A *P* value of less than 0.05 was considered significant. Unless otherwise stated, *, $P < 0.05$; **, $P < 0.01$; ***, $P < 0.001$; ns, not statistically significant. In all mouse experiments, *N* refers to the number of animals from which samples were taken. Sample sizes (i.e. the number of animals per group) were not estimated *a priori* since effect sizes in our system cannot be predicted.

Data and software availability

16S rDNA sequencing data has been deposited in the European Nucleotide Archive under the accession number PRJEB21705 (https://www.ebi.ac.uk/ena/data/view/PRJEB21705). Metagenomic sequencing data is available in the European Nucleotide Archive under accession number PRJEB15095 (https://www.ebi.ac.uk/ena/data/view/PRJEB15095)

CHAPTER THREE[†]

DYSBIOSIS-ASSOCIATED CHANGE IN HOST METABOLISM GENERATES LACTATE TO SUPPORT *SALMONELLA* GROWTH

Introduction

In the anaerobic environment of the intestine, commensal bacteria have evolved sophisticated strategies to compete for limiting amounts of complex polysaccharides to support growth. Bacterial pathogens invading this ecosystem are likely to have evolved unique metabolic adaptations to circumvent nutritional competition with commensal microbes.

The invasive enteric pathogen *Salmonella enterica* Typhimurium (*S.* Tm) is a common cause of bacterial food-borne gastroenteritis (reviewed in [115-117]). In murine models of *S*. Tm infection, two spatially distinct but cooperative populations of the pathogen exist in the gut [61]. One population invades and replicates in the gut mucosa, a process that depends on two distinct type three secretion systems (T3SS-1 and T3SS-2) [49, 118-120]. Tissue invasion and replication trigger inflammatory host immune responses that keep the infection localized to the intestinal tract. The induction of a potent host inflammatory response is essential for effective colonization of the gastrointestinal tract [5, 44, 45]. A subpopulation of *S*. Tm in the gut lumen relies on mucosal inflammation to fundamentally change the environment of the gut. The creation of a novel niche in the lumen of the intestinal tract fosters an outgrowth of *S.* Tm at the expense of the microbiota [5, 44]

Recent studies have identified nutrients that specifically enhance growth of *S*. Tm during gut inflammation. For example, production of reactive oxygen and nitrogen species generates the alternative electron acceptors tetrathionate and nitrate [63, 70, 71]. Inflammation-associated changes in epithelial metabolism allow molecular oxygen to diffuse from the tissue into the gut lumen [85]. Respiration facilitates the utilization of poorly fermentable carbon sources such as ethanolamine, 1,2-propanediol, fructose-asparagine, and succinate [73, 77-79]. Furthermore, oxidation of sugars by nitric oxide gives rise to the aldaric acids galactarate and glucarate [72]. Collectively, these studies suggest that inflammation-driven changes in the nutritional environment of the gut lumen are critical for *S*. Tm niche creation and competition with the microbiota.

A survey of more than 300 compounds demonstrated that *S.* Tm is able to utilize over 70 structurally diverse compounds as carbon sources *in vitro* [121]. Comprehensive analyses of the *S*. Tm metabolism during systemic infection revealed significant redundancy in nutrient acquisition [122, 123]. Thus, it is conceivable that during gut colonization *S*. Tm relies on a variety of carbon sources, the identity and source of which are unknown.

Here, we performed metabolic profiling to identify nutrients that are accessible to *S*. Tm in the niche of the inflamed gut lumen. We discovered that luminal lactate levels are increased during *S*. Tm infection. Lactate availability in the gut was dependent on both the gut microbiota and host metabolism. Alterations in the gut microbiota led to decreased butyrate levels, prompting host cell metabolism to switch from an oxidative metabolism to lactate fermentation. Utilization of host-derived lactate enhanced fitness of *S*. Tm. These results identify lactate as a connection between host and microbial metabolism.

Results

Lactate levels in the gut lumen are increased during S. Tm infection.

To better understand how the metabolic landscape of the intestine changes during *S.* Tm infection, we performed semi-quantitative profiling of extracellular metabolites in the gut lumen. Groups of Swiss Webster mice were intragastrically inoculated with the *S.* Tm wild-type strain or mock-treated with LB broth. Seven days after infection, the cecal content was collected and subjected to gas chromatography mass spectrometry (GC/MS) (**Appendix A**). This analysis identified several extracellular metabolites with differential abundance in the cecal contents of infected mice compared to mock-treated mice. In this profiling, lactate was the most abundant metabolite during *S.* Tm infection while only small amounts of this compound were detected in mock-treated mice. To validate this finding, we developed a quantitative gas chromatography tandem mass spectrometry-based assay (GC/MS/MS) to measure lactate concentrations in the intestinal content (**Fig. 1A**). Compared to mock-treated animals, cecal lactate levels were significantly increased during *S.* Tm infection, confirming the results of the metabolic profiling. This finding led us to hypothesize that lactate may be a nutrient for *S.* Tm during infection.

Lactate utilization provides a fitness advantage in the inflamed gut.

The *S.* Tm chromosome is predicted to encode two respiratory lactate dehydrogenases, LldD and Dld [124]. To investigate the function of the *S.* Tm enzymes, we performed competitive growth assays *in vitro* (**Fig. 2**). To this end, we generated a mutant lacking both *lldD* and *dld* (Δ*lldD* Δ*dld* mutant). Mucin broth was inoculated with 1:1 mixture of the wild-type strain (AJB715) and a Δ*lldD* Δ*dld* mutant and incubated for 18 h. The relative titer of each strain was

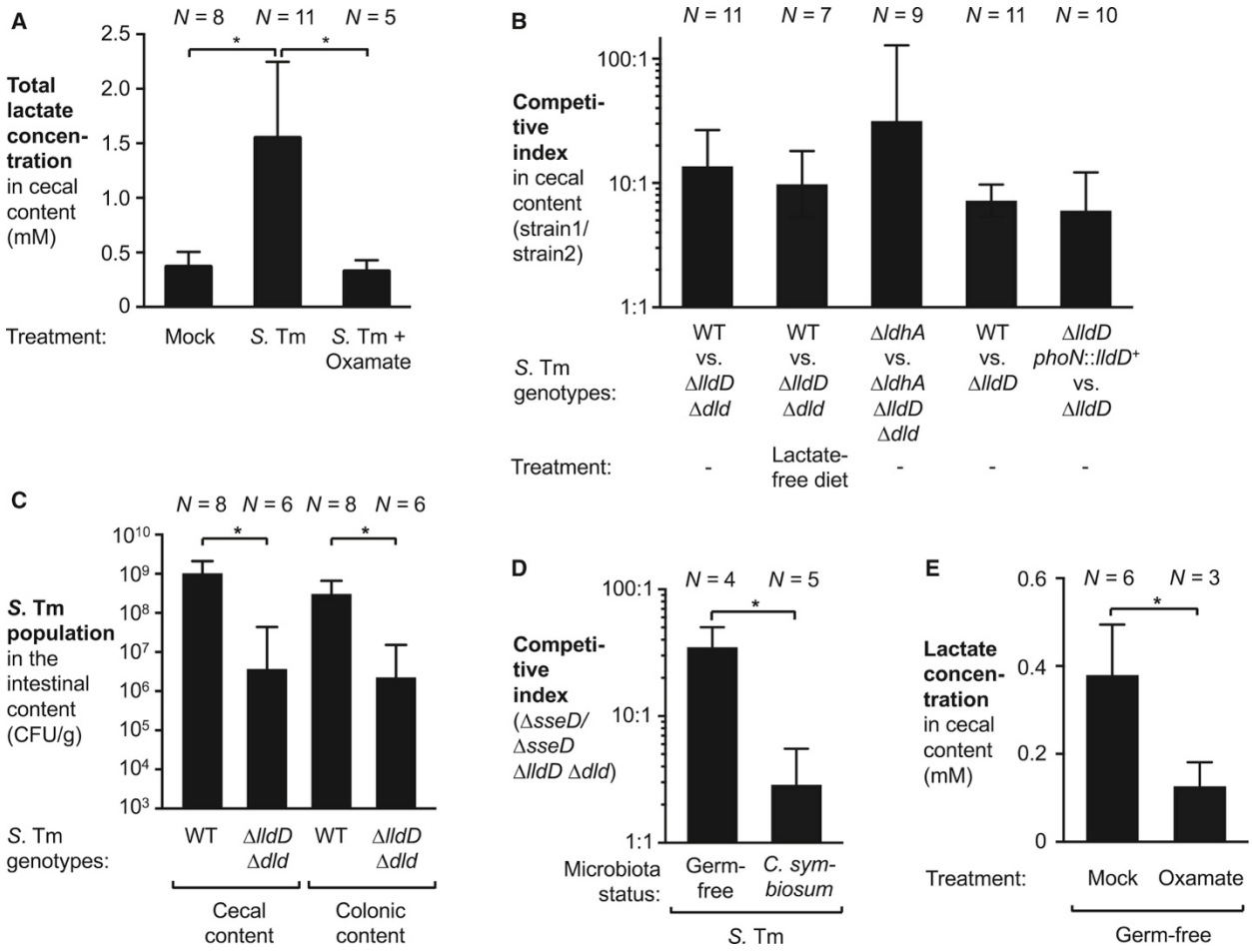

Figure 1. The host is a source of lactate during *S.* Tm infection (A) Groups of Swiss Webster mice were inoculated with the *S.* Tm wild-type strain (WT) or mock-treated with LB broth. One group of *S.* Tm-infected mice received 0.5 % sodium oxamate in their drinking water for the duration of the experiment. After 8 days of infection the mice were sacrificed, and lactate concentration in the cecal content was analyzed by GC/MS/MS. (B) Groups of Swiss Webster mice were intragastrically inoculated with a 1:1 ratio of the indicated *S.* Tm strains. Samples were collected 8 days after infection. Competitive indices were calculated using the relative abundance of each strain in the cecal content, corrected by the ratio in the inoculum. (C) Two groups of Swiss Webster mice were intragastrically infected with the *S.* Tm wild-type strain or the Δ*lldD* Δ*dld* mutant, respectively. The *S.* Tm populations in the cecal and colonic content (CFU/g) were determined after 8 days. (D) Groups of germ-free mice were pre-colonized with *C. symbiosum* or were mock-treated. After 3 days, both groups were intragastrically inoculated with an equal mixture of a Δ*sseD* and a Δ*sseD* Δ*lldD* Δ*dld* mutant. Cecal content was collected 10 days after infection to determine the CI. (E) Germ-free Swiss Webster mice were treated with oxamate in their drinking water for 2 days or were mock-treated. Lactate concentrations in the cecal content were quantified by GC/MS/MS. Bars represent geometric means ± standard error. *, $P < 0.05$. The number of animals per group (*N*) is indicated above each bar.

enumerated on selective agar and the ratio of wild-type strain to mutant bacteria, corrected by the ratio in the inoculum, was used to calculate the competitive index (**Fig. 2A**). Both strains were recovered in similar quantities in the absence of lactate suggesting that there was no general anaerobic growth defect for the Δ*lldD* Δ*dld* mutant. When the media was supplemented with both lactate and exogenous electron acceptors, the wild-type strain outcompeted the Δ*lldD* Δ*dld* mutant (**Fig. 2A and B**), a finding that is consistent with the respiratory function of membrane-bound LldD and Dld.

We then evaluated whether respiratory lactate dehydrogenases provide a fitness advantage to *S.* Tm in a model of infection. We intragastrically inoculated conventionally-raised Swiss Webster mice with equal amounts of both the *S.* Tm wild-type strain and a Δ*lldD* Δ*dld* mutant. Eight days after infection, host responses in cecal and colonic tissue as well as luminal bacterial populations were analyzed. Infection with *S.* Tm resulted in substantial pathological changes in the cecal mucosa (**Fig. 3A - D**), while infrequent and limited changes were observed in the colon (data not shown). The wild-type strain was recovered from the cecal content at significantly higher numbers than the Δ*lldD* Δ*dld* mutant (13-fold; $P < 0.05$ when comparing the individual wild-type and Δ*lldD* Δ*dld* populations) (**Fig. 1B**). To determine whether lactate oxidation provides a fitness advantage in competition with the gut microbiota, we intragastrically inoculated groups of Swiss Webster mice with the *S.* Tm wild-type strain and the Δ*lldD* Δ*dld* mutant, respectively (single infection). Eight days after infection, colonization of the cecal and colonic lumen by the Δ*lldD* Δ*dld* mutant was significantly reduced compared to the wild-type strain (**Fig. 1C**). Respiratory lactate dehydrogenase activity did not significantly enhance *S.* Tm fitness during systemic

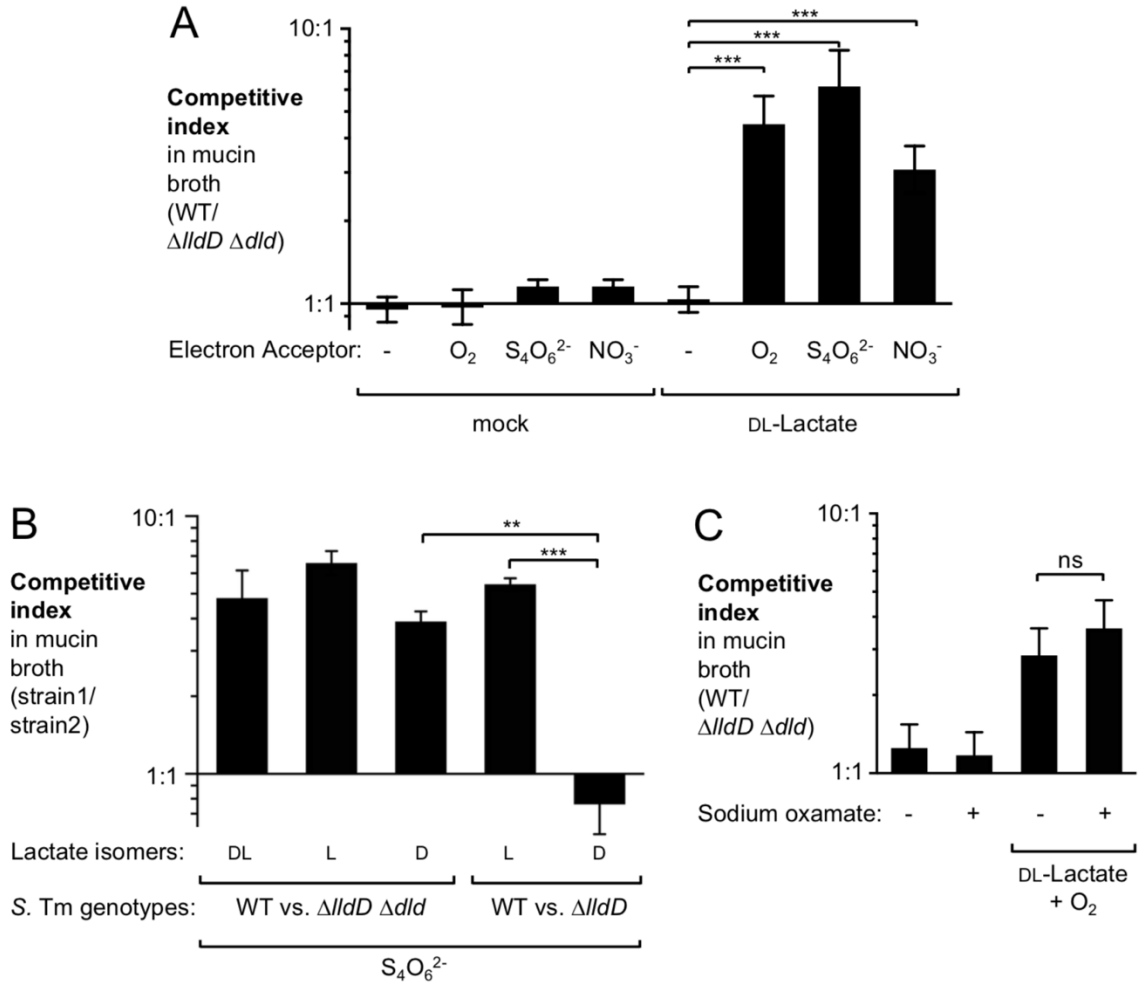

Figure 2: Lactate utilization by *S.* Tm *in vitro*. (A-C) Mucin broth supplemented with 20 mM lactate and 40 mM of the indicated electron acceptors was inoculated with an equal mixture of the *S.* Tm wild-type strain (WT) and the indicated mutants. The culture was incubated anaerobically (mock, tetrathionate, nitrate) or aerobically (O_2) with shaking for 18 h. After incubation, diluted samples were plated on selective media to determine the competitive index. (A) Effect of various terminal electron acceptors on LldD- and Dld-mediated lactate utilization. (B) Stereospecificity of LldD in *S.* Tm. (C) Effect of sodium oxamate on *S.* Tm lactate oxidation *in vitro*. Sodium oxamate was added at a final concentration of 5 % (w/v) as indicated. $S_4O_6^{2-}$, tetrathionate; NO_3^-, nitrate. DL-lactate is an equal mixture of the two enantiomers. Composite data for at least 4 biological replicates is shown. Bars represent geometric means ± standard error. **, $P < 0.01$; ***, $P < 0.001$. ns, not statistically significant.

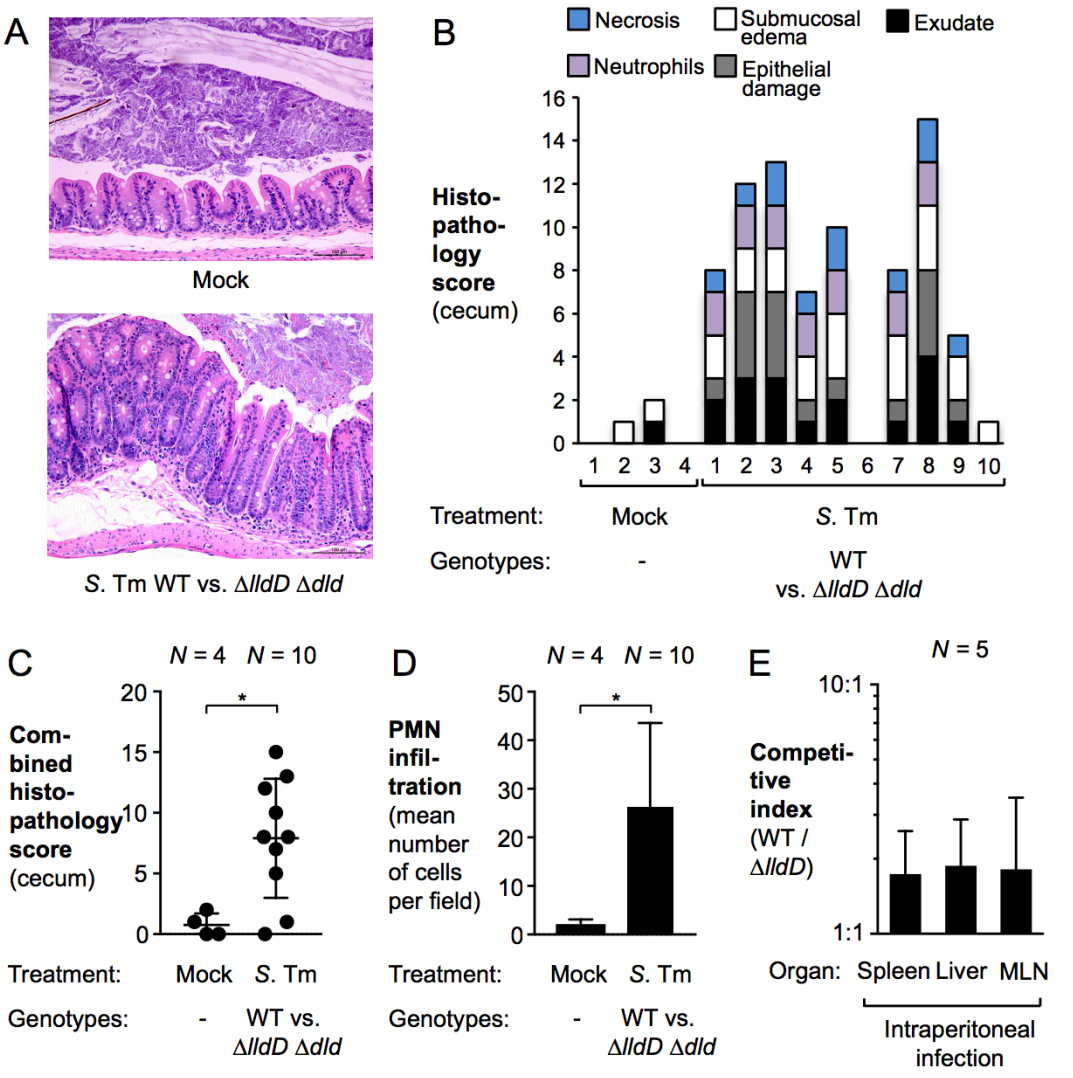

Figure 3: *S.* Tm-induced pathological changes in the cecal mucosa of Swiss Webster mice. (A-D) Groups of Swiss Webster mice were intragastrically inoculated with a 1:1 ratio of the *S.* Tm wild-type strain (WT) and the Δ*lldD* Δ*dld* mutant or were mock-treated with LB broth as described in Fig. 1B. Samples were collected 8 days after infection. One mouse was not analyzed due to the lack of samples. (A) Representative images of H+E stained cecal tissue. Scale bar, 100 μm (B) Individual histopathology scores for pathological changes in the cecum. Each bar represents one animal. (C) Combined Histopathology Score from data shown in panel B. Each symbol represents one animal; centerlines represent the average ± standard deviation. (D) Infiltration of PMNs into the cecal tissue. 10 fields per animal were examined. Bars are means ± standard deviation. (E) C57BL/6 mice were infected with *S.* Tm wild-type and the Δ*lldD* mutant in equal numbers via intraperitoneal injection. 3 days after infection samples of liver, spleen, and mesenteric lymph nodes (MLN) were collected, homogenized, and plated on selective agar to determine the competitive index. Bars are geometric means ± SEM. The number of animals per group (*N*) is indicated above each bar. *, $P < 0.05$.

infection (**Fig. 3E**). Collectively, these data indicated that during gut colonization, *S.* Tm accessed the lactate pool and that lactate degradation provided a fitness advantage for the pathogen.

Lactate utilized by S. Tm is host-derived.

Next, we investigated the source of lactate in the gut lumen. As a simple fermentation end product, lactic acid can be generated by virtually all members in the tree of life, including gut bacteria [125] and mammalian cells [126]. To determine if lactate originated from the mouse diet, we repeated the *S.* Tm competition experiment in mice that were fed a defined, lactate-free diet (**Fig. 1B**). In this experiment, the wild-type strain outcompeted the lactate utilization deficient strain to a similar extent as with our standard rodent diet (9-fold, $P < 0.05$ when comparing the individual wild-type and Δ*lldD* Δ*dld* populations), indicating that dietary lactate only plays a minor role during *S.* Tm infection.

The *S.* Tm genome encodes a third lactate dehydrogenase, *ldhA*, which is involved in fermentative lactate production. It is conceivable that cross-feeding of lactate could occur between two *S.* Tm subpopulations in the gut lumen. To explore this possibility, we determined the competitive fitness of a Δ*ldhA* mutant and a Δ*ldhA* Δ*lldD* Δ*dld* mutant. In the absence of *ldhA*, respiratory lactate dehydrogenase activity still provided a fitness advantage in colonizing the cecal lumen (**Fig. 1B**), demonstrating that lactate does not originate from *S.* Tm.

Given that many members of the microbiota can produce lactate [125], we tested the hypothesis that the microbiota was the predominant source of lactate during *S.* Tm infection using a gnotobiotic mouse model. Mice reared in a germ-free environment rapidly succumb to *S.* Tm infection due to uncontrolled systemic replication. To circumvent this limitation, we generated a *S.* Tm mutant that lacks a functional T3SS-2 (Δ*sseD* mutant) and thus is unable to replicate at

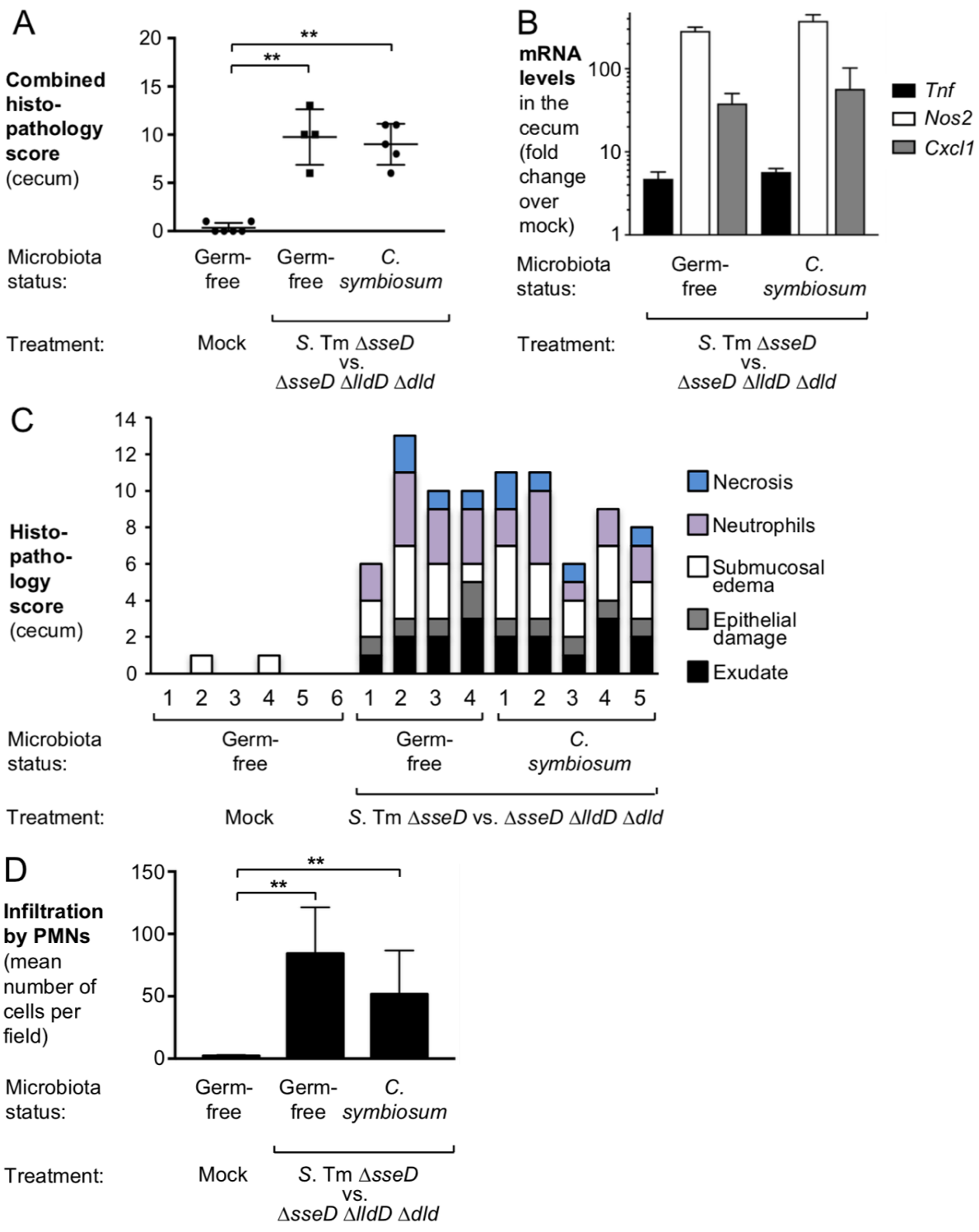
A
Combined histo-pathology score (cecum)
20
15
10
5
0
**
**
Microbiota status:
Germ-free
Germ-free
C. symbiosum
Treatment:
Mock
S. Tm ΔsseD vs. ΔsseD ΔlldD Δdld
B
mRNA levels in the cecum (fold change over mock)
100
10
1
Tnf
Nos2
Cxcl1
Microbiota status:
Germ-free
C. symbiosum
Treatment:
S. Tm ΔsseD vs. ΔsseD ΔlldD Δdld
C
Histo-patho-logy score (cecum)
14
12
10
8
6
4
2
0
1 2 3 4 5 6 1 2 3 4 1 2 3 4 5
Necrosis
Neutrophils
Submucosal edema
Epithelial damage
Exudate
Microbiota status:
Germ-free
Germ-free
C. symbiosum
Treatment:
Mock
S. Tm ΔsseD vs. ΔsseD ΔlldD Δdld
D
Infiltration by PMNs (mean number of cells per field)
150
100
50
0
**
**
Microbiota status:
Germ-free
Germ-free
C. symbiosum
Treatment:
Mock
S. Tm ΔsseD vs. ΔsseD ΔlldD Δdld

Figure 4: *S.* Tm-induced pathological changes in the gnotobiotic mouse model. (A-D) Groups of germ-free Swiss Webster mice were pre-colonized with *C. symbiosum* or were mock-treated. After 3 days, both groups were intragastrically inoculated with an equal mixture of an Δ*sseD* and an Δ*sseD* Δ*lldD* Δ*dld* mutant. After 10 days, cecal tissue was collected for analysis. (A) Combined histopathology score. (B) Fold-change in mRNA levels of *Tnf, Nos2,* and *Cxcl1* by RT-qPCR. Bars represent geometric means ± standard error. (C) Individual histopathology scores for cecal tissue. Each bar represents one animal. (D) Infiltration of PMNs into the cecal tissue. 10 fields per animal were evaluated. Bars are means ± standard deviation. **, $P < 0.01$. The number of animals per group (*N*) is indicated in panel C.

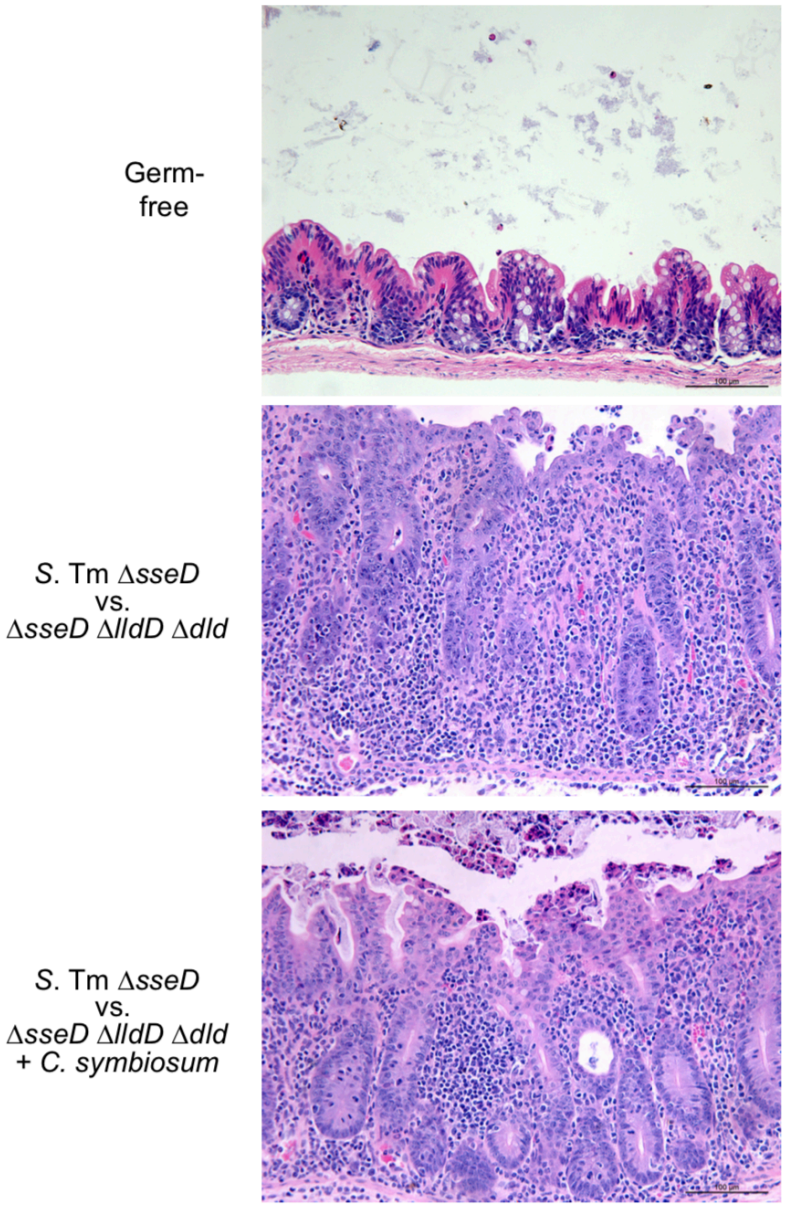

Figure 5: *S.* Tm-induced pathological changes in the gnotobiotic mouse model. Groups of germ-free Swiss Webster mice were pre-colonized with *C. symbiosum* or were mock-treated. After 3 days, both groups were intragastrically inoculated with an equal mixture of an Δ*sseD* and an Δ*sseD* Δ*lldD* Δ*dld* mutant. After 10 days, cecal tissue was collected for analysis. Representative images of H+E stained sections of the cecum. Scale bar, 100 μm.

systemic sites [118]. Germ-free mice were intragastrically inoculated with an equal mixture of the Δ*sseD* mutant and an isogenic Δ*sseD* Δ*lldD* Δ*dld* mutant. Significant cecal inflammation was observed ten days after infection (**Fig. 4 and 5**). Importantly, the Δ*sseD* mutant was recovered in higher numbers than the isogenic Δ*sseD* Δ*lldD* Δ*dld* mutant (35-fold, $P < 0.05$ when comparing the individual wild-type and Δ*lldD* Δ*dld* populations; **Fig. 1D**), suggesting that lactate utilization still provides a fitness advantage for *S.* Tm even in the absence of the microbiota.

We next investigated whether the host could be a major source of lactate. As a proof of principle experiment, germ-free Swiss Webster mice were either mock-treated or received sodium oxamate, an inhibitor of fermentative lactate dehydrogenases, in the drinking water for 2 days. We measured the concentration of lactate in the cecal content using GC/MS/MS (**Fig. 1E**). Lactate was abundant in the cecal lumen of germ-free mice (~ 0.38 mM). Oxamate treatment significantly reduced lactate levels, suggesting that host lactate dehydrogenases are a major source of lactate in germ-free animals. Also, oxamate treatment of conventionally-raised, *S.* Tm-infected mice significantly decreased lactate concentrations (**Fig. 1A**), an observation that is consistent with the notion that increases in lactate levels during *S.* Tm infection were likely of host origin.

S. Tm can utilize both L-(+)- and D-(-)- lactate *in vitro* (**Fig. 2B**). The lactate-degrading, respiratory lactate dehydrogenases LldD and Dld allow for the utilization of L-(+)- and D-(-)-lactate, respectively (**Fig. 2B**). Lactate-generating mammalian lactate dehydrogenases solely generate the L-enantiomer, while fermenting microbes in the gut microbiota produce both enantiomers. Based on our hypothesis that the majority of lactate during *S.* Tm infection is host-derived, we predicted that *S.* Tm would predominantly utilize L-lactate during infection. A mutant lacking only LldD activity (Δ*lldD* mutant) recapitulated the fitness defect of the Δ*lldD* Δ*dld* double

mutant (**Fig. 1B**), supporting this hypothesis. This fitness advantage is also seen when we competed a genetically complemented strain (Δ*lldD phoN*::*lldD*$^{+}$) against the L-lactate utilization deficient mutant (Δ*lldD*) (**Fig. 1B**). A mutant lacking only Dld activity did not display a competitive colonization defect (data not shown). Collectively, these experiments suggest that utilization of host-derived lactate enhances *S*. Tm fitness in the inflamed gut.

Depletion of microbial butyrate changes epithelial cell metabolism to lactate fermentation.

Under homeostatic conditions, fermentation of host-inaccessible complex polysaccharides by members of the microbiota, primarily Clostridia clusters IV and XIVa, gives rise to the short chain fatty acid butyrate [80, 127]. In IEC, butyrate is consumed through β-oxidation and energy is generated by oxidative phosphorylation. In the absence of butyrate, e.g. in germ-free mice, intestinal epithelial cells change their metabolism from fatty acid oxidation to glucose fermentation with lactate as the main fermentation end product [89]. In animal models of infectious and non-infectious colitis, a depletion of members in the class Clostridia and concomitant decreases in butyrate availability have been reported to alter colonocyte metabolism [84, 85, 90, 91]. Thus, we hypothesized that ablation of Clostridia through antibiotic treatment would recapitulate these changes in the absence of a pathogen and result in lactate accumulation in the gut lumen. To test this idea, conventional C57BL/6 mice were orally treated with a single dose of streptomycin (**Fig. 6**). Streptomycin treatment decreased Clostridia populations by more than 4 orders of magnitude, with Clostridia populations returning to normal levels after 3 to 4 days (**Fig. 6A**). Concomitant with the ablation of Clostridia, a significant decrease in butyrate concentrations in the cecal content was observed (**Fig. 6B**). In contrast, lactate levels were significantly increased 2, 3, and 4 days after streptomycin-induced perturbation (**Fig. 6C**),

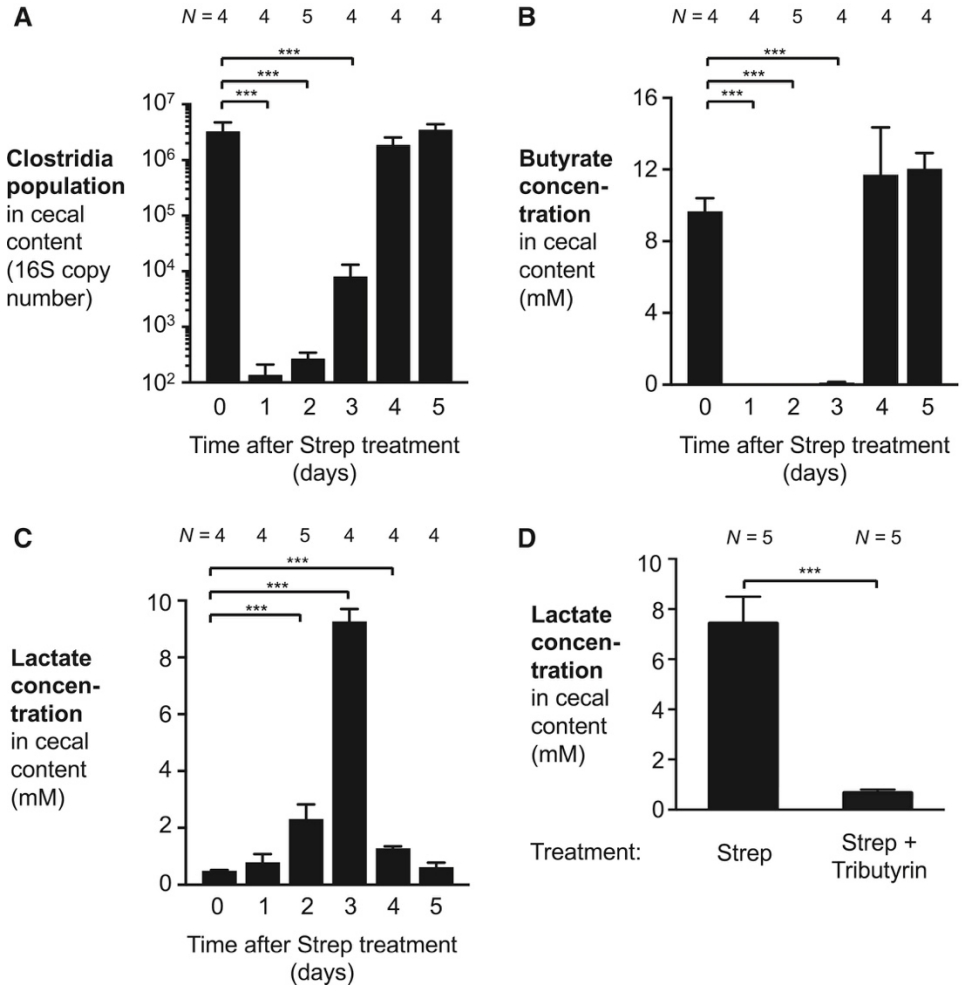

Figure 6. Perturbation of the gut microbiota by oral streptomycin treatment results in elevated lactate levels. (A-C) Groups of C57BL/6 mice received a single oral dose of streptomycin (Strep). Samples of cecal content were taken 1 to 5 days after streptomycin administration. Mock-treated controls represent the 0-day time point. (A) qPCR analysis of DNA extracted from the cecal content to assess Clostridia populations in the microbiota. (B and C) The concentration of butyrate (B) and lactate (C) in the cecal content was quantified by GC/MS. (D) Groups of C57BL/6 mice were treated with a single dose of streptomycin. Animals then received oral tributyrin treatment through gavage and fortified chow, or were mock-treated. Lactate levels in the cecal content were measured 3 days after streptomycin treatment. Bars represent geometric means ± standard error. ***, $P < 0.001$. The number of animals per group (*N*) is indicated above each bar.

mirroring the decline in butyrate levels. To determine whether exogenous supplementation with butyrate was sufficient to suppress the spike in lactate levels, streptomycin-treated mice were orally treated with tributyrin (glyceryl tributyrate) (**Fig. 6D**). This exogenous supplementation with a butyrate source significantly decreased the cecal lactate concentration three days after streptomycin treatment.

In germ-free mice, colonocytes perform lactate fermentation due to a lack of microbial short chain fatty acids [89]. We reasoned that colonization of gnotobiotic mice with a butyrate-producing bacterial strain would decrease availability of lactate. To test this idea, we repeated the competitive infection experiment with the Δ*sseD* and the Δ*sseD* Δ*lldD* Δ*dld* mutant in germ-free mice that had been mono-associated with *Clostridium symbiosum* 3 days prior to infection. The fitness advantage conferred by *S.* Tm lactate dehydrogenases in the absence of other microbes was significantly reduced in the presence of *C. symbiosum* (**Fig. 1D**). No significant differences in cecal inflammation between the germ-free mice and those that had been pre-colonized with *C. symbiosum* prior to infection were noted (**Fig. 4 and 5).** Taken together, these experiments indicate that the lack of microbial butyrate induces a shift in host metabolism to lactate fermentation.

Lactate utilization during post-antibiotic expansion of the S. Tm population.

Antibiotic therapy predisposes to infection with non-typhoidal *Salmonella* serovars in both immune-competent and immune-suppressed individuals [128]. In murine models, oral pre-treatment with streptomycin decreases colonization resistance and leads to a pronounced post-antibiotic expansion of the *Salmonella* population in the gut lumen [5]. We investigated the role of *S.* Tm lactate metabolism in streptomycin pre-treated mice. Conventional C57BL/6 mice were intragastrically treated with one dose of streptomycin. One day later, these animals were

intragastrically inoculated with *S.* Tm. Five days after infection, the cecal contents were collected for 16S qPCR analysis and measurements of lactate and butyrate concentrations (**Fig. 7; Fig. 8E**). Compared to healthy control mice, streptomycin-treated and *S.* Tm infected mice exhibited a significant decrease in Clostridia and Bacteroidetes populations and a bloom of the Enterobacteriaceae population (**Fig. 7A**). Cecal butyrate levels were significantly decreased while lactate levels were elevated in streptomycin-treated and *S.* Tm infected mice compared to mock-treated controls (**Fig. 7B and C**). Respiratory lactate dehydrogenases (5.4-fold), in particular the L-lactate dehydrogenase LldD (5.1-fold), provided a fitness advantage in colonizing the murine cecum since the *S.* Tm wild-type strain was recovered in higher numbers than isogenic Δ*lldD* Δ*dld* and Δ*lldD* mutants in competitive infection experiments (**Fig. 7D**). Similarly, lactate utilization provided a fitness advantage in the absence of T3SS-1 and T3SS-2-induced inflammation (Δ*invA* Δ*spiB* mutant background) (**Fig. 7D - E; Fig. 8A - C**).

Streptomycin is effective at removing Gram-positive Clostridia. In contrast, oral pre-treatment with neomycin, an antibiotic that primarily targets Gram-negative bacteria [129], did not enable lactate utilization by *S.* Tm (**Fig. 7D**). We therefore concluded that streptomycin-induced perturbation of the microbiota is sufficient for lactate accumulation to occur.

To evaluate whether inhibition of fermentative host lactate dehydrogenases is sufficient to decrease lactate availability during S. Tm infection, groups of streptomycin pre-treated mice were intragastrically inoculated with the *S.* Tm wild-type strain and the Δ*lldD* Δ*dld* mutant and were either mock-treated or received sodium oxamate in the drinking water and determined the competitive index 4 days after infection. Administration of sodium oxamate abolished the fitness advantage conferred by lactate oxidation in *S.* Tm *in vivo* (**Fig. 7F**). Sodium oxamate did not

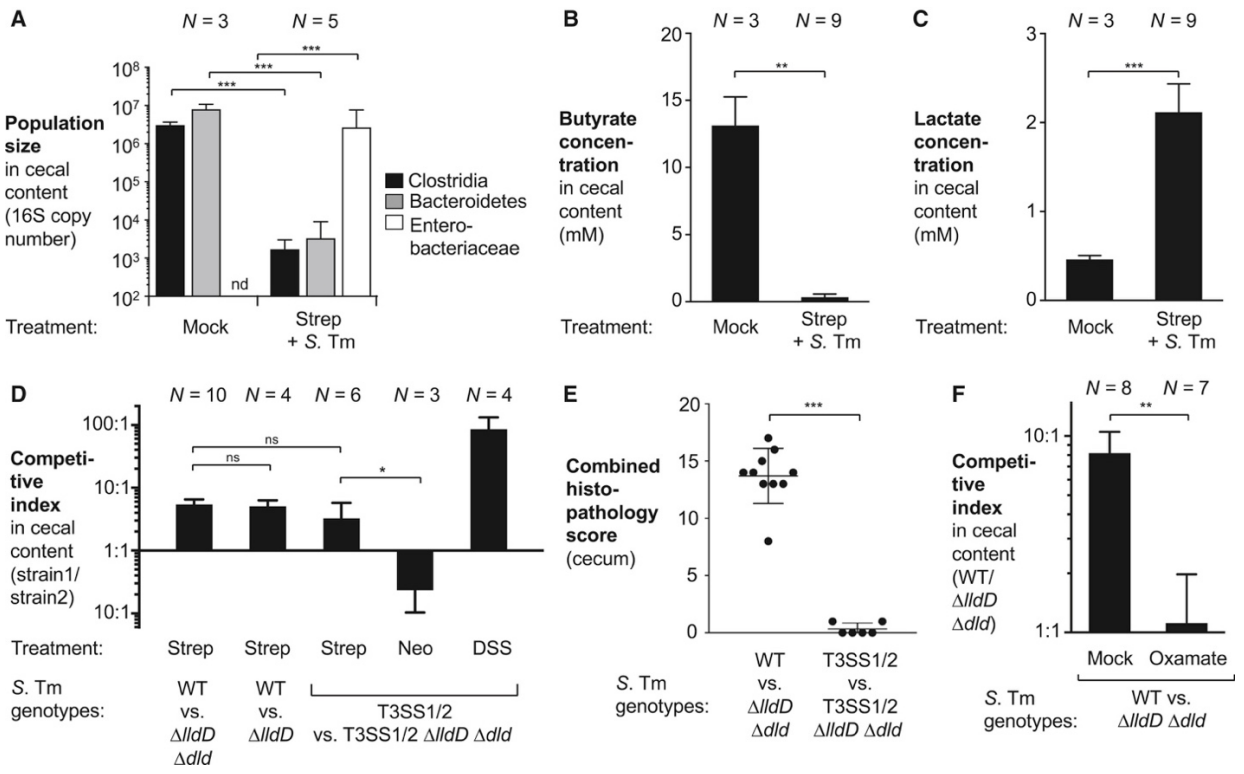

Figure 7. *S.* Tm utilizes lactate during post-antibiotic expansion (A-C) Groups of C57BL/6 mice, pretreated with a single dose of oral streptomycin (Strep) were infected with the *S.* Tm wild-type strain (WT) or were mock-treated. Five days after infection, cecal content was collected for analysis. (A) 16S qPCR analysis of Clostridia, Bacteroidetes, and Enterobacteriaceae populations in the cecal microbiota. (B - C) Concentrations of butyrate (B) and lactate (C) in the cecal content were measured by targeted GC/MS. (D-E) C57BL/6 mice were pre-treated with a single dose of streptomycin (Strep), neomycin (Neo), or 4 days of dextran sulfate sodium (DSS) treatment and were subsequently infected with an equal mixture of the indicated *S.* Tm strains through the intragastric route. DSS treatment was continued throughout the duration of the experiment, as indicated. Five days after infection, samples were collected for analysis. T3SS1/2, Δ*invA* Δ*spiB* mutant. (D) Competitive indices of the indicated strains in the cecal content. (E) Combined histopathology score of cecal tissue. Each dot represents one animal while lines represent the average ± standard deviation. (F) Streptomycin-pretreated mice, infected with the *S.* Tm wild-type strain and the Δ*lldD* Δ*dld* mutant, were treated with sodium oxamate in the drinking water or mock treated beginning one day after infection until the end of the experiment. The competitive index in the cecal content was determined 4 days after infection. Bars represent geometric means ± standard error. *, $P < 0.05$; **, $P < 0.01$; ***, $P < 0.001$; ns, not statistically significant; nd, not detected. The number of animals per group (*N*) is indicated above each bar.

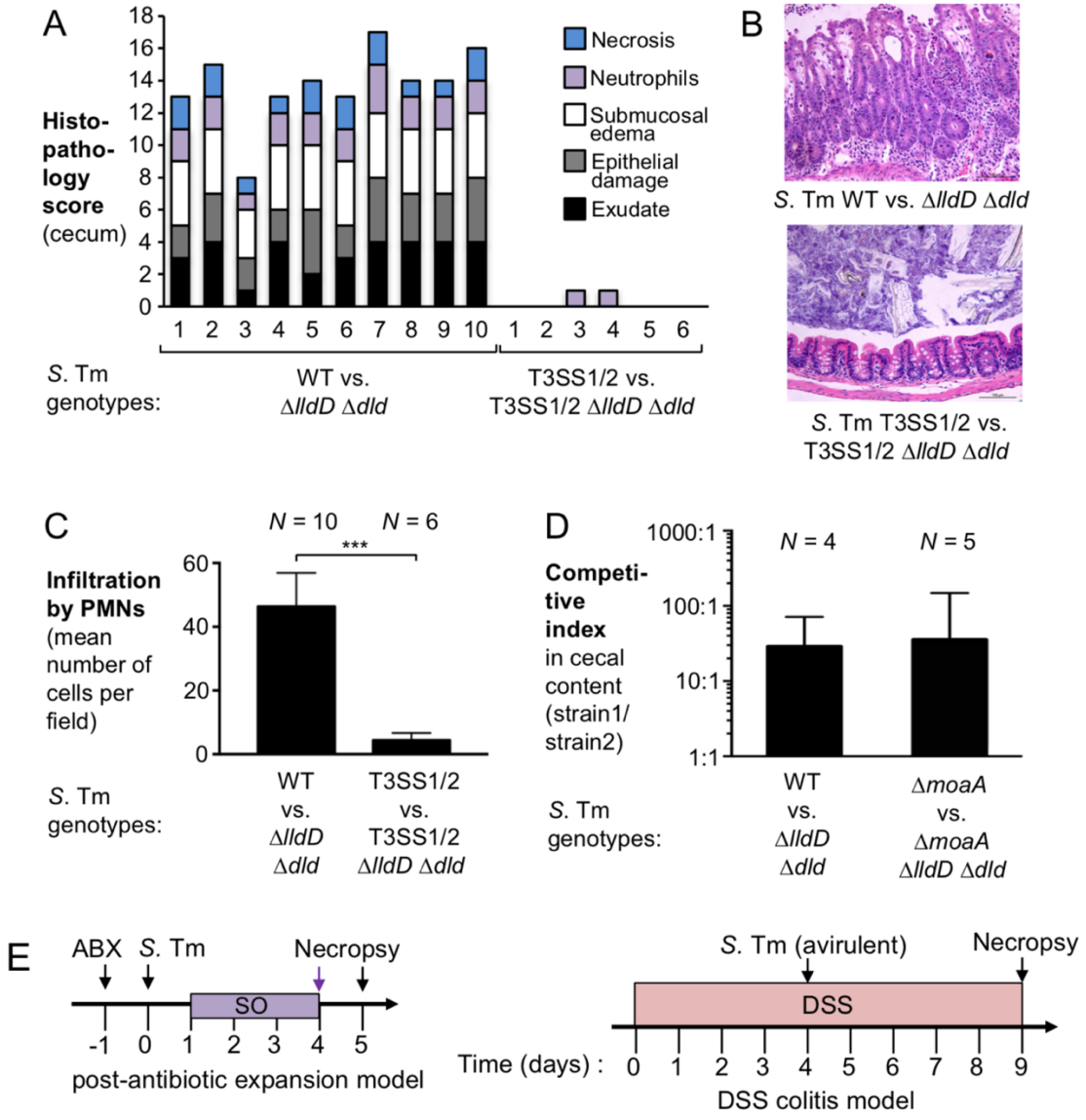

Figure 8. Lactate utilization in the streptomycin-treated mouse model of salmonellosis. (A-D) Streptomycin-pretreated C57BL/6 mice were intragastrically infected with an equal mixture of the indicated *S.* Tm strains. Five days after infection, samples were collected for analysis. T3SS1/2, Δ*invA* Δ*spiB* mutant. (A) Individual histopathology scores of cecal tissue. Each bar represents one animal. (B) Representative images of H&E stained cecal sections. Scale bar, 100 μm. (C) Infiltration of PMNs into cecal tissue. 10 fields were evaluated per animal. Bars represent average ± standard deviation. (D) Cecal content was collected, and the competitive index of the indicated strains was determined. Bars represent geometric means ± standard error. (E) Schematic representation of the post-antibiotic expansion model and the dextran sulfate sodium (DSS)-induced colitis model. ABX, oral antibiotic treatment. In one experiment, animals were treated with sodium oxamate (SO). ***, $P < 0.001$. The number of animals per group (*N*) is indicated above each bar.

directly inhibit respiratory LldD and Dld activity (**Fig. 2C**) *in vitro*. Taken together, the experiments provide further support for the idea that during *S.* Tm infection, increased lactate levels are caused by altered host metabolism.

S. Tm-*induced dysbiosis is characterized by a depletion of butyrate-producing Clostridia.*

To investigate microbiota changes induced by *S.* Tm, groups of conventional Swiss Webster mice were intragastrically inoculated with the *S.* Tm wild-type strain or mock-treated. After 8 days, the cecal content of these mice was collected for 16S rDNA sequencing (**Fig. 9A - C**). Unweighted principal coordinate analysis of microbiota composition showed distinct clustering of the microbiota of mock treated mice compared with that of infected mice (**Fig. 9A**). Taxonomic analysis of microbiota composition of mock treated mice revealed that during *S.* Tm infection, the phyla Bacteroidetes and Firmicutes were significantly decreased (**Fig. 9B**). In particular, populations of the class Clostridia were significantly diminished (3-fold; $P < 0.05$). In contrast, a bloom of Gammaproteobacteria, the class to which *S.* Tm belongs, was observed (**Fig. 9C**). In agreement with our initial profiling (**Appendix A**), targeted measurements of butyrate by GC/MS demonstrated that mock-treated mice had nearly 10-fold higher levels of butyrate in their cecal content compared to that of *S.* Tm infected mice (**Fig. 9D**) and a concomitant increase in lactate concentrations (**Fig. 1A**). The fitness advantage conferred by lactate oxidation was time-dependent and correlated with the magnitude of cecal inflammation (**Fig. 10**). In a model of chemically-induced colitis (dextran sulfate sodium-induced colitis model; **Fig. 8E**), lactate oxidation provided a fitness advantage for *Salmonella* in the absence of bacterial virulence factors, consistent with the idea that gut inflammation is sufficient to increase luminal lactate levels (**Fig. 7D**). Collectively, these data suggest that *Salmonella*-induced inflammation is associated with a

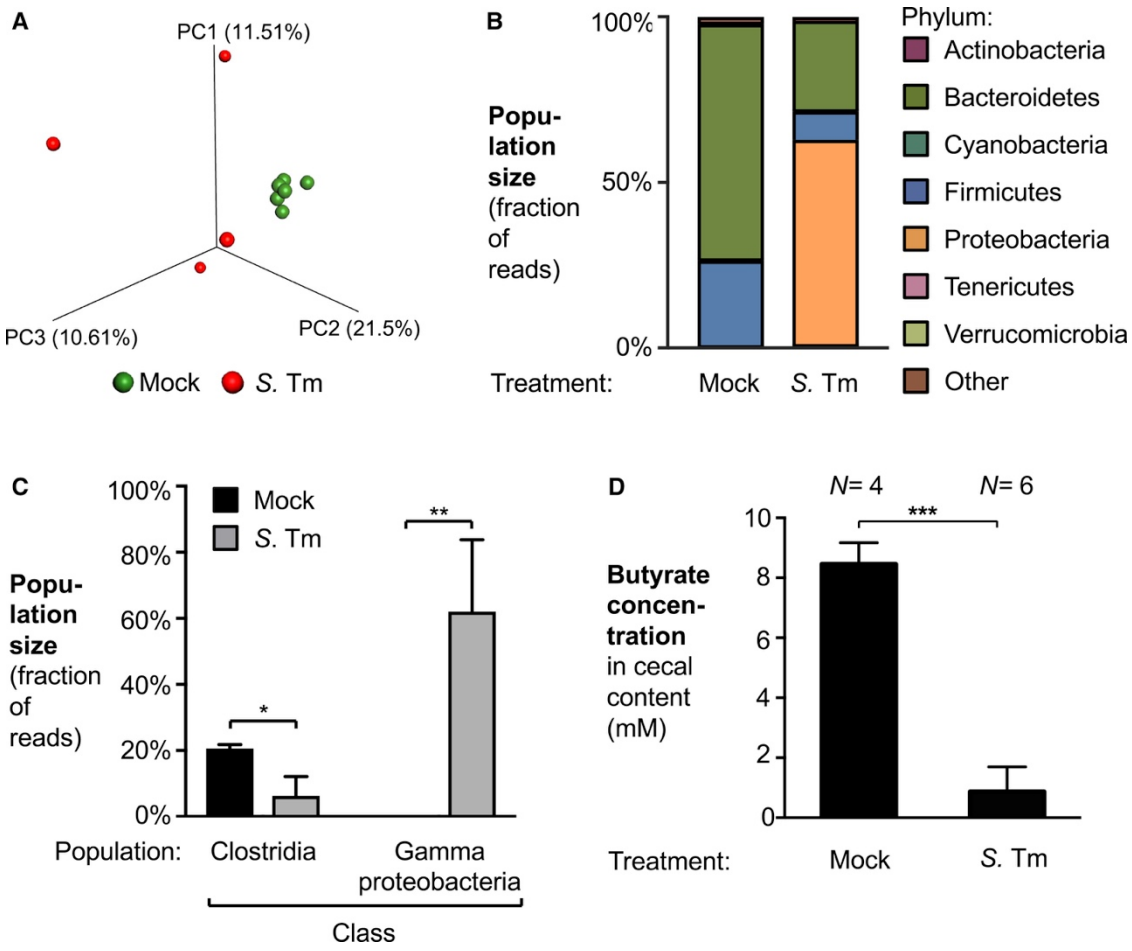

Figure 9. Gut microbiota changes during *S.* Tm infection. (A – C) Groups of Swiss Webster mice were intragastrically infected with the *S.* Tm wild-type strain (WT) or mock-treated. Eight days after infection, cecal content was collected for 16S rDNA profiling. (A) Principal coordinate (PC) plot of unweighted UniFrac distances generated from cecal microbial communities. Mock treatment, green spheres; *S.* Tm infection, red spheres. (B) Cecal microbiota composition at the phylum level. (C) Abundance of the classes Clostridia and Gammaproteobacteria in the ceca of mock-treated (black bars) and *S.* Tm-infected mice (gray bars). In mock-treated animals, Gammaproteobacteria were detected at very low abundance (less than 0.15%) (D) Swiss Webster mice were infected as described above. Butyrate concentrations in the cecal contents were determined 8 days after infection using GC/MS. Bars represent geometric means ± standard error. *, $P < 0.05$; **, $P < 0.01$; ***, $P < 0.001$. The number of animals per group (N) is indicated above each bar.

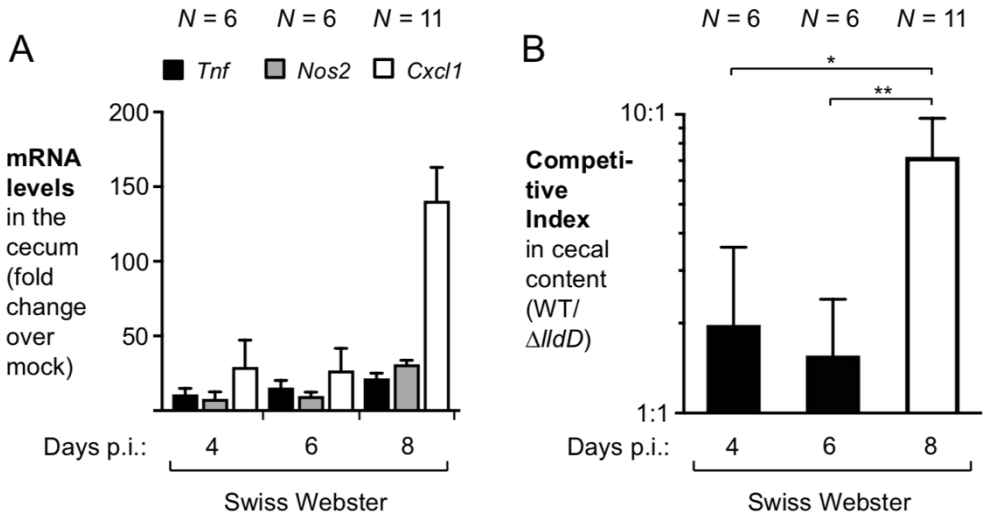

Figure 10. Time course of *S.* Tm infection in Swiss Webster mice. Swiss Webster mice were intragastrically infected with an equal mixture of the *S.* Tm wild-type strain (WT) and the Δ*lldD* mutant. Samples were collected 4, 6, and 8 days post infection (p.i.). (A) mRNA levels of *Tnf* (black bars), *Nos2* (gray bars), and *Cxcl1* (white bars) in cecal tissue were determined by RT-qPCR. (B) The competitive index in the cecal content at each time point was determined. The data for the day 8 time point (white bar) is also shown in Fig. 1B and is given here for reference. Bars represent the geometric mean ± standard error. *, $P < 0.05$; **, $P < 0.01$. The number of animals per group (*N*) is indicated above each bar.

depletion of butyrate-producing Clostridia, which in turn correlates with increased availability of lactate.

Manipulation of PPARγ signaling influences lactate production during S. Tm infection.

PPARγ is a transcription factor that controls fatty acid-based metabolism in the host. PPARγ is expressed in intestinal epithelial cells [96] and orchestrates the switch from fermentation of glucose to β-oxidation in this cell type [84] (**Fig. 11A**). We therefore hypothesized that lactate production by the intestinal epithelium could be prevented by pharmacological activation of PPARγ signaling. We administered the PPARγ agonist rosiglitazone or a vehicle control via intraperitoneal injection to streptomycin-treated C57BL/6 mice to drive epithelial β-oxidation (**Fig. 11B and C**). As expected, rosiglitazone did not interfere with the streptomycin-induced depletion of butyrate in the cecal content (**Fig. 11B**). Interestingly, cecal lactate levels were significantly reduced during rosiglitazone treatment (**Fig. 11C**). Administration of rosiglitazone in the streptomycin-treated mouse model of *Salmonella* infection decreased the fitness advantage conferred by L-lactate utilization (**Fig. 11D**). These experiments support the idea that PPARγ controls the metabolic switch that is responsible for host epithelial lactate production during *S.* Tm infection.

Oxygen is the terminal electron acceptor for lactate utilization.

We next wanted to determine the identity of the terminal electron acceptor for lactate utilization. Under homeostatic conditions, β-oxidation consumes most of the oxygen available at the gut mucosal interface [91]. During *S*. Tm infection, unconsumed oxygen leaks into the gut lumen where it enables respiration by the facultative anaerobic pathogen [85]. In addition, *S*. Tm respires nitrate and tetrathionate, byproducts of the inflammatory oxidative burst [63, 70, 71]. *In*

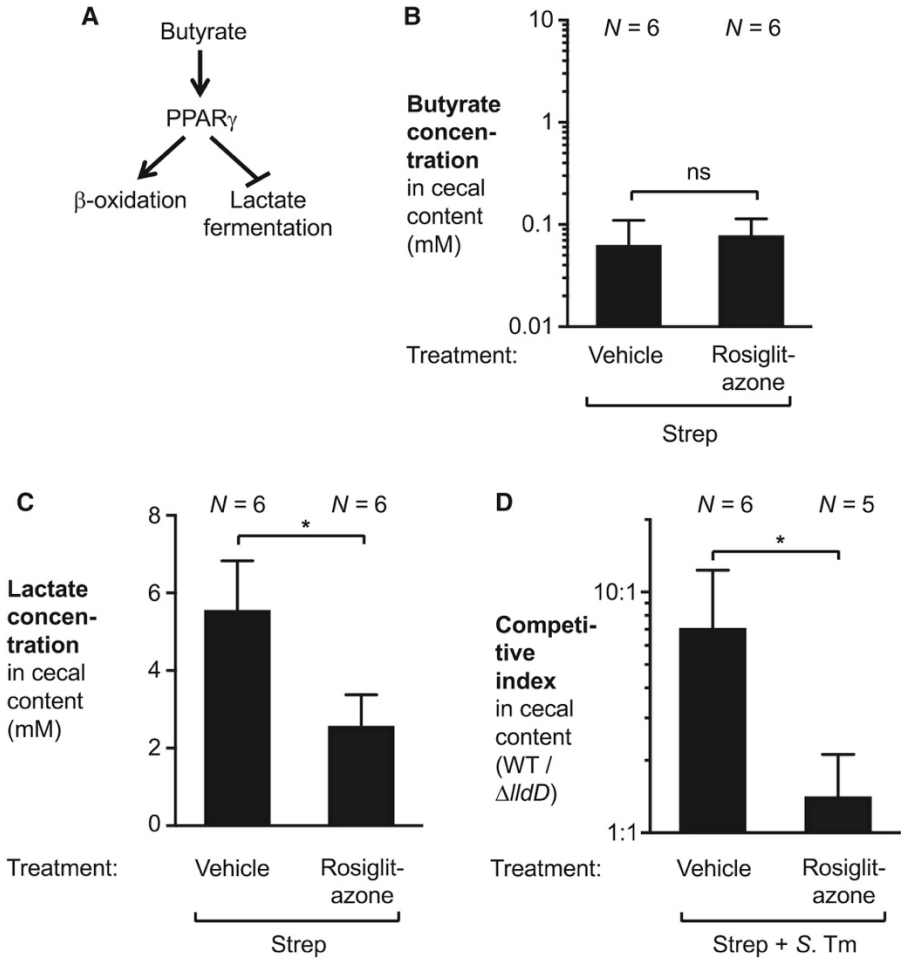

Figure 11. Effect of PPARγ signaling on lactate availability during *S.* Tm colitis. (A) Schematic model of the effect of PPARγ on host cell metabolism. (B and C) Groups of C57BL/6 mice were given a single oral dose of streptomycin (Strep). The following day, rosiglitazone or vehicle (50 % DMSO in PBS) was administered intraperitoneally. Concentrations of butyrate (B) and lactate (C) in the cecal content were measured by GC/MS the day after. (D) Groups of streptomycin-pretreated C57BL/6 mice were infected with an equal mixture of the *S.* Tm wild-type strain and an Δ*lldD* mutant for 5 days. Rosiglitazone or vehicle control was administered intraperitoneally for the last 3 days of infection.
Bars represent geometric means ± standard error. *, $P < 0.05$; ns, not statistically significant. The number of animals per group (*N*) is indicated above each bar.

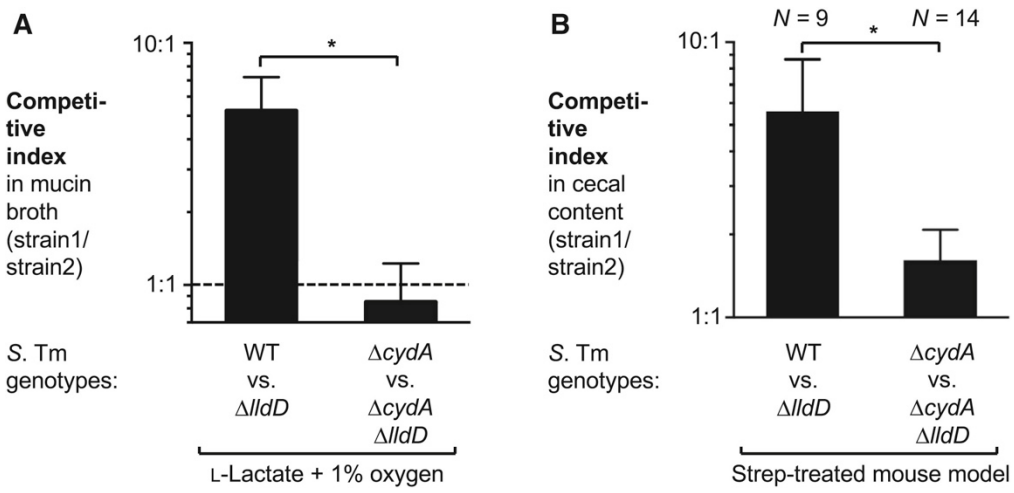

Figure 12. Impact of aerobic respiration on lactate utilization in *S.* Tm (A) Mucin broth supplemented with L-lactate was inoculated with an equal mixture of the *S.* Tm wild-type strain (WT) and an Δ*lldD* mutant or a Δ*cydA* and a Δ*cydA* Δ*lldD* mutant and incubated in a microaerobic chamber with 1 % oxygen. Fitness was measured by determining the competitive index. The experiment was performed independently at least four times. (B) Groups of C57BL/6 mice were pre-treated with streptomycin (Strep) and subsequently infected with the indicated *S.* Tm strains. Five days after infection, cecal content was collected to determine the competitive index.
Bars represent geometric means ± standard error. *, $P < 0.05$. The number of animals per group (*N*) is indicated above each bar.

vitro, lactate utilization occurs in fully aerated media and under microaerobic conditions (1 % oxygen) (**Fig. 2A and 12A**). Under anaerobic *in vitro* conditions, lactate dehydrogenases provide a growth advantage only in the presence of nitrate or tetrathionate (**Fig. 2A**). To test if anaerobic nitrate or tetrathionate respiration is required for lactate utilization, we created a mutant that lacked *moaA*. The *moaA* gene product catalyzes the first step of molybdopterin biosynthesis, an essential cofactor in the anaerobic tetrathionate and nitrate reductases. We then performed competition experiments in the streptomycin-treated C57BL/6 model (**Fig. 8D**). The fitness advantage conferred by lactate dehydrogenase genes was recapitulated in the absence of molybdopterin biosynthesis, i.e. in the *moaA* mutant background, suggesting that molybdenum cofactor-dependent anaerobic respiratory pathways are dispensable for lactate utilization. To test the idea that oxygen could be the terminal electron acceptor for lactate utilization, we created a mutant lacking cytochrome bd oxidase (CydAB) activity. CydAB is a terminal oxidase that is expressed under microaerobic conditions. Using the streptomycin-treated mouse model, we then determined the competitive fitness of the Δ*cydA* mutant against an isogenic strain that is unable to utilize L-lactate (Δ*cydA* Δ*lldD*). The fitness advantage conferred by LldD (**Fig. 7D and 12B**) was negated in the absence of CydAB activity (**Fig. 12A and B**), suggesting that oxygen is the preferred electron acceptor for oxidation of L-lactate during *S.* Tm infection.

Discussion

The nutritional mechanisms that support *S.* Tm outgrowth during inflammation, specifically the carbon sources that can be accessed by *S.* Tm in the inflamed intestine, remain poorly characterized. To address this question, we took an untargeted metabolic profiling approach

to identify metabolites that become more abundant during *S.* Tm induced inflammation. This experiment identified lactate as a potential nutrient that increased in abundance in the infected cecum. Disruption of the normal microbiota composition through antibiotic treatment or the onset of mucosal inflammation can lead to accumulation of microbial metabolites, for example because consumers of small metabolites are depleted [40, 130, 131]. We thus had initially hypothesized that most of the lactate in the gut lumen during *S.* Tm infection was of microbial origin. Contrary to this initial hypothesis, increased lactate levels were not primarily due to changes in gut microbial community composition or their metabolism. Instead, the increase in gut lactate levels was caused by a shift in the central metabolism of the host, most likely IEC. While the microbiota was not directly responsible for increased lactate levels in our animal models, it played a major functional role by providing butyrate, the preferred carbon source of IEC. Depletion of butyrate-producing Clostridia, either through streptomycin administration, DSS treatment, or during *S.* Tm induced dysbiosis, was sufficient to induce the production of host-derived lactate. The picture emerging from this study is that during *S.* Tm infection, butyrate and lactate link the metabolism of the gut microbiota, the host, and the pathogen at the mucosal interface (**Fig. 13**).

Recent work by Rivera-Chavez *et al.* demonstrates how a change in intestinal epithelial cell metabolism from β-oxidation to fermentation results in the leakage of oxygen from the tissue into the intestinal lumen, supporting growth of facultative anaerobic *S.* Tm [85]. In our study, we found that terminal oxidase activity (CydAB) was required for *S.* Tm to benefit from lactate utilization, indicating that oxygen was the terminal electron acceptor for lactate degradation *in vivo.* A respiratory metabolism allows *S.* Tm to be much more energetically competitive with the gut microbiota, which is largely comprised of strict anaerobes that solely rely on fermentative

processes. While oxygen is required for L-lactate oxidation *in vivo*, luminal oxygenation is not sufficient for *S*. Tm to utilize lactate from other sources (e.g. microbiota), since inhibition of host lactate production with oxamate abolished the fitness advantage conferred by lactate oxidation. Our findings suggest that lactate dehydrogenases and terminal oxidases form a disease-specific metabolic module. Thus, manipulation of epithelial metabolism through *S.* Tm-induced dysbiosis produces both the electron donor and an electron acceptor for lactate oxidation.

S. Tm also exploits a corresponding shift in host cell metabolism during systemic infection. During persistent *S.* Tm infection, anti-inflammatory M2 macrophages represent a major replicative niche for the pathogen, especially during later stages of infection [132-134]. M2 macrophages perform a fatty acid oxidation-based metabolism, which is controlled by the transcriptional regulator PPARγ. Reliance on β-oxidation for energy production liberates intracellular glucose for consumption by *S.* Tm, which supports replication inside of M2 macrophages [132]. In intestinal epithelial cells, reprogramming of central metabolism is controlled by PPARγ [84]. Consistent with this recent report, we found that activation of PPARγ during *S*. Tm infection decreased availability of lactate in the gut lumen.

The inverse relationship between elevated fecal L-lactate and decreased butyrate levels during episodes of inflammation has been known for almost fifty years. Elevated levels of fecal L-lactate are frequently found in patients with non-infectious chronic diarrhea, especially during severe ulcerative colitis and in a subset of Crohn's disease patients with colon involvement. Interestingly, in Crohn's disease patients in which disease activity is restricted to the ileum, no

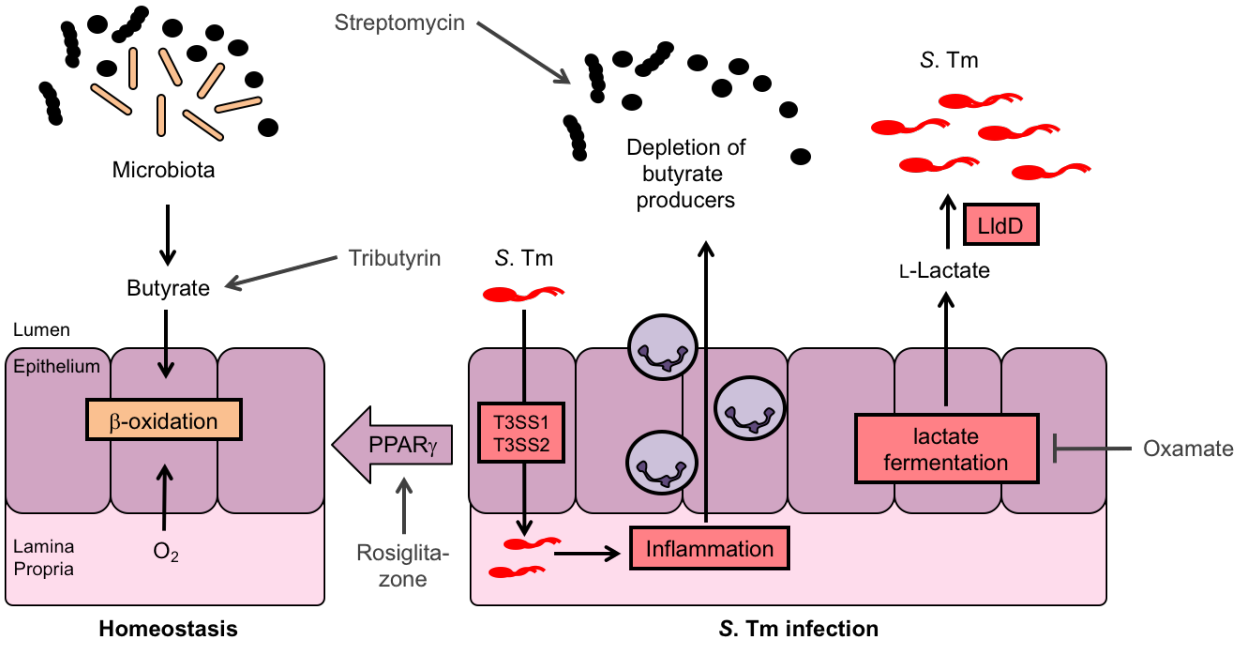

Figure 13. Central model of lactate utilization during *S.* Tm infection.
See text for details.

such trend is observed [135-140]. In many of these patient samples a decrease in butyrate concentrations was noted [139, 140]. This metabolic switch has also been shown in germ-free mice [89] and in *ex vivo*-cultured colonocytes from DSS-treated mice [90], a chemical model of experimental colitis. The inverse correlation between elevated luminal lactate levels and severe colonic inflammation is consistent with our results showing that inflammation-associated dysbiosis induces a metabolic reprogramming (e.g. lactate production) and suggests that this mechanism could also be occurring in patients with chronic non-infectious diarrhea. In patients with inflammatory bowel disease, it was speculated that disease-associated increases in certain metabolites were due to malabsorption or altered microbiota metabolism; in contrast, our studies in animal models of *S.* Tm colitis raise the possibility that increases in lactate, and possibly other metabolites, are in fact generated by the host metabolism during disease. Overall, by combining bacterial genetics with targeted and untargeted metabolomics, our work revealed a metabolic connection between the gut microbiota, the host, and the enteric pathogen *S.* Tm and expands our understanding of how microbiota dysbiosis affects tissue homeostasis.

CHAPTER FOUR[‡]

HOST-DERIVED METABOLITES MODULATE TRANSCRIPTION OF *SALMONELLA* GENES INVOLVED IN L-LACTATE UTILIZATION DURING GUT COLONIZATION

Introduction

Salmonella enterica serovar Typhimurium (*S.* Tm) is an enteric pathogen that causes subacute, self-limiting gastroenteritis in the immunocompetent host [141]. *S.* Tm virulence is primarily mediated by two distinct type three secretion systems. The type three secretion system encoded by the *Salmonella* Pathogenicity Island 1[51], enables *S.* Tm to invade cultured epithelial cells and the mucosa of infected animals [48, 49]. A second type three secretion system encoded by *Salmonella* Pathogenicity Island 2 enables intracellular replication inside of macrophages [54, 142] and is required for full virulence in murine and bovine models of infection [56, 57, 119]. Both type three secretion systems are required for efficient induction of host inflammatory responses. Development of inflammation drives changes in the microbiota composition (dysbiosis), including an expansion of the pathogen population [5, 44]. Increased colonization of the intestinal tract by *Salmonella* enhances fecal shedding and host transmission through the fecal-oral route [62, 85].

The onset of intestinal inflammation changes the metabolic environment of the gut. Recent studies have shown that inflammation leads to the production of the terminal electron acceptors nitrate [70, 71] and tetrathionate [63], as well as leakage of oxygen from host tissue into the gut lumen [85]. The availability of electron acceptors supports outgrowth of *S.* Tm, which is capable

of anaerobic and aerobic respiration. In contrast, the microbiota mostly consists of obligate anaerobes that cannot use these electron acceptors. Exogenous electron acceptors allow *S.* Tm to run a complete, oxidative TCA cycle [73]. This in turn facilitates the catabolism of poorly-fermentable carbon sources such as ethanolamine and succinate [73, 77]. Recently, we have shown that host-derived L-lactate serves as a nutrient source during *S.* Tm expansion in the inflamed gut [143].

Under homeostatic conditions, non-digestible polysaccharides are fermented into the short chain fatty acid butyrate by members of the class Clostridia. Butyrate is oxidized as the primary fuel source for intestinal epithelial cells, a process which consumes oxygen and keeps the gut lumen anaerobic [88, 91]. Butyrate is also a cue for the transcription factor PPARγ which controls central metabolism of these cells and drives their metabolism towards oxidative metabolism [84, 85, 143]. During *S.* Tm infection, inflammation results in a depletion of butyrate-producing Clostridia from the gut as part of gut microbiota dysbiosis [5, 85]. Butyrate deprivation alters host cell metabolism, leading to leakage of oxygen and L-lactate into the gut lumen [85, 143]. The respiratory L-lactate dehydrogenase LldD facilitates degradation of host-derived L-lactate in a stereospecific manner [143]. The terminal electron acceptor for L-lactate utilization is host-derived oxygen, as lactate oxidation is entirely dependent on the cytochrome bd oxidase CydAB [143]. Since L-lactate and oxygen become available in the gut through the same mechanism, i.e. inflammation-associated changes in host metabolism, lactate oxidation by the LldD-CydAB electron transport chain constitutes a disease-specific metabolic module that contributes to *S.* Tm outgrowth through manipulation of host metabolism [143].

Here, we investigated how L-lactate utilization is regulated during *S.* Tm infection in the murine gut. LldD is encoded in an operon that contains other genes with putative functions in L-lactate utilization. The first gene in the operon, *lldP,* encodes a putative L-lactate permease. The second gene, *lldR,* encodes a putative regulatory protein. The gene products of *lldPRD* in *S.* Tm 14028 exhibit considerable sequence identity at the amino acid level to the orthologues in *E. coli* K-12 MG1665 (94 %, 86 %, and 94 % for LldP, LldR, and LldD, respectively). While some work has been done to understand the regulation of the homologous operon in *E. coli* under *in vitro* conditions [144-146], the regulation of the L-lactate utilization operon in *S.* Tm, especially *in vivo,* remains largely uncharacterized. Our results from *in vitro* experiments and murine models of colitis indicate that host-derived oxygen and L-lactate induced transcription of L-lactate utilization genes, suggesting that sensing of these host derived metabolites governs transcriptional control of the *lldPRD* operon.

Results

Oxygen, nitrate, and L-lactate induce lactate utilization genes.

To investigate expression of the *S.* Tm *lldPRD* operon, we first analyzed transcription of individual genes in response to key host-derived metabolites *in vitro*. Mucin broth containing L-lactate, or the electron acceptor nitrate was inoculated with the *S.* Tm wild-type strain (IR715). After 3 hours of growth under microaerobic or anaerobic conditions, we extracted bacterial RNA and evaluated the transcription of *lldP*, *lldR,* and *lldD* by RT-qPCR (**Fig. 14)**. In the absence of exogenous electron acceptors, addition of L-lactate alone was insufficient to induce transcription of *lldP*, *lldR,* and *lldD*. In contrast, addition of the electron acceptors oxygen and nitrate was

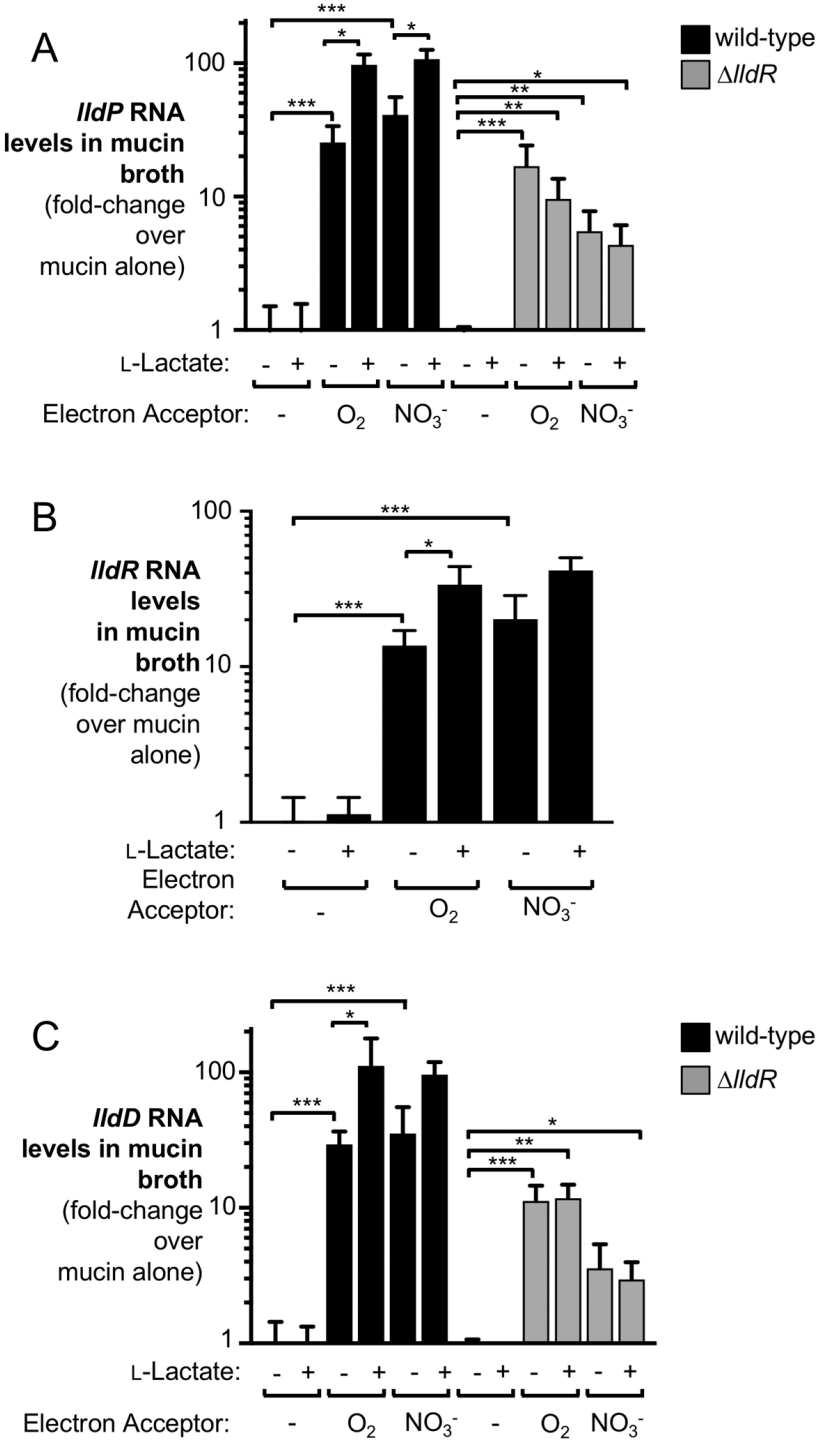
A
wild-type
ΔlldR
lldP RNA levels in mucin broth (fold-change over mucin alone)
100
10
1
***
*
*
***
*
**
**
***
L-Lactate: - + - + - + - + - + - +
Electron Acceptor: - O2 NO3- - O2 NO3-
B
lldR RNA levels in mucin broth (fold-change over mucin alone)
100
10
1
***
*
***
L-Lactate: - + - + - +
Electron Acceptor: - O2 NO3-
C
wild-type
ΔlldR
lldD RNA levels in mucin broth (fold-change over mucin alone)
100
10
1
***
*
***
*
**
***
L-Lactate: - + - + - + - + - + - +
Electron Acceptor: - O2 NO3- - O2 NO3-

Figure 14. Analysis of *lldPRD* transcription in response to varying stimuli *in vitro*. The *S.* Tm wild-type strain (black bars) and an Δ*lldR* mutant strain (gray bars) were grown in mucin broth. Nitrate (NO_3^-) and L-lactate were added as indicated at a concentration of 40 mM and 20 mM, respectively. Cultures were grown for 3 hours anaerobically (no electron acceptor and nitrate conditions) or in the presence of 1 % oxygen. RNA was extracted, and *lldP* (A), *lldR* (B), and *lldD* (C) mRNA levels were assessed by RT-qPCR. Transcription was normalized to the housekeeping gene *gmk.* All experiments were conducted with at least 3 biological replicates. To determine differences between groups, a two-tailed, unpaired Student's *t*-test on ln-transformed data was used. Bars indicate the geometric mean ± standard error. *, $P < 0.05$; **, $P < 0.01$; ***, $P < 0.001$.

sufficient to significantly upregulate expression by more than 10-fold. Exposure to L-lactate in the presence of oxygen further increased transcription beyond that of the electron acceptor alone, up to about 100-fold over uninduced conditions (**Fig. 14**). In addition to LldD, *S.* Tm expresses a second respiratory lactate dehydrogenase termed Dld [147]. Unlike LldD, Dld is specific for D-lactate [143]. Under the conditions tested, *dld* was not inducible by oxygen, nitrate, or L-lactate (**Fig. 15**).

Previous reports suggest that under inflammatory conditions, the gut environment becomes microaerobic [84, 85]. We thus analyzed how varying levels of oxygenation affected *lldD* transcription with no L-lactate and 20 mM L-lactate in Lysogeny Broth (LB broth) **(Fig. 16A)**. For this experiment, we created a transcriptional fusion of the *lldD* gene and *lacZ* (CG254), leaving the coding sequence of *lldD* intact to avoid any changes in expression due to the absence of LldD. We exposed cultures of *S.* Tm CG254 to 0 % (anaerobic), 1 % (microaerobic), 8 % (tissue oxygenation), and 21 % (atmospheric) oxygen and assessed *lldD* transcription in a standard β-galactosidase assay. Increasing levels of oxygen correlated with increased *lldD* expression, with 21 % oxygen inducing the strongest response. Addition of 20 mM L-lactate further increased expression in the presence of oxygen.

The two-component system ArcAB *represses lldD expression in the absence of oxygen.*

ArcB is a sensor kinase that detects the redox state of the quinone pool and phosphorylates the response regulator ArcA. Phosphorylated ArcA then regulates the transcription of a wide variety of genes [148]. In *E. coli*, the ArcAB two-component system represses lactate utilization genes [75, 145, 146, 149]. In *S.* Tm, *lldP* and *lldR* were also found to be repressed under anaerobic conditions in a broad survey of the ArcA regulatory program [148]. We thus hypothesized that

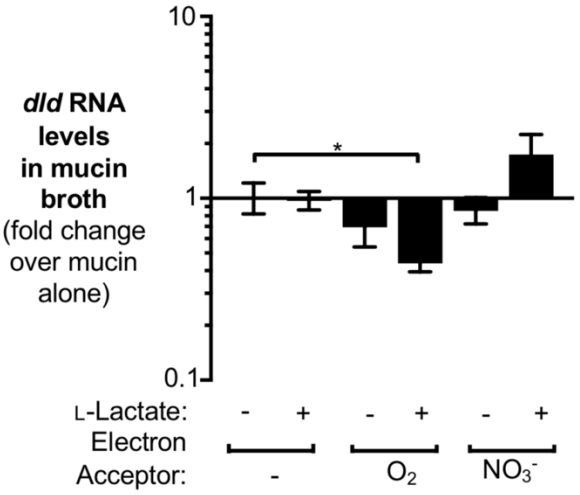

Figure 15. Effect of L-lactate and electron acceptors on *dld* transcription. The *S.* Tm wild-type strain was grown in mucin broth. Nitrate (NO_3^-) and L-lactate were added as indicated at a concentration of 40 mM and 20 mM, respectively. Cultures were grown for 3 hours anaerobically (no electron acceptor and nitrate conditions) or in the presence of 1 % oxygen. RNA was extracted and *dld* mRNA levels determined by RT-qPCR. To determine differences between groups, a two-tailed, unpaired Student's *t*-test was applied to the ln-transformed data. Transcription was normalized to the housekeeping 16S rDNA gene. ∗, $P < 0.05$.

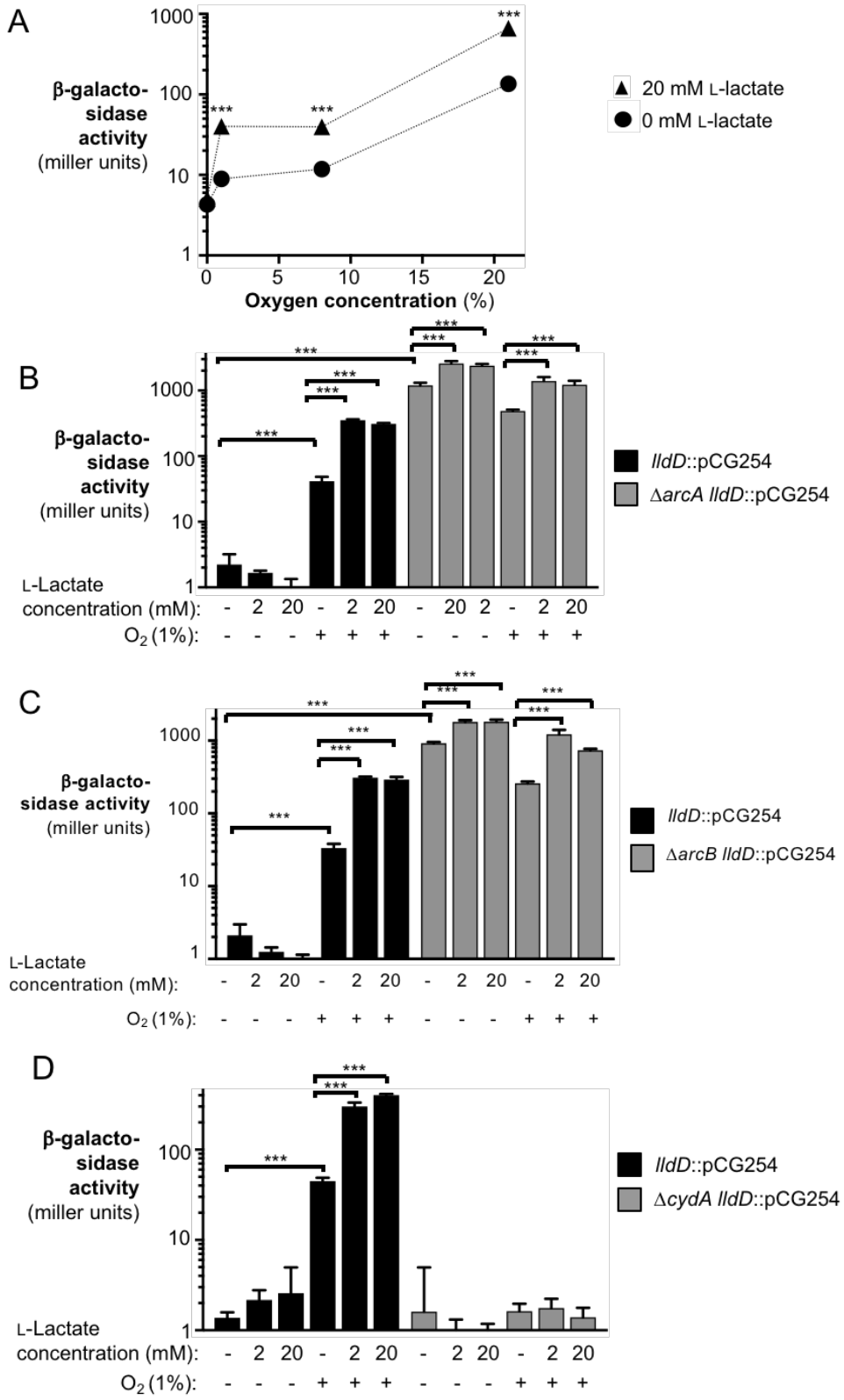
A
β-galacto-sidase activity (miller units)
1000
100
10
1
***
***
***
0
5
10
15
20
Oxygen concentration (%)
20 mM L-lactate
0 mM L-lactate
B
β-galacto-sidase activity (miller units)
lldD::pCG254
ΔarcA lldD::pCG254
L-Lactate concentration (mM): - 2 20 - 2 20 - 20 2 - 2 20
O2 (1%): - - - + + + - - - + + +
C
β-galacto-sidase activity (miller units)
lldD::pCG254
ΔarcB lldD::pCG254
L-Lactate concentration (mM): - 2 20 - 2 20 - 2 20 - 2 20
O2 (1%): - - - + + + - - - + + +
D
β-galacto-sidase activity (miller units)
lldD::pCG254
ΔcydA lldD::pCG254
L-Lactate concentration (mM): - 2 20 - 2 20 - 2 20 - 2 20
O2 (1%): - - - + + + - - - + + +

Figure 16. Influence of oxygen levels, ArcAB regulation, and CydAB-mediated respiration on *lldD* transcription. (A) The *lldD-lacZ* transcriptional reporter strain CG254 (*lldD*::pCG254) was grown in LB broth in the presence of varying concentrations of oxygen. Media was supplemented with 20 mM L-lactate (black triangles) or mock-treated (black circles). After 135 min, β-galactosidase activity was quantified. Note: The size of the error bar is smaller than the symbol representing the geometric mean. (B-D) The *S*. Tm strains CG254 (*lldD*::pCG254), CG267 (Δ*arcA lldD*::pCG254), CG268 (Δ*arcB lldD*::pCG254) and CG270 (Δ*cydA lldD*::pCG254) were grown anaerobically (no oxygen conditions) or with 1 % oxygen in LB broth supplemented with L-lactate as indicated. After 5 h, β-galactosidase activity was determined. (B) β-galactosidase activity in the wild-type background (black bars) and an Δ*arcA* mutant background (gray bars). (C) β-galactosidase activity in the wild-type background (black bars) and an Δ*arcB* mutant background (gray bars). (D) β-galactosidase activity in the wild-type background (black bars) and a Δ*cydA* mutant background (gray bars). All experiments were conducted with at least 3 biological replicates. To determine differences between groups, a two-tailed, unpaired Student's *t*-test was applied to the ln-transformed data. Bars indicate the geometric mean ± standard error. ***, $P < 0.001$.

ArcAB would also be involved in the regulation of *lldD*. To test this idea, we compared *lldD* expression in the wild-type background (CG254) and strains which lack ArcA (CG267) or ArcB (CG268). LB broth supplemented with and without L-lactate was inoculated with the indicated strains and incubated anaerobically or microaerobically. Since the Δ*arcA* and Δ*arcB* mutants displayed a slight growth defect under aerobic conditions, the cultures were incubated for 5 h. *lldD* expression was then evaluated by β-galactosidase assay (**Fig. 16B and C**). Under anaerobic conditions, the wild-type strain had minimal *lldD* expression, even in the presence of L-lactate, while transcription was induced in the oxygenated condition as well as in the presence of oxygen and L-lactate. In contrast, the transcription of *lldD* in the Δ*arcA* and Δ*arcB* mutants was de-repressed, and induction by oxygen was lost entirely (**Fig. 16B and C**). Of note, these strains still exhibited significant induction by the addition of L-lactate, both in the presence and absence of oxygen. Taken together, these experiments suggest that ArcAB is responsible for transcriptional repression of *S*. Tm *lldD* under anaerobic conditions.

The terminal oxidase CydAB is necessary for lldD expression under microaerobic conditions.

In our previous study, we found that L-lactate utilization was dependent on the activity of the terminal oxidase CydAB *in vivo* [143]. ArcB senses electron flux via the redox state of quinone pool [150], and thus we hypothesized that aerobic respiration would contribute to de-repression of *lldD*. To test this, we performed β-galactosidase assays as described above using a mutant strain which lacks the terminal oxidase CydAB (CG270) **(Fig. 16D)**. While the wild-type strain had increased *lldD* transcription with the addition of oxygen and oxygen with L-lactate, the Δ*cydA* mutant exhibited no increase in *lldD* transcription in the presence of oxygen. Our data suggests

that under microaerobic conditions, the electron flux mediated by CydAB is sensed by ArcAB, which in turn enables *lldD* expression.

Induction of lldD transcription occurs at physiological levels of lactate.

In our previous work, we had shown that lactate levels in the murine gut vary considerably [143]. The experiments described thus far have used an initial concentration of 20 mM L-lactate. To test if lactate utilization genes were still induced *in vitro* at physiologically relevant concentrations of L-lactate, we performed a dose-response experiment with 1 % oxygen and varying concentrations of L-lactate (**Fig. 17A**). There was a significant, dose-dependent increase in the level of *lldD* transcription over the oxygen-only condition (dashed line) for a large number of L-lactate concentrations, ranging from 0.3125 mM to 20 mM L-lactate.

Next, we analyzed lactate concentrations in the murine gut lumen during *S.* Tm infection. Streptomycin-pretreated C57BL/6 mice were intragastrically inoculated with the *S.* Tm Δ*lldD* mutant and lactate concentrations in the cecal content quantified by GC/MS. Consistent with our previous results [143], the lactate concentration in mock-treated animals (no streptomycin/*S.* Tm treatment) was approximately 0.6 mM (**Fig. 17B**). Lactate levels in the Salmonella-infected animals rose to about 11.7 mM (**Fig. 17B**). As such, the responsiveness of *lldD* transcription to lactate *in vitro* (**Fig. 17A**) encompasses the relevant *in vivo* concentrations of lactate (**Fig. 17B**).

Host cells produce the L-enantiomer of lactate. To determine the potential contribution of D-lactate to induction of *lldD* expression, we repeated this experiment with various concentrations of the D-enantiomer **(Fig. 17A)**. In contrast to our previous results with L-lactate, exposure to D-lactate did not increase *lldD* expression significantly, with the exception of 20 mM, the highest concentration tested. The commercially available D-lactate compounds is 98 % enantiopure and

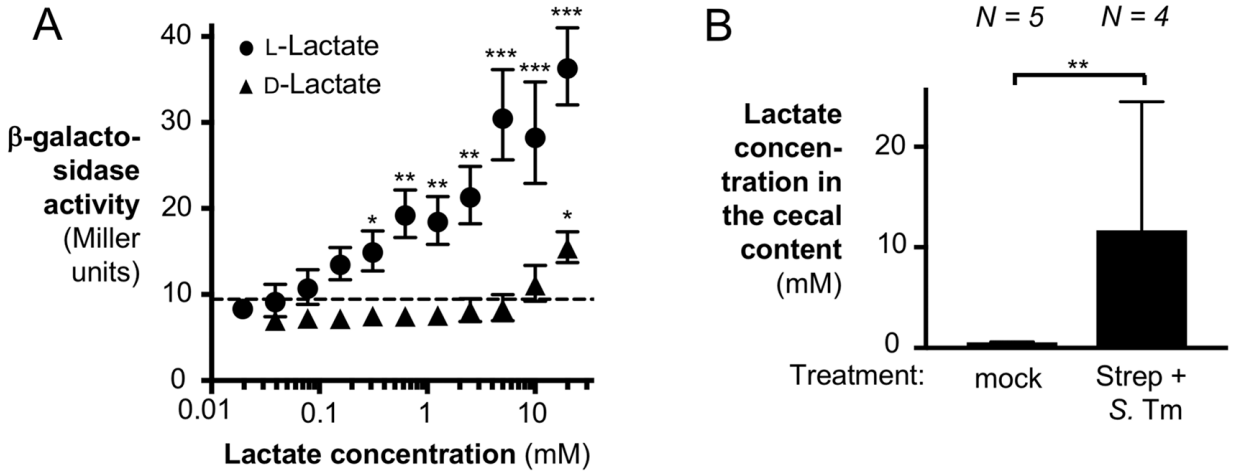

Figure 17. Analysis of *lldPRD* transcription in response to varying concentrations of L-lactate and D-lactate. (A) The *lldD-lacZ* transcriptional reporter strain CG254 (*lldD*::pCG254) was grown in LB broth for 135 min in the presence of 1 % oxygen with varying concentrations of L-lactate (black circles) or D-lactate (black triangles). *lldD* transcription was assessed via β-galactosidase activity. The dashed line indicates β-galactosidase activity in the absence of lactate. All experiments were conducted with at least 3 biological replicates. Note: In some instances, the size of the error bar is smaller than the symbol representing the geometric mean. (B) C57BL/6 mice were treated intragastrically with streptomycin followed by infection with the *S.* Tm Δ*lldD* mutant (CG6) one day later. Mock-treated mice received water followed by LB broth one day later. Cecal content was collected 5 days after infection for lactate quantification by GC-MS. To determine differences between groups, a two-tailed, unpaired Student's *t*-test on ln-transformed data was used. Bars and symbols indicate the geometric mean ± standard error. *, $P < 0.05$; **, $P < 0.01$; ***, $P < 0.001$.

thus the 20 mM D-lactate condition likely contains 0.4 mM of L-lactate, which would be sufficient to induce expression. As such, the observed increase in *lldD* expression with 20 mM D-lactate was likely a reflection of this impurity (**Fig. 17A**).

The transcriptional regulator LldR enables the response to L-lactate in vitro.

The L-lactate utilization operon includes the putative transcriptional regulator LldR. In *E. coli,* LldR has been shown to increase transcription of L-lactate utilization genes [144, 145]. Given that the L-lactate utilization genes in *S.* Tm are also inducible by L-lactate in the presence of electron acceptors, we hypothesized that LldR could also be responsible for the increase in *lldPD* expression in the presence of lactate. To test this, we evaluated transcription of *lldP* and *lldD* in a Δ*lldR* mutant (**Fig. 14A and C, gray bars**). Unlike the wild-type strain, the Δ*lldR* mutant was unable to increase transcription of *lldP* and *lldD* when L-lactate was added to the media, even in the presence of oxygen and nitrate. This data strongly supports the idea that the increase in *lldPD* expression in the presence of L-lactate is mediated by LldR.

LldR *mediates lldPD transcription in the murine gut.*

We next sought to examine transcription of *lldPRD in vivo* in mouse model of *Salmonella* infection. One of the pathological features of non-typhoidal salmonellosis is the development of a neutrophilic infiltrate into the intestinal mucosa [151, 152]. Transmigrated neutrophils and other leukocytes are frequently detected in the feces of patients [60, 153]. The streptomycin-treated C57BL/6 model has been used extensively by numerous groups as it allows for reproducible colonization of C57BL/6 mice and neutrophils infiltrate the intestinal mucosa upon oral *S.* Tm infection [154]. Perturbation of the microbiota by streptomycin prior to *S.* Tm infection ensures depletion of Clostridia and leads to lactate production by the host **(Fig. 17B)** and leakage of oxygen

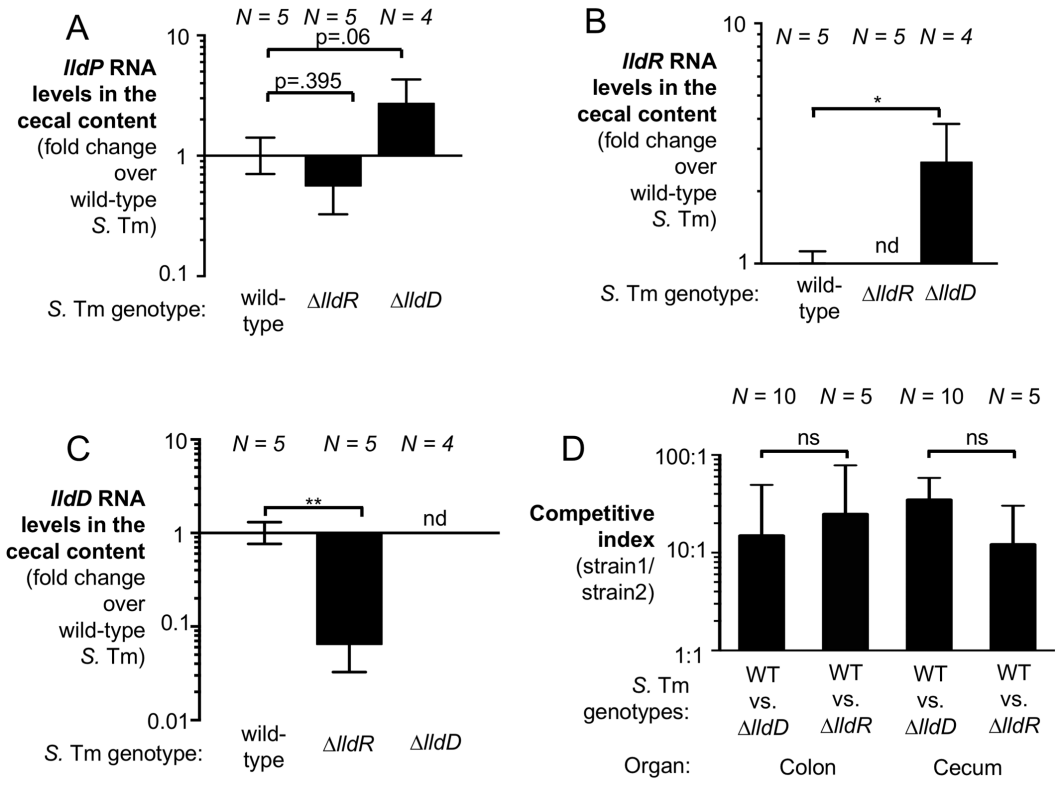

Figure 18. Effect of LldR on *S.* Tm *lldPRD* transcription and fitness *in vivo.* (A-C) Groups of wild-type C57BL/6 mice were treated with streptomycin by oral gavage. One day later, animals were intragastrically infected with the *S.* Tm wild-type strain (IR715), an Δ*lldD* mutant (CG6), or an Δ*lldR* mutant (CG200). Cecal content was collected for RNA extraction 5 days after infection. *S.* Tm RNA levels were assessed for *lldP* (A), *lldR* (B), and *lldD* (C). Transcription was normalized to *S.* Tm 16S rRNA. (D) Swiss Webster mice were inoculated with a 1:1 ratio of *S.* Tm wild-type strain (AJB715) and an Δ*lldD* mutant (CG6), or the wild-type strain (AJB715) and an Δ*lldR* mutant (CG200). Colonic and cecal content were collected 8 days after infection. Wild-type and mutant populations were enumerated on selective agar, and the competitive index was calculated. The number of mice per group (*N*) is indicated for each bar. To determine differences between groups, a two-tailed, unpaired Student's *t*-test was applied to the ln-transformed data. Bars are the geometric mean ± standard error. *, $P < 0.05$; **, $P < 0.01$, nd, not detected, ns, not significant.

into the gut lumen [84, 85, 143]. Therefore, we initially chose to assess transcription of genes required for lactate utilization in the streptomycin-treated C57BL/6 model. To assess how *lldP* transcription occurs in the murine cecum, we treated wild-type C57BL/6 mice with streptomycin sulfate by oral gavage. One day later, we intragastrically infected mice with *S.* Tm wild-type (IR715), a Δ*lldR* mutant (CG200), or a Δ*lldD* mutant (CG6). Five days after infection, the mice were sacrificed and cecal content was collected for bacterial RNA extraction and RT-qPCR (**Fig. 18 A-C**). We were initially concerned that members of the gut microbiota express genes similar to *S.* Tm *lldPRD*, thus possibly interfering with our RT-qPCR assay. However, no *lldR* or *lldD* mRNA was detected in mice infected with the *S.* Tm Δ*lldR* or the Δ*lldD* mutant (**Fig. 18A-C**), respectively, demonstrating that the RT-qPCR assay is specific for intended *S.* Tm mRNA targets. Similarly, no *lldP* transcription was detected in mice infected with a Δ*lldP* mutant (**Fig. 19)**. mRNA for all three genes of the *lldPRD* operon was detected during *S.* Tm colonization of the cecal lumen. Consistent with our *in vitro* data showing that LldR is required for full expression of L-lactate utilization genes in the presence of L-lactate, expression of *lldD* was decreased in the Δ*lldR* mutant ($P < 0.01$). A similar trend was observed for *lldP*, however, this decrease was not statistically significant. Intriguingly, *lldP* and *lldR* expression increased in the Δ*lldD* mutant (**Fig. 18A and B**). We speculate that this was due to an accumulation of lactate within the cell as the Δ*lldD* mutant cannot degrade lactate. To ensure that differences in *lldPRD* expression were not due to attenuation of the mutant strains, we analyzed inflammatory cytokines in cecal tissue, which revealed significant inflammation in the streptomycin-treated, *S.* Tm infected-cecum. Inflammation levels were similar across all groups, with the exception of the Δ*lldD* mutant, which exhibited somewhat lower *Nos2* and *Cxcl1* expression (**Fig. 20**).

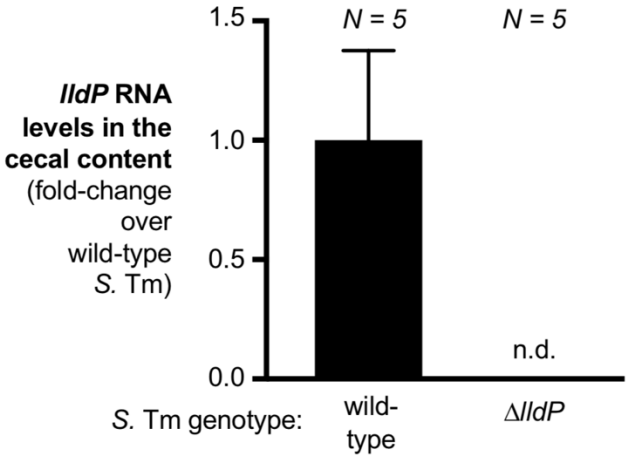

Figure 19. Specificity of *lldP* qPCR primers *in vivo.* Wild-type C57BL/6 mice were treated with streptomycin by oral gavage. One day later, animals were intragastrically infected with the *S.* Tm wild-type strain (IR715) and an Δ*lldP* mutant (CG226). Cecal content was collected for RNA extraction 5 days after infection. *S.* Tm RNA levels were assessed for *lldP*. Transcription was normalized to the *S.* Tm 16S rDNA gene. The number of mice per group (*N*) is indicated for each bar. Bars are the geometric mean ± standard error. n.d., not detected.

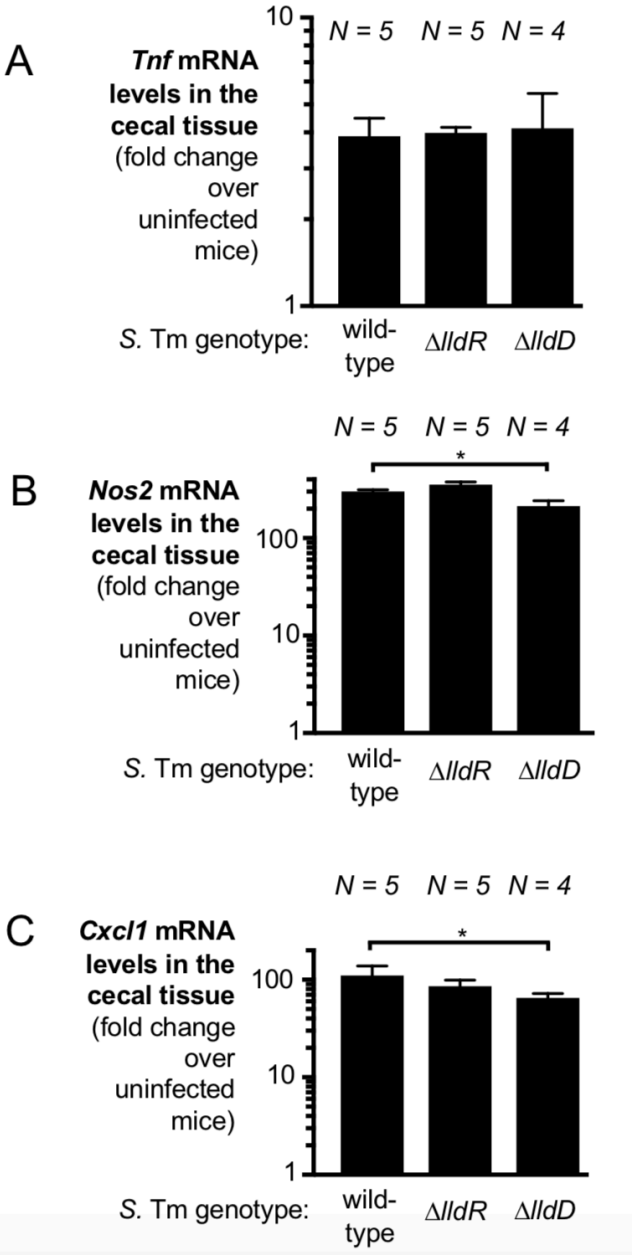

Figure 20. mRNA levels of inflammatory cytokines during *S.* Tm infection. Groups of C57BL/6 mice were treated with intragastric streptomycin. One day later, animals were infected with the *S.* Tm wild-type strain (IR715), an Δ*lldD* mutant (CG6), or an Δ*lldR* mutant (CG200). 5 days after infection, cecal tissue was flash frozen and RNA was extracted. RNA levels were assessed for *Tnf* (A), *Nos2* (B), and *Cxcl1* (C). Transcription was normalized to the murine *Gapdh* housekeeping gene. To determine differences between groups, a two-tailed, unpaired Student's *t*-test was applied to the ln-transformed data. The number of mice per group (*N*) is indicated for each bar. Bars are the geometric mean ± standard error. *, $P < 0.05$.

LldR *is required for optimal fitness in the intestinal tract.*

We next wanted to explore the contribution of LldR to fitness of *S.* Tm *in vivo*. To do this, we assessed the role of LldR in Swiss Webster mice. Swiss Webster mice do not require antibiotic pre-treatment to develop neutrophilic inflammation, and thus the perturbation of the microbiota that occurs is dependent on *S.* Tm virulence factors and not direct killing of the microbiota by antibiotics [143]. To determine if LldR provides a fitness advantage in the murine gut, we performed competitive colonization experiments (**Fig. 18D**). Groups of Swiss Webster mice were intragastrically inoculated with an equal ratio of the *S*. Tm wild-type (AJB715) and a Δ*lldD* mutant (CG6) or the *S*. Tm wild-type (AJB715) and a Δ*lldR* mutant (CG200) and determined the abundance of these strains in the cecal and colonic content 8 days after infection. As we have shown before, the Δ*lldD* mutant was recovered in lower numbers than the wild-type strains. Similarly, LldR also provided a significant fitness advantage in both the colonic and cecal content. The competitive fitness for the Δ*lldD* mutant and the Δ*lldR* mutant were not significantly different from one another. We also attempted to analyze transcription of *lldD* in this mouse model. *S.* Tm gut colonization is considerably lower in Swiss Webster mice compared to streptomycin-treated C57BL/6 mice, which prevented us from reproducibly quantifying *lldD* transcription in the Swiss Webster model. Collectively, these data suggest that LldR regulates L-lactate utilization on the transcriptional level *in vivo*, and that LldR-mediated regulation contributes to optimal gut colonization.

Discussion

While the majority of *Salmonella enterica* serovars are associated with gastroenteritis, a subset of serovars causes disseminated disease such as typhoid and paratyphoid fever. The genomes of extraintestinal serovars typically exhibit an increased accumulation of pseudogenes compared to intestinal serovars [155, 156], which may reflect adaptations to different niches within the host [157]. We have shown previously that *S.* Tm exploits changes in host metabolism, such as the release of oxygen and L-lactate into the gut lumen (**Fig. 21**) [85, 143]. Our data suggest that the inducibility of the *lldPRD* operon by L-lactate may be a specific adaptation to changes in mammalian L-lactate production during infection with intestinal serovar Typhimurium. Consistent with this idea, *lldP* and *lldR* were identified as pseudogenes in the extraintestinal serovars *Salmonella enterica* serovar Gallinarum and *Salmonella enterica* serovar Choleraesuis, respectively [155, 158, 159]. Furthermore, during experimental *S.* Tm infection of mice, LldD contributes gut colonization but is dispensable for fitness at systemic sites [143].

Our results indicate that the regulation the *lldPRD* operon is stereospecific to L-lactate. Mammalian cells produce L-lactate [160], whereas members of the microbiota can produce both isomers [125]. Little is known about changes in short chain fatty acids and lactate during human Salmonellosis. Of note, patients with non-infectious diarrhea exhibit increased L-lactate levels in the feces [137]. Increases in fecal L-lactate in ulcerative colitis are due to augmented excretion by the mucosa [136]. In patients with ulcerative colitis suffering from pancolitis and active Crohn's disease, the average fecal L-lactate concentration exceeds 10 mM, compared to less than 4 mM in quiescent patients [137].

Here, we report that induction of the *S.* Tm L-lactate dehydrogenase LldD *in vitro* occurred at L-lactate concentrations that span the experimentally determined *in vivo* lactate concentrations.

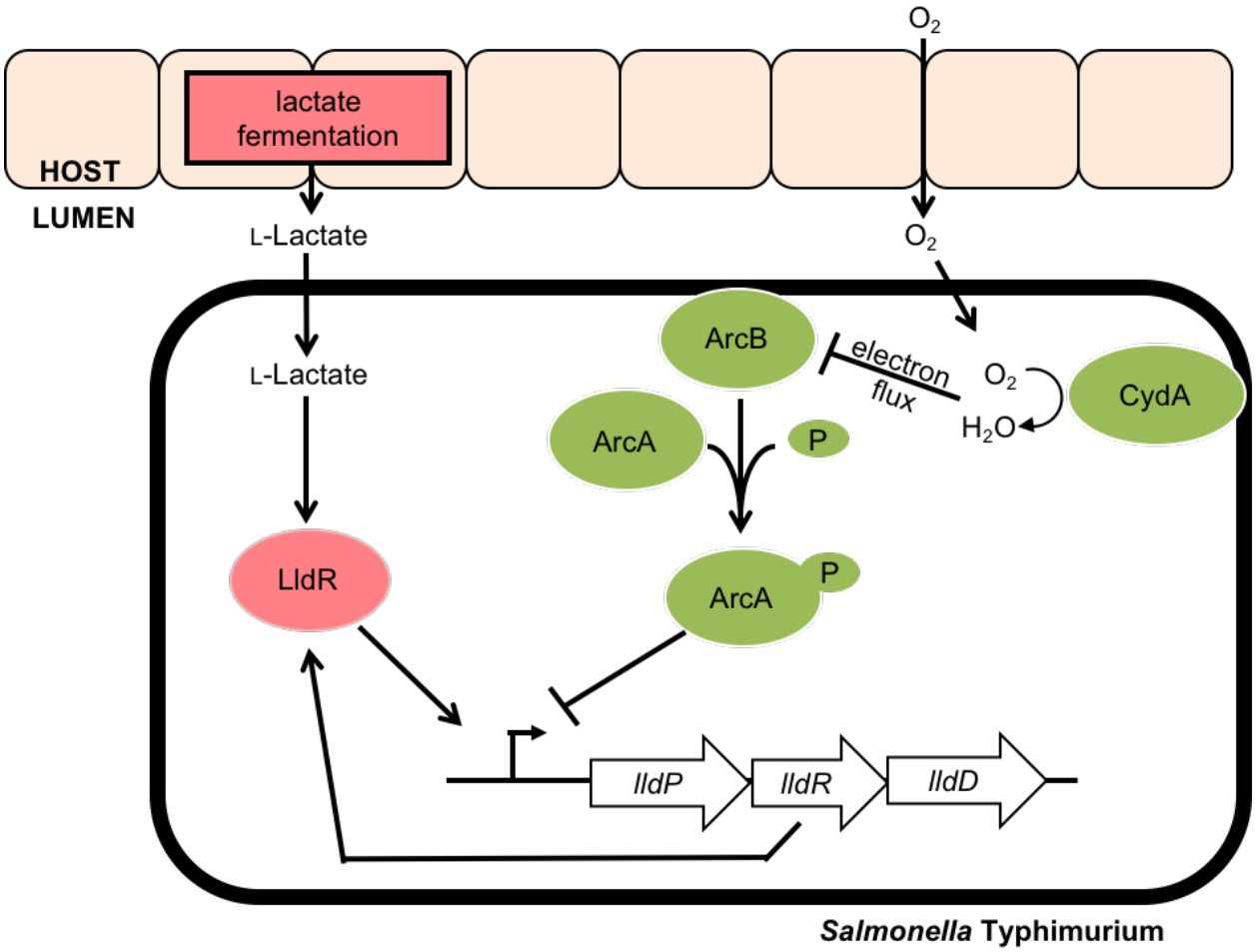

Figure 21. Central model of regulation of lactate utilization during *S.* Tm infection. See text for details.

In contrast, exposure to D-lactate had little effect on *lldD* transcription. Consistent with the idea that L-lactate utilization is an adaption to the environment of the inflamed gut, the D-lactate dehydrogenase Dld was not inducible by oxygen, nitrate, or L-lactate. Furthermore, Dld activity does not provide a fitness advantage in the murine gut [143].

Unlike the cytoplasmic lactate dehydrogenase LdhA used during fermentation, LldD is membrane-bound and donates electrons directly to the quinone pool [161]. In the murine gut, oxygen likely is the terminal electron acceptor for *S*. Tm L-lactate utilization [143]. Our data showed that oxygen availability and aerobic respiration modulated L-lactate utilization genes *in vitro*. Signaling through the respiration-responsive regulatory system ArcAB was required for repression under anaerobic conditions, when electron acceptors are not available for coupling with L-lactate conversion to pyruvate. Similarly, activity of the terminal oxidase CydAB was essential for expression of L-lactate utilization genes under microaerobic conditions. This shows a dual function for CydAB during lactate-oxidation, which serves as the terminal electron acceptor and modulates the electron flux that relieves ArcAB-mediated repression of L-lactate utilization genes. Taken together, our study demonstrates that sensing of host-derived metabolites provides an important cue for a dynamic transcriptional program that benefits *S.* Tm in the murine gut through lactate-oxidation and thus ensures successful *S.* Tm outgrowth.

CHAPTER FIVE

LACTATE PRODUCTION BY THE HOST DURING NON-INFECTIOUS COLITIS AND LACTATE UTILIZATION BY ENTEROBACTERIACEAE

Introduction

The microbial ecology of the distal gut changes dramatically during inflammatory settings. The dysbiosis that occurs in a wide variety of inflammatory disorders is characterized by the outgrowth of the facultative anaerobic Proteobacteria, in particular the family Enterobacteriaceae (reviewed in [162]). However, the mechanisms that enable the expansion of Enterobacteriaceae remain incompletely described.

Recent work by our lab demonstrated that during the expansion of Enterobacteriaceae in animal models of colitis, aerobic respiration is one of the metabolic signatures of the change in the composition of the microbiota [40]. The oxygen consumed by Enterobacteriaceae during colitis arises due to the changes in host metabolism in the absence of butyrate [84]. Our previous study of lactate utilization during *S.* Tm infection showed that depletion of Clostridia through streptomycin administration was sufficient to produce lactate (**Fig. 6; Fig 11B and C**) and to promote *S.* Tm fitness through lactate utilization in a post-antibiotic expansion model of salmonellosis, even in the absence of *S.* Tm virulence factors (**Fig. 7**). Similarly, pre-treatment of mice with DSS also significantly increased the fitness advantage of lactate utilization in the absence of *S.* Tm-induced inflammation (**Fig. 7D**). In contrast, treatment with neomycin, an antibiotic that does not kill Clostridia, did not promote *S.* Tm fitness through lactate utilization (**Fig. 7D**) [143]. We therefore hypothesized that changes in host cell metabolism during

inflammation-induced dysbiosis could give rise to lactate that could then be utilized by commensal Enterobacteriaceae.

In this study, we investigated the role of host lactate production during the DSS colitis model of intestinal inflammation. We found that DSS treatment resulted in decreased butyrate, consistent with previous reports [84], and increased lactate levels. Through metagenomic analysis, we identified that genes predicted to encode homologues of *lldD* were enriched in the microbiota of mice treated with DSS compared to mock-treated mice. We also identified putative L-lactate dehydrogenases in the adherent-invasive *E. coli* strain NRG 857C and began to characterize their function *in vitro* and *in vivo*. Overall, our results indicated that lactate accumulated during intestinal inflammation and may play a role as a nutrient source for Enterobacterial expansion; however, further work is required to delineate the role of L-lactate utilization in the outgrowth of Enterobacteriaceae.

Results

DSS treatment decreases butyrate and elevates lactate levels.

We hypothesized that DSS treatment would lead to butyrate depletion and lactate accumulation in the gastrointestinal tract. To test this idea, we treated wild-type C57BL/6 mice with DSS for 8 days. 9 days after DSS treatment, mice were euthanized, and the concentrations of butyrate and lactate were assessed by GC/MS. Consistent with our predictions, DSS treatment significantly lowered the concentration of butyrate in the cecal content (**Fig. 22A**). Additionally, the concentration of lactate was significantly elevated during treatment with DSS (**Fig. 22B**). This

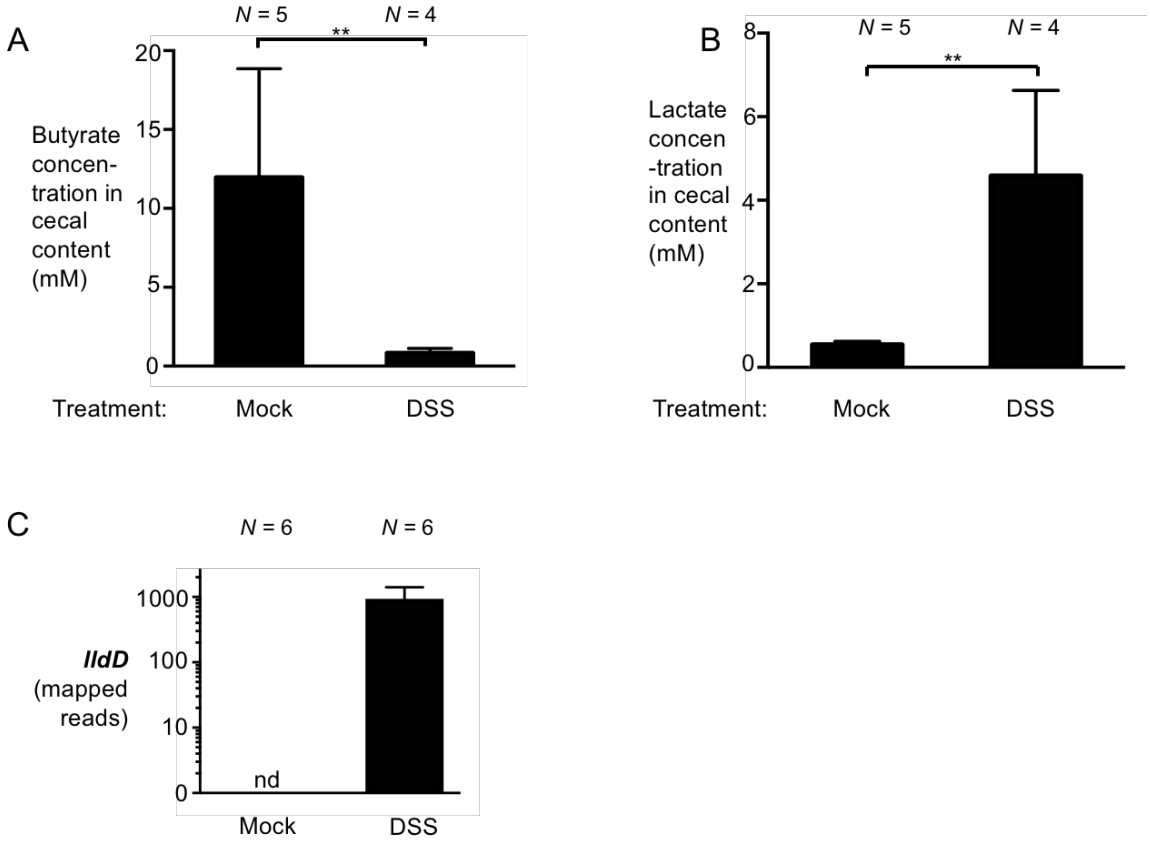

Figure 22. Effect of DSS treatment on butyrate levels, lactate levels, and the coding capacity of the microbiome. Groups of C57BL/6 mice received 3 % dextran sulfate sodium (DSS) in their drinking water for 8 days (or sterile water for mock). Samples of cecal content were taken 9 days after the start of DSS. (A) The concentration of butyrate (B) and lactate in the cecal content was quantified by GC/MS. Bars represent geometric means ± standard error. (C) DNA was extracted from cecal content of mock and DSS-treated mice and subjected to metagenomic sequencing. The number of reads of *lldD* from mice in each group was enumerated. Bars represent means ± standard error.
**, $P < 0.01$. The number of animals per group (N) is indicated above each bar. nd, not detected.

suggests that the inflammation induced by DSS also leads to elevated lactate production by the host.

Metagenomic sequencing revealed an increase in the amount of lldD encoded by the microbiota during intestinal inflammation.

Our previous study had demonstrated that L-lactate is an important nutrient source for *S.* Tm during infection [143]. Other members of the Enterobacteriaceae family, such as *E. coli,* also possess homologous, membrane-bound, respiratory L-lactate dehydrogenases akin to LldD in *S.* Tm [145]. We performed metagenomic analysis on cecal content from mice with and without DSS treatment [40]. As expected, DSS treatment led to an expansion of Enterobacteriaceae [40]. Subsequently, we wanted to identify if DSS treatment would favor the expansion of bacteria that encode homologues of *lldD*. No reads for *lldD* were detected from the cecal content of the mock-treated mice. However, the number of reads mapped to *lldD* increased significantly during DSS treatment (**Fig. 22C**). This suggests that there is an expansion of bacteria that have the genetic capacity to use L-lactate as a nutrient source during intestinal inflammation.

L-Lactate utilization by E. coli NRG 857C.

We next wanted to establish a cause-and-effect relationship between lactate utilization and Enterobacterial outgrowth during inflammation. To do this, we chose to use *E. coli* as a model organism. *E. coli* is a member of the Enterobacteriaceae family and is commonly used as a model organism due to its tractable genetics. The *E. coli* strain NRG 857C is an AIEC strain that was isolated from a human patient with CD, a form of IBD [163]. AIEC strains are able to adhere to and invade intestinal epithelial cells [163]. Genomic analysis has highlighted several putative virulence determinants that are associated with AIEC and pathogenic strains but not commensal

strains, including adhesins and iron acquisition and transport systems [164]. Given that NRG 857C is a strain of *E. coli* that was isolated from a CD patient, we hypothesized that it is well-adapted to the inflamed gut environment and may take advantage of the increase in L-lactate that occurs during intestinal inflammation.

The *E. coli* NRG 857C genome encodes several putative L-lactate dehydrogenases. They include a homolog of LldD, a well-characterized enzyme in *E. coli* and *S.* Tm [145, 161]. The *E. coli* NRG 857C genome also contains the genes *ykgEFG*, which have been implicated in L-lactate utilization. *ykgEFG* were identified during the characterization of L-lactate dehydrogenase genes *lldEFG* in another bacterium, which share 30 %, 38 %, and 32 % identity, respectively, to *ykgEFG* in *E. coli* NRG 857C [165]. Subsequently, Sweeney *et al.* found that genetic ablation of *lldD* and *ykgE* produced a strain that cannot catabolize L-lactate in *E. coli* W3110 [166]. There are also two putative L-lactate dehydrogenase genes, NRG857_20285 and NRG857_14970. NRG857_20285 is a putative dehydrogenase [164]. NRG857_14970 is a putative L-lactate or malate dehydrogenase [164]. The function of these genes was annotated using the NCBI Prokaryotic Genomes Automatic Annotation Pipeline and thus require experimental validation [164].

We sought to identify if these putative L-lactate dehydrogenases were involved in L-lactate utilization *in vitro* as well as identify if they provide a benefit to *E. coli* NRG 857C during expansion in the inflamed gut. To this end, we generated mutants that lacked *lldD, ykgF,* and NRG857_20285, as well as the subsequent combinations of mutations (Δ*lldD* ΔNRG857_20285, Δ*ykgF* ΔNRG857_20285, Δ*lldD* Δ*ykgF,* and Δ*lldD* Δ*ykgF* ΔNRG857_20285). We performed *in vitro* competition assays with the wild-type strain and the putative L-lactate dehydrogenase mutants in mucin broth with 20 mM L-lactate and 1 % O_2, as we had done with *S.* Tm [143]. This

experiment demonstrated that both the Δ*lldD* Δ*ykgF* and Δ*lldD* Δ*ykgF* ΔNRG857_20285 mutants had a significant fitness defect during *in vitro* competitions (**Fig. 23A**). This finding is consistent with the idea that the gene products of *lldD* and *ykgF* may be respiratory L-lactate dehydrogenases; however, more experiments are required to validate these results.

We next wanted to assess if the Δ*lldD* Δ*ykgF* mutant would have a fitness disadvantage during expansion in the inflamed gut. To this end, we performed competitive colonization assays in mice treated with DSS. On day 4 of DSS treatment, we infected mice with an equal mixture of the wild-type and Δ*lldD* Δ*ykgF* strains. Mice were sacrificed 9 days after the beginning of DSS treatment, and colonic and cecal content was collected. Diluted colonic and cecal content was plated on selective agar to enumerate the wild-type and mutant populations and determine the competitive index. This experiment showed that there was ~3-fold fitness advantage for the wild-type strain over the Δ*lldD* Δ*ykgF* strain in this model (**Fig. 23B)**. This mutant was selected to test *in vivo* due to the fitness disadvantage they have *in vitro.* However, experiments examining the *in vivo* role of all of the putative lactate dehydrogenases in the *E. coli* NRG 857C genome need to be performed in the future, as these genes may support fitness *in vivo* but not *in vitro*. Additionally, further experiments need to be done to characterize the L-lactate dehydrogenases that commensal and pathobiont *E. coli* and other Enterobacteriaceae use during inflammation. This will allow us to identify if L-lactate utilization supports fitness during outgrowth under inflamed conditions (**Fig. 24**).

Discussion

The expansion of Enterobacteriaceae such as *E. coli* are a hallmark of dysbiosis during intestinal inflammation (reviewed in [162]). Intestinal inflammation alters the metabolic

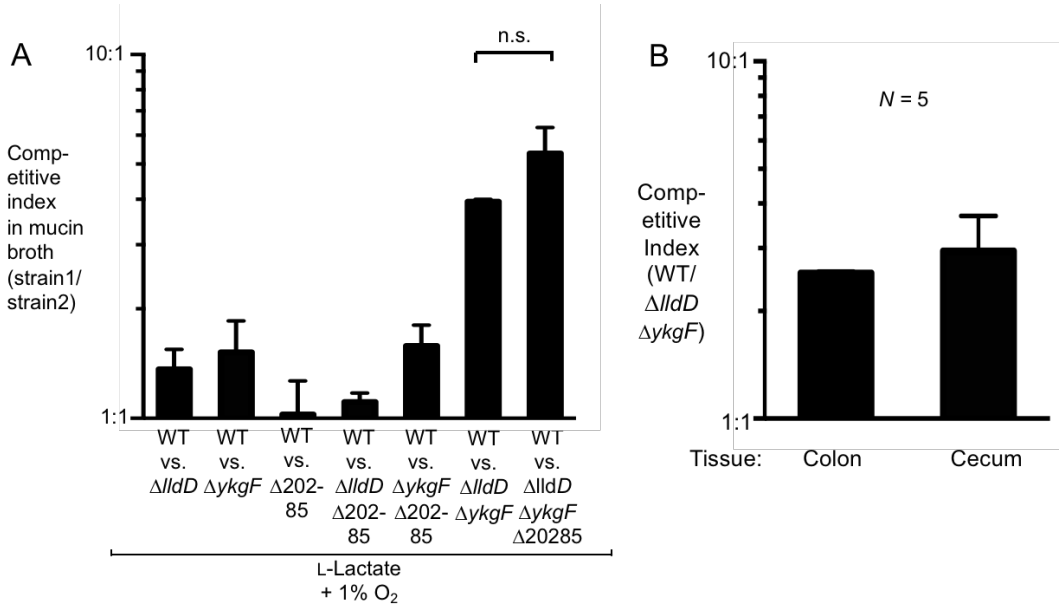

Figure 23: Lactate utilization by *E. coli.* (A) Mucin broth with 20 mM L-lactate was inoculated with an equal ratio of the *E. coli* NRG 857C wild-type strain (WT) and the indicated mutants. The culture was incubated under microaerobic (1 % O_2) conditions for 18 h. After incubation, samples were diluted and plated on selective media to determine the competitive index. Each experiment was conducted with at least 3 biological replicates. Δ20285 = NRG857_ 20285. (B) Wild-type C57BL/6 mice were treated with 3 % DSS for 8 days. On day 4 of the experiment, mice were infected with an equal amount of the wild-type strain and the Δ*lldD* Δ*ykgF* mutant strain. Mice were sacrificed on day 9 of the experiment. Colonic and cecal content was diluted and plated on selective agar to calculate the competitive index. Note: The size of the error bar is smaller than the bar representing the geometric mean. Bars represent geometric means ± standard error. The number of animals per group (*N*) is indicated above each bar. n.s. = not significant.

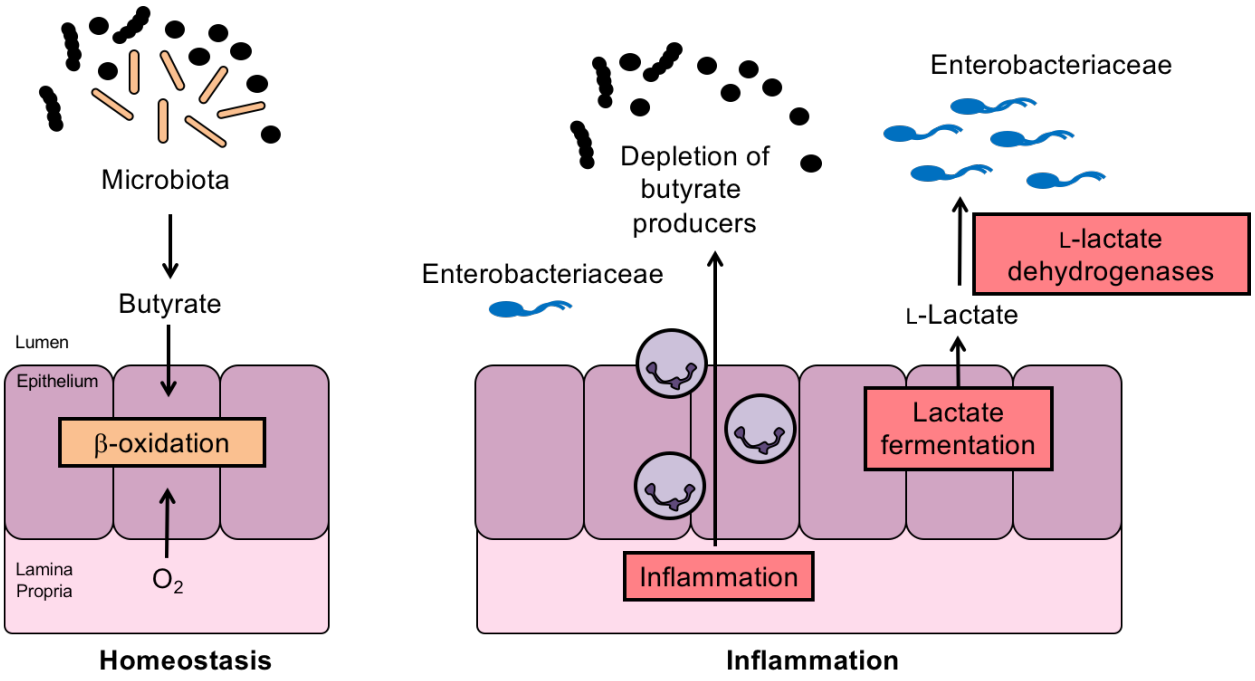

Figure 24. Proposed central model of lactate accumulation during non-infectious colitis. See text for details.

environment of the gut lumen in a manner that is advantageous to the expansion of Enterobacteriaceae and detrimental to the survival of the obligate anaerobic microbiota. The specific mechanisms that enable Enterobacteriaceae to thrive in the inflamed gut remain incompletely described.

Analyses of batch fermentation by commensal gut microbes, both *ex vivo* from the feces of human volunteers and in pure culture, have suggested that commensal microbes may consume microbiota-derived D- and L-lactate as a substrate for the production of short chain fatty acids [125, 167-169]. Disruption of this type of metabolic cross-feeding was hypothesized to be the cause of increased lactate concentrations in human patients with severe intestinal inflammation [135-137, 139, 140, 170]. However, our studies with *S.* Tm infection, antibiotic treatment, and the DSS model of colitis suggest that host-derived lactate could be responsible for lactate accumulation during colitis. However, more investigation into the role of host-derived lactate during inflammation needs to be conducted.

Additionally, further studies on lactate utilization by commensal *E. coli* and AIEC strains may reveal strain-specific differences between different types of *E. coli.* Given that lactate accumulates during intestinal inflammation in both animal models of colitis (**Fig. 22B**) and human patients with IBD [135-137, 139, 140, 170], we speculate that AIEC strains may be particularly well-adapted to lactate utilization during intestinal inflammation, although this hypothesis has not yet been tested. Additionally, there may be differences in *E. coli* strains that are isolated from humans, like NRG 857C, and *E. coli* strains isolated from mice. Host-specific differences could explain why the fitness disadvantage for the Δ*lldD* Δ*ykgF E. coli* NRG 857C in the DSS colitis was only 3-fold. An AIEC strain isolated from mice may be more reliant on lactate utilization

during DSS treatment of mice. Unknown regulatory mechanisms could also necessitate multiple L-lactate dehydrogenases that are used under different conditions, which may explain the potentially redundant L-lactate dehydrogenase genes in the *E. coli* NRG 857C genome. However, much more experimentation is required to evaluate these hypotheses.

Recently, the role of nutritional competition between commensal Enterobacteriaceae and pathogenic Enterobacteriaceae, such as *S.* Tm, has been investigated. For example, in order to colonize the gut successfully, *S.* Tm must acquire iron, which the host sequesters during inflammation [171]. Many bacteria express iron-scavenging molecules known as siderophores. *E. coli* and *S.* Tm possess the siderophore enterobactin (also known as enterochelin) (reviewed in [172]). The host prevents acquisition of iron through the protein lipocalin-2, which binds enterobactin [173, 174]. *S.* Tm overcomes sequestration of iron by lipocalin-2 in the gut through the siderophore salmochelin, which is not recognized by lipocalin-2 [171].

Deriu *et al.* identified that the *E. coli* strain Nissle 1917 was able to limit colonization of the gut by *S.* Tm through competition for iron in the inflamed gut [175]. Genomic analysis of the probiotic *E. coli* strain Nissle 1917 showed that this strain lacks many virulence factors (such as α-hemolysins and P-fimbrial adhesins) [176]. However, this strain possesses a number of factors that enable successful colonization of the gastrointestinal tract, including microcins and iron uptake systems [176]. These lipocalin-2-resistant iron uptake systems in *E. coli* Nissle allow the commensal strain to compete with the pathogen, which limits *S.* Tm colonization and inflammation in the gut [175].

The competition for iron in the gut illustrates the idea of nutritional competition between commensals and invading pathogens, in which the shared nutritional strategies of pathogenic and

commensal Enterobacteriaceae limits the availability of nutrients for the pathogen. Similarly, commensal *E. coli* and other Enterobacteriaceae family members, such as *Klebsiella* species, could also take advantage of the lactate-oxidation metabolic niche, as suggested by our metagenomic sequencing. Given that lactate-oxidation is an important metabolic pathway during expansion of *S.* Tm during infection, we speculate that lactate utilization by commensal Enterobacterial species could serve as a mechanism of colonization resistance during enteric infection, although further study must be carried out to investigate this hypothesis.

CHAPTER SIX

DISCUSSION AND CONCLUDING REMARKS

Discussion

In this section, we will highlight several concepts related to this study. First, we will discuss metabolic mechanisms of control over microbes by the host, and how pathogens can subvert these mechanisms. In particular, we will dissect how pathogens are able to exploit metabolic switches in host cells to support their metabolism. Next, we will explore the ways in which metabolites can serve as cues for bacterial gene expression. This will be followed by a discussion of PPARγ as a drug target for treatment of dysbiosis-associated diseases. Finally, we will discuss the role of lactate in homeostasis in the small intestine and how bacteria can sense lactate to discriminate between regions of the gastrointestinal tract.

Host control mechanisms limit Enterobacterial populations during homeostasis.

The evolutionary development of the mammalian gastrointestinal tract is intertwined with the microbes that inhabit it. These microbes perform essential functions for the host, and perturbations in the microbiota are associated with negative consequences for the host. The host possesses a number of control mechanisms to confine the microbiota to the lumen of the distal gut while maintaining the beneficial functions of the microbial population. These mechanisms include the secretion of antimicrobial peptides such as RegIIIγ, which maintain the spatial segregation between the host and the microbes in the lumen of the small intestine [177]. Another key mechanism is maintaining the anaerobic status of the gut through β-oxidation of butyrate by IEC (reviewed in [95]). This oxidative metabolism not only generates energy for the host cells, but also

protects the obligate anaerobes of the microbiota from oxygen damage to oxygen-sensitive iron-sulfur cluster proteins [178]. It also limits the growth of members of the Enterobacteriaceae family, which are not metabolically competitive in the anaerobic gastrointestinal tract (reviewed in [18]). Thus, limitation of oxygen through consumption of a microbial metabolite could be considered a form of nutritional colonization resistance by preventing the outgrowth of pathogens such as *S.* Tm [85] or potentially deleterious Enterobacteriaceae family members [40, 84].

The murine pathogen *Citrobacter rodentium* is an enteric pathogen that forms attaching and effacing (AE) lesions. Pathological changes in the mucosa create a so-called pedestal structure that houses an individual bacterium [179]. Intriguingly, Lopez *et al.* discovered that *C. rodentium* also utilizes aerobic respiration during infection, albeit through a different mechanism than *S.* Tm or non-pathogenic Enterobacteriaceae. The pathological hallmark of *C. rodentium* infection is colonic crypt hyperplasia [179], and as a result the intestinal epithelium becomes populated with immature IEC. Unlike mature IEC, immature IEC do not consume oxygen through β-oxidation. Subsequently, oxygen from the host tissue leaks into the lumen of the gastrointestinal tract, where it can be used by *C. rodentium* for aerobic respiration [180]. This suggests that acquisition of oxygen via manipulation of the host through a variety of mechanisms is a sought-after advantage for aerobic enteric pathogens. It is not known if host-derived lactate is a nutrient for *C. rodentium* during infection. *C. rodentium* encodes a homolog of *lldD,* however, this gene is annotated as having a frameshift mutation [181]. There may be an uncharacterized lactate dehydrogenase in *C. rodentium* that enables lactate utilization, but further study is required to ascertain this.

S. Tm *subverts host control mechanisms by inducing inflammation to expand in the gut lumen.*

During infections with the enteric pathogen *S.* Tm, many of the mechanisms designed to protect the host actually enable the success of the pathogen. This suggests that pathogens have evolved mechanisms to overcome or manipulate the host response in order to ensure successful transmission to new hosts. The repertoire of effector molecules in the *S.* Tm genome induces the host immune response, leading to the killing of the invading organisms within the tissue [61]. However, it is the host immune response that modifies the gastrointestinal lumen into an environment that allows *S.* Tm to thrive metabolically through respiratory metabolism [63, 70, 71, 85]. Successful competition for nutrients enables *S.* Tm to dominate the distal gut and therefore transmit to new hosts [62].

The role of lactate metabolism during growth of S. aureus under nitric oxide stress

In contrast to many pathogenic and commensal bacterial species, *S. aureus* is particularly well adapted to survival under nitrosative stress. One interesting mechanism that enables survival of the pathogen is metabolic adaptation through lactate fermentation. Nitric oxide inhibits the activity of the enzymes pyruvate dehydrogenase and pyruvate-formate lyase, thus disabling crucial pathways that would generate acetyl-CoA. To survive, *S. aureus* upregulates the L-lactate dehyrogenase *ldh1,* which is inducible by nitric oxide. This allows the pathogen to maintain redox balance and grow. *ldh1* was found to be required for fitness and virulence during a murine model of sepsis. The virulence defect of a *ldh1* mutant was abrogated in mice that were treated with an iNOS inhibitor or in *Nos2*-deficient mice. In contrast, the coagulase-negative species *Staphylococcus epiderimidis* and *Staphylococcus saprophyticus* lacked an inducible L-lactate dehydrogenase and were unable to grow under nitric oxide stress [182]. Subsequent studies by Vitko and colleagues found that *S. aureus*' ability to survive through lactate fermentation was

highly dependent on the availability of glycolytic substrates [183]. Interestingly, under low nitric oxide conditions, *S. aureus* is able to re-assimilate L-lactate via the L-lactate-quinone oxidoreductase Lqo [184]. Lactate metabolism in *S. aureus* during infection highlights the importance of pathogen adaptation to the metabolic changes that occur during the host inflammatory response, and how subversion of these inflammatory defenses can separate pathogens from commensals.

Pathogens exploit PPAR-mediated metabolic switches in host cells during infection.

Many intracellular pathogens are adept at exploiting metabolic changes in host cells to acquire nutrients. As previously discussed, *S.* Tm is found preferentially in alternatively activated macrophages (AAMs, also called M2 macrophages) during murine models of long term persistence. During acute phases of infection, the microbicidal, classically activated macrophages (CAMs, also called M1 macrophages) predominate. CAMs have a metabolism characterized by anaerobic glycolysis, which preserves oxygen for use in the production of reactive species during the oxidative burst. This restricts the amount of glucose available for the consumption by *S.* Tm during intracellular growth. However, during later stages of infection, anti-inflammatory AAMs become abundant. The AAMs phenotype is dependent on PPARδ, another important transcription factor in the PPAR family. Like PPARγ, PPARδ is a master regulator of metabolism and drives macrophage metabolism towards β-oxidation of fatty acids, which liberates glucose for exploitation by *S.* Tm during intracellular replication. Thus, *S.* Tm is able to persist intracellularly by exploiting macrophage-derived glucose [132].

Similarly, the intracellular pathogen *Brucella abortus* also exploits AAMs. Xavier *et al.* found that during *B. abortus* persistence, the bacteria were predominantly found in AAMs, where

the intracellular pathogen can take advantage of the increased glucose found in AAMs due to their fatty acid oxidation-based metabolism. Interestingly, in *B. abortus* infection PPARγ was essential for enhanced bacterial replication inside of AAMs. This suggests that exploitation of AAM metabolism is a niche that is occupied by multiple intracellular pathogens [185].

In contrast, Thurlow *et al.* discovered that PPARγ-mediated AAM activation was required for the clearance of methicillin-resistant *Staphylococcus aureus* (MRSA) skin and soft tissue infections (SSTIs). AAM activation deprived extracellular MRSA of glucose and oxygen within resolving abscesses, demonstrating the importance of PPARγ in limiting nutrient availability for extracellular pathogens [186]. This suggests that host-directed antimicrobial therapies, targeting PPARγ or PPARδ, could be developed to control both intracellular and extracellular pathogens through their metabolism. Such treatments could potentially be used during *S.* Tm infection to limit access to nitrate, oxygen, and lactate in the lumen of the gut or to inhibit persistence within macrophages, although substantially more research is needed to validate PPARγ or PPARδ as antimicrobial drug targets.

Metabolites can serve as both nutrition sources and environmental cues for enteric pathogens.

Enteric pathogens such as *S.* Tm can use metabolites for both nutrition and to sense the environment around them. For example, butyrate can serve as both a cue to repress virulence and as a nutrient during early stages of *S.* Tm infection. Butyrate is known to suppress expression of T3SS-1 genes [187]. Early in infection, *S.* Tm is able to consume butyrate through anaerobic β-oxidation, which supports the metabolism of *S.* Tm [188]. Consumption of butyrate intracellularly removes the inhibitory signal for invasion, and thus the utilization of butyrate facilitates invasion and worsens inflammation [188].

Interestingly, the genes required for anaerobic β-oxidation of butyrate are absent from the genomes of *S.* Typhi and *S.* Paratyphi A [155]. Bronner *et al.* demonstrated that genetic ablation of butyrate utilization in combination with addition of the *viaB* locus from *S.* Typhi and the deletion of *fepE* in the *S.* Tm genome resulted in decreased invasion, decreased intestinal inflammation, and increased colonization of the spleen in a mouse model of typhoid fever [188]. The *viaB* locus in *S.* Typhi contains the regulation, biosynthesis, and export machinery for the production of the Vi capsular polysaccharide [189], which prevents the induction of intestinal inflammation in the streptomycin-treated mouse model of salmonellosis when introduced into *S.* Tm [190]. Another genetic feature of *S.* Typhi is that *fepE* is a pseudogene [191]. Genetic ablation of *fepE* in *S.* Tm results in the loss of very long O antigen chains, which facilitates the production of Vi capsule and thus immune evasion during colitis [192]. The reduction in intestinal virulence when these mutations are made in conjunction with genetic ablation of butyrate utilization in *S.* Tm suggests that the absence of the butyrate utilization genes in *S.* Typhi is a mechanism to quell the induction of inflammation in the intestine [188].

E. coli O157:H7, also known as enterohemorrhagic *E. coli* (EHEC), is a human pathogen that causes bloody diarrhea [193]. Like *Citrobacter rodentium,* EHEC forms AE lesions on the host epithelium [194]. The genes required for AE formation are encoded in the locus of enterocyte effacement (LEE genes) [195]. The expression of LEE genes is induced by a number of host and microbial signals (reviewed in [196]). Ethanolamine, a derivative of cell membranes, can serve as the sole nitrogen source for EHEC both *in vitro* and in bovine intestinal content [197] as well as a cue for AE formation [198]. Interestingly, ethanolamine also plays a role in *S.* Tm infection. In addition to the fitness advantage conferred by ethanolamine utilization during tetrathionate

respiration [77], ethanolamine also serves as a cue for *S.* Tm to express T3SS-2 during intracellular replication [199]. In summary, ethanolamine serves as an important nutrient and cue for signaling in enteric pathogens in a variety of settings. These studies highlight the importance of sensing of the metabolic milieu of the inflamed gut for enteric pathogens, both for the purposes of virulence gene expression and the prudent expression of metabolic genes.

PPARγ and host metabolism is a potential therapeutic target for preventing dysbiosis during intestinal inflammation.

PPARγ has been appreciated for its role in animal models of intestinal inflammation [84, 96]. Genetic polymorphisms in PPARγ have also been associated with an increased risk of ulcerative colitis [200, 201]. Additionally, a series of studies from the 1980's and 1990's found a correlation between severe colitis and lactate abundance in the stool. Vernia and colleagues identified that patients with severe ulcerative colitis had nearly 20 mM L-lactate in their stool, compared with only 0.2 mM in healthy controls. Similarly, these same patients had a decrease in the amount of butyrate present in their stool [139, 140].

Similarly, Hove *et al.* found elevated L-lactate in CD patients with ileocolitis, but not in patients without disease in the colon [137]. Further experiments were performed by Hove and colleagues using enema bags containing butyrate in an electrolyte solution that were inserted in the rectums of control patients, patients with quiescent UC, and patients with active UC. These experiments showed no difference in butyrate absorption by patients with active UC; however, these patients did have significantly more L-lactate diffuse into the enema bag than did the control patients or the patients with quiescent disease [136]. The results of these studies have been recently recapitulated by studies with larger sample sizes and modern analytical chemistry methodologies

[135, 170]. Collectively, this suggests that the absence of a signal for PPARγ (e.g. inflammation-induced depletion of butyrate) could lead to the accumulation of lactate in patients with IBD.

While these correlations have been known for decades, further work is needed to identify if changes in host metabolism are responsible for the increase in lactate observed in patients with IBD. However, it does suggest that there could be a role for therapies that activate PPARγ in treating dysbiosis during intestinal inflammation. Indeed, the drug 5-aminosalicylic acid (5-ASA), which is commonly used in the treatment of IBD, targets PPARγ [202]. This suggests that this drug could not only have a direct anti-inflammatory effect on the host, but also modulate the expansion of potentially deleterious Enterobacteriaceae that can exacerbate inflammation [43] without harming the rest of the microbiota (reviewed in [95]).

Lactate is an important cue for gut development, regeneration, and immune surveillance in the small intestine.

Our studies have largely focused on lactate metabolism in the cecum and large intestine. However, lactate also plays an important role in maintaining homeostasis in the small intestine, including in the development of the immune system. A subset of myeloid cells in the terminal ileum express the chemokine receptor CX3CR1 (CX3CR1+ cells). CX3CR1+ cells form dendrites that cross the intestinal epithelium and can sample antigens in the gut lumen [203]. However, the exact mechanism that leads to luminal dendrite protrusion was unknown. Morita *et al.* found that the methanol-soluble fraction of luminal content from SPF mice, but not germ-free mice, can stimulate dendrite protrusion *ex vivo*. Chemical analysis of luminal content revealed that L-lactate, D-lactate, and pyruvate are responsible for dendrite protrusion. Furthermore, L-lactate, D-lactate, and pyruvate activate the G-coupled protein receptor Gpr31, which is required for dendrite

protrusion into the lumen. Colonization of mice with *Lactobacillus helveticus*, which produces both lactate and pyruvate, increased dendrite protrusion. The absence of dendrite protrusion into the lumen resulted in immune dysfunction due to decreased antigen sampling [204].

Similarly, microbiota-derived lactate is an important signal for the development and regeneration of the small intestinal epithelium. Lee *et al.* found that small intestinal organoids cultured with lactate-producing bacteria conditioned media, gut contents from newborn mice, or lactate alone are larger than those cultured in standard medium. Similarly, those organoids co-cultured with lactate-producing bacteria-conditioned media or lactate have increased expression of genes in the Wnt/β-catinin pathways, as well as increased numbers of Lgr5+ stem cells and Paneth cells. In contrast to the protrusion of dendrites, in which Gpr31 was required for the response to lactate, the G-protein coupled receptor Gpr81 in stromal cells was required for enhanced epithelial differentiation. Lactate-stimulated Gpr81 signaling exerts an even stronger effect over organoids from newborn mice than organoids from adult mice, suggesting that this signaling mechanism may be related to development. Furthermore, pre-exposure to lactate or lactate-producing bacteria was protective against gut injury. This suggests that microbiota-derived lactate is an important signal to support regeneration of the small intestinal epithelium [205]. Evidence from human patients showed that administration of lactic acid-producing bacteria prior to radiation treatment in patients with cervical cancer reduces the severity of radiation-induced diarrhea, although the exact mechanism for this effect in humans is still unknown [206].

Host-derived lactate also supports stem cell function in the small intestinal crypt. Rodriguez-Colman and colleagues found that Lgr5+ stem cells and Paneth cells in the intestinal crypt perform very different types of metabolism. Paneth cells possess a metabolism based on

lactate fermentation. The lactate generated by Paneth cells can then be transported into adjacent Lgr5+ stem cells, where it can be converted back into pyruvate and shuttled into the mitochondria for use in oxidative phosphorylation. The reactive oxygen species generated by oxidative phosphorylation support the phosphorylation of the p38 MAP kinase, which maintains crypt formation and differentiation [207].

The pathogen *Campylobacter jejuni* relies upon sensing of metabolites in the gastrointestinal tract [208]. *C. jejuni* is a common foodborne pathogen that causes diarrhea in humans (reviewed in [209]) but is a commensal organism in avian hosts [210]. During colonization of the avian gut, *C. jejuni* is more commonly found in the lower digestive tract and found in low abundance in the stomach and small intestine [210]. *C. jejuni* may use sensing of lactate and short chain fatty acids to discriminate between the upper and lower gastrointestinal tract, respectively. This allows *C. jejuni* to appropriately express genes that are required for commensalism in the avian host [208].

These examples of the importance of lactate metabolism in the small intestine highlight the metabolic differences between the small intestine and the large intestine, both of the host and the microbiota that occupy the lumen of these organs. The lumen of the murine small intestine has relatively few bacteria due to a number of host control mechanisms, such as secretion of antimicrobial peptides from Paneth cells [177]. In the murine small intestine, Lactobacillaceae are more abundant than in the distal gut [211], potentially because the facultative anaerobic Lactobacillaceae are more tolerant to oxygen than other commensals found in the distal gut (reviewed in [212]). Thus, microbiota-derived lactate may be a more abundant metabolite in the

small intestinal lumen under homeostatic conditions and facilitate the development of the innate immune system and the small intestinal crypt.

In contrast, the lumen of the distal gut is densely colonized by strict anaerobes [1]. In our studies, lactate was not very abundant under uninflamed conditions in the murine cecum. However, host-derived lactate increased significantly when the relationship between Clostridial metabolism and host metabolism was perturbed, such as during *S.* Tm infection, streptomycin treatment, and potentially DSS treatment. Thus, lactate serves as an indicator of perturbation of the microbiota and disruption of host metabolism in the distal gut, rather than being a cue or indicator of homeostasis as it may be in the small intestine.

Concluding Remarks

The gut microbiota is a vastly complex network between many types of bacteria, viruses, fungi, and host cells. In recent decades, there has been an increased appreciation for the wide variety of effects that the gut microbiota exerts upon human biology and health. However, untangling a complex system like host-microbiota interactions is difficult. Interestingly, enteric pathogens are evolutionarily adapted to disrupt host-microbiota interactions in order to gain a foothold in the gut, thus making enteric pathogen infection an effective model to study the mechanisms that maintain host-microbiota homeostasis.

The picture emerging from our studies is that there is an inverse relationship between the metabolism of the host and the metabolism of the microbes that dominate the distal intestinal tract. Under homeostatic conditions, the fermentation of complex polysaccharides into a fermentation end product, butyrate, supports β-oxidation in the host intestinal epithelium. However, this process

is disrupted during intestinal inflammation, such as enteric pathogen infection or DSS colitis. In this case, pathogenic or commensal Enterobacteriaceae dominate the gut through an oxidative metabolism. In the absence of a substrate for β-oxidation, the intestinal epithelium must instead rely on fermentation. The pathogen *Mycobacterium tuberculosis* exploits a similar change in host metabolism during infection. During infection with *M. tuberculosis,* the metabolism of the host lung becomes dependent on lactate fermentation, most likely from changes in immune cell metabolism [213]. *M. tuberculosis* can use host-derived lactate as a nutrient using a quinone-dependent L-lactate dehydrogenase during infection of human peripheral blood mononuclear cell-derived macrophages [214]. A similar lactate-oxidation metabolic strategy is also employed by *B. abortus* during infection of HeLa and THP-1 cells [215]. We refer to this inverse metabolic relationship as 'metabolic mirroring' between the host and microbes. In conclusion, our usage of enteric pathogen infections as a model for dysbiosis illustrates the value of studying bacterial pathogenesis of enteric pathogens, both for the knowledge learned about the pathogen itself and the systems that maintain homeostasis in the host.

Table 1. Bacterial strains used in this study

Strain	Characteristic(s)	Reference
AJB715	*S.* Tm IR715 *phoN*::Kan^r	[216]
ATCC 14940	*Clostridium symbiosum*	ATCC
CG6	*S.* Tm IR715 Δ*lldD*	[143]
CG8	*S.* Tm IR715 Δ*dld*	[143]
CG9	*S.* Tm IR715 Δ*lldD* Δ*dld*	[143]
CG12	*S.* Tm IR715 Δ*dld* Δ*invA* Δ*spiB phoN*::Kan^r	[143]
CG30	*S.* Tm IR715 Δ*lldD* Δ*dld* Δ*invA* Δ*spiB phoN*::Kan^r	[143]
CG89	*S.* Tm IR715 Δ*ldhA*	[143]
CG107	*S.* Tm IR715 Δ*moaA phoN*::Kan^r	[143]
CG110	*S.* Tm IR715 Δ*lldD* Δ*dld phoN*::Kan^r	[143]
CG111	*S.* Tm IR715 Δ*ldhA* Δ*lldD* Δ*dld*	[143]
CG115	*S.* Tm IR715 Δ*moaA* Δ*lldD* Δ*dld*	[143]
CG116	*S.* Tm IR715 Δ*ldhA phoN*::Kan^r	[143]
CG124	*S.* Tm IR715 Δ*cydA*	[143]
CG127	*S.* Tm IR715 Δ*cydA* Δ*lldD*	[143]
CG131	*S.* Tm IR715 Δ*cydA phoN*::Kan^r	[143]
CG142	*S.* Tm IR715 Δ*lldD phoN*::pCG142 (= *phoN*::*lldD*$^+$)	[143]
CG168	*E. coli* NRG 857C Δ*lldD*	This study
CG169	*E. coli* NRG 857C Δ*lldH*	This study

CG184	*E. coli* NRG 857C Δ*lldD* Δ*ykgF*	This study
CG185	*E. coli* NRG 857C Δ*lldD* ΔNRG857_ 20285	This study
CG188	*E. coli* NRG 857C Δ*ykgF* ΔNRG857_ 20285	This study
CG189	*E. coli* NRG 857C Δ*lldD* Δ*ykgF* ΔNRG857_ 20285	This study
CG190	*E. coli* NRG 857C Δ*ykgF*	This study
CG200	*S.* Tm IR715 Δ*lldR*	[217]
CG226	*S.* Tm IR715 Δ*lldP*	[217]
CG254	*S.* Tm IR715 *lldD*::pCG254	[217]
CG267	*S.* Tm IR715 Δ*arcA lldD*::pCG254	[217]
CG268	*S.* Tm IR715 Δ*arcB lldD*::pCG254	[217]
CG270	*S.* Tm IR715 Δ*cydA lldD*::pCG254	[217]
DH5α λ*pir*	*E. coli* DH5α λ*pir*; F^- *endA1 hsdR17* (r^-m^+) *supE44 thi-1 recA1 gyrA relA1* Δ (*lacZYA-argF*)*U189* φ*80lacZ*ΔM15 λ*pir*	[218]
FF283	*S.* Tm IR715 Δ*moaA*	[79]
IR715	Nalidixic acid resistant strain of *Salmonella enterica* serovar Typhimurium ATCC14028.	[219]
LB33	*E. coli* NRG 857C Δ*lacZ*	[40]
MW118	*S.* Tm IR715 Δ*arcB*	[217]

MW119	IR715 Δ*arcA*	[217]
MW285	*S*. Tm IR715 Δ*sseD*	[143]
MW287	*S*. Tm IR715 Δ*sseD phoN*::Cm^r	[143]
MW292	*S*. Tm IR715 Δ*sseD* Δ*lldD* Δ*dld*	[143]
NRG 857C	Adherent invasive E. coli isolate (O83:H1) Carb^r Cm^r Tet^r	[163]
S17-1 λ*pir*	*E. coli* S17-1 λ*pir*; *zxx::*RP4 2-(Tet^r::Mu) (Kan^r::Tn7) λ*pir*	[220]
SPN487	*S*. Tm IR715 Δ*invA* Δ*spiB*	[221]
SW284	*S*. Tm IR715 *phoN*::Cm^r	[222]

Table 2. Plasmids used in this study

Plasmid	Characteristic(s)	Reference
pCG1	Upstream and downstream regions of *S.* Tm *dld* in pRDH10	[143]
pCG2	Upstream and downstream regions of *S.* Tm *lldD* in pRDH10	[143]
pCG89	Upstream and downstream regions of *S.* Tm *ldhA* in pRDH10	[143]
pCG124	Upstream and downstream regions of *S.* Tm *cydA* in pRDH10	[143]
pCG142	Promoter and coding regions of *S.* Tm *lldD* in pSW327	[143]
pCG168	Upstream and downstream regions of *E. coli* NRG 857C *lldD* in pGP706	This study
pCG169	Upstream and downstream regions of *E. coli* NRG 857C NRG857_ 20285 in pGP706	This study
pCG190	Upstream and downstream regions of *E. coli* NRG 857C *ykgF* in pGP706	This study
pCG200	Upstream and downstream regions of *S.* Tm *lldR* in pRDH10	[217]
pCG226	Upstream and downstream regions of *S.* Tm *lldP* in pRDH10	[217]
pCG254	Fragment of *lldD* in pFUSE	[217]

pFUSE	*ori*(R6K) *mobRP4* Cm^r *lacZYA*	[223]
pGP704	*ori*(R6K) *mobRP4* Carb^R	[224]
pGP706	*ori*(R6K) *mobRP4 sacRB* Kan^r	[143]
pMW1	Upstream and downstream regions of *S.* Tm *sseD* in pGP706	[143]
pMW89	Upstream and downstream regions of *S.* Tm *arcB* in pRDH10	[217]
pMW195	Upstream and downstream regions of *S.* Tm *arcA* in pRDH10	[217]
pRDH10	*ori*(R6K) *mobRP4* Cm^r Tet^r *sacRB*	[225]
pSW327	Fragment of *phoN* cloned into pGP704.	[73]

Table 3. Primers for Mutagenesis

Target/ Purpose	Sequence	Reference
Deletion of *lldD* in *S.* Tm	5'- GCCATCTCCTTGCATGC GTGATTGTGATGCCAAAAC -3' 5'- ACTGATTTCTCATGATTTATTCTCCCTGG -3' 5'- TAAATCATGAGAAATCAGTGGCGATTCAC -3' 5'- CAAGGAATGGTGCATGC TTACGACCGCAATACCGC -3'	[143]
Deletion of *dld* in *S.* Tm	5'- GCCATCTCCTTGCATGCCAGGTCATATTCAGGCC -3' 5'- GCACGGTGTGTGGTGGGACAAAATATC-3' 5'- CCACCACACACCGTGCGGTTTACCGT-3' 5'- CAAGGAATGGTGCATG CCAGACGCCGGAAATGAAAG -3'	[143]
Deletion of *ldhA* in *S.* Tm	5'-GCCATCTCCTTGCATGATA ACGTATCTGCTGAATGAC-3' 5'-GCGACAGGTGACCTTCTCCAGTGATG-3' 5'-GAAGGTCACCTGTCGCTCCCCTGCGC-3' 5'CAAGGAATGGTGCATGGCA CATGTTTCGCCAGGGATGAAAG-3'	[143]

Deletion of *sseD* in *S.* Tm	5’-CTAGAGGTACCGCATGCAGCTGCAAAAGTGCTTG-3’ 5’-ACCTCGTTTCAGATTAAGCGCGATAG-3’ 5’-CTTAATCTGAAACGAGGTAAACATGGTGCAAG-3’ 5’-AGCTCGATATCGCATGCGCCAACTCCATGGCTGG-3’	[143]
Amplification of *lldD* promoter region in *S.* Tm	5’-CTAGAGGTACCGCATGTGAAGTAACAACACTCCC-3’ 5’-TTCTCCCTGAGAACCACACGCATAATG-3’	[143]
Amplification of *lldD* coding sequence in *S.* Tm	5’-TGGTTCTCAGGGAGAATA AATCATGATTATTTCAGCAGC-3’ 5’-AGCTCGATATCGCATGTCAGGCGGCATCGCCTTT-3’	[143]
Deletion of *cydA* in *S.* Tm	5’-GCCATCTCCTTGCATGAA TGTGGAATGTTTTTTACTGG-3’ 5’-CTCCTGTCCATGACTCCTTGCTCATC-3’ 5’-GAGTCATGGACAGGAGTCGTCAAATG-3’ 5’-CAAGGAATGGTGCATGACTGGAAGAAGTTACCGG-3’	[143]

Deletion of *S.* Tm *lldR*	5’-GCCATCTCCTTGCATGTTA ACGTTCCGGTACCGTATC-3’ 5’-GTTTTAACCTGGATGAT TCCGTGAATGATTATTTCA -3’ 5’-TTCCGTGAATGATTATTTCAGCAGCCAGCGATTATC-3’ 5’- GTCGGCCTGAACGGTCGCCATGCACCATTCCTTG-3’	[143]
Deletion of *S.* Tm *arcA*	5’-GCCATCTCCTTGCATGCACCGTGCTTAACGAGCGCG-3’ 5’- TTTGGCGCCTGGGCCGAAAAATTGCCA-3’ 5’-GGGCCGAAAAATTGCCAACTAAATCGAAAC-3’ 5’- CGTATTGTCGACAGCCAGCATGCACCATTCCTTG -3’	[143]
Deletion of *S.* Tm *arcB*	5’-GCCATCTCCTTGCATGCT CCACAACGATATCATCAACCGGG-3’ 5’- ACCCCGGTCAAACCGGGGTTCCTTCAC-3’ 5’-AACCGGGGTTCCTTCACCACAACTTC-3’ 5’- GAAATAGGCCAGATAGCGT TGCATGCACCATTCCTTG-3’	[143]
Deletion of *S.* Tm *lldP*	5’-GGGCGCCATCTCCTTGCA TGTCGAAGAAGCAAACACTTATAC-3’ 5’-GTTCTCAGGAGACCTGCATTGTGATGCC-3’ 5’-GAGACCTGCATTGTGATGCCAAAACGCC-3’ 5’-CGGAACAACACCAGGCAGC ATGCACCATTCCTTGCGGC-3’	[143]

Creation of pCG254	5’-GCCGCTCTAGAACTAGTGGA TCCCCGGTGTCGAATCACGGCGG-3’ 5’- CTTTATGTACTGCGTGAC CGGGAATTCCGATCCGACAAC-3’	[143]
Deletion of *E. coli* NRG 587C *lldD*	5’-GCTTCTTCTAGAGGTACCGC ATGGCGAAACTGGTAAGCGAAG-3’ 5’-CATTCGAGGGAGAAAAACGCGGTTAGACGA-3’ 5’-AGAAAAACGCGGTTAGACGAATATCTGC-3’ 5’-CGTTGAAATGCTGATCCACA TGCGATATCGAGCTCTCC-3’	This study
Deletion of *E. coli* NRG 857C *ykgF*	5’-GCTTCTTCTAGAGGTAC CGCATGGGAAAAACTCGGCTGTCG-3’ 5’-CCGCTGAGGATATAAAGTCGGAGCGAA-3’ 5’-GGATATAAAGTCGGAGCGAATTTTTGAATAAC-3’ 5’-GGTGTATCTGATTATTGAGG ACATGCGATATCGAGCTCTCC-3’	This study
Deletion of *E. coli* NRG 857C NRG857_ 20285	5’-GCTTCTTCTAGAGGTACC GCATGAGAAAAACGCTTGATCGG-3’ 5’-CTAATGTGAGGAAATCAACGTTCTGGTCGA-3’ 5’-GAAATCAACGTTCTGGTCGATAAACTTG-3’ 5’-GTAGCAGTTTTACCTGCAC ATGCGATATCGAGCTCTCC-3’	This study

Table 4. Primers for real-time PCR

Target (Organism)	Sequence	Reference
16S (Clostridia)	5'-ACTCCTACGGGAGGCAGC-3' 5'-GCTTCTTTAGTCAGGTACCGTCAT-3'	[44]
16S (Bacteroidetes)	5'-GGTTCTGAGAGGAGGTCCC-3' 5'-GCTGCCTCCCGTAGGAGT-3'	[44]
16S (Enterobacteriaceae)	5'-GTGCCAGCMGCCGCGGTAA-3' 5'-GCCTCAAGGGCACAACCTCCAAG-3	[44]
Gapdh (*mus musculus*)	5'-TGTAGACCATGTAGTTGAGGTCA-3' 5'-AGGTCGGTGTGAACGGATTTG-3'	[226]
Cxcl1 (*mus musculus*)	5'-TGCACCCAAACCGAAGTCAT-3' 5'-TTGTCAGAAGCCAGCGTTCAC-3'	[226]
Nos2 (*mus musculus*)	5'-TTGGGTCTTGTTCACTCCACGG-3' 5'-CCTCTTTCAGGTCACTTTGGTAGG-3'	[227]
Tnfa (*mus musculus*)	5'-AGCCAGGAGGGAGAACAGAAAC-3' 5'-CCAGTGAGTGAAAGGGACAGAACC-3'	[40]
lldP (*S.* Tm)	5'-TGCTGGCGTTCGCGTTTATC-3' 5'- CTCTCTACAGGCTACCGCGG-3'	[217]
lldR (*S.* Tm)	5'-ACCGCTGCCGACAAAGAGAA-3' 5'- CTTTCATCTGGCGATCGCGG-3'	[217]
lldD (*S.* Tm)	5'-TCCGTAACGGGCTGGATGTC-3' 5'- GAAGGTCGCCATGACCCTGA-3'	[217]

dld (*S.* Tm)	5'-CCGGAGCAGATCCTGAGCAA-3' 5'- TTTGAATCTTCCGGCTGCGC -3'	[217]
gmk (*S.* Tm)	5'-TTGGCAGGGAGGCGTTT-3' 5'- GCGCGAAGTGCCGTAGTAAT-3'	[228]
16S rRNA (*S.* Tm)	5'-CAGAAGAAGCACCGGCTAACTC-3' 5'-GCGCTTTACGCCCAGTAATT-3'	[228]

Table 5. Histopathology Scoring Criteria.

Score	Exudate	Epithelial Damage	Infiltration of PMNs*	Necrosis	Submucosal Edema
0	No changes	No changes	No changes (0-5)	No changes	No changes
1	Slight accumulation	Desquamation	6-20	Slight	Detectable (<10 %)
2	Mild accumulation	Mild erosion	21-60	Mild	Mild (10-20 %)
3	Moderate accumulation	Marked erosion	61-100	Moderate	Moderate (20-40 %)
4	Marked accumulation	Ulceration	>100	Marked	Marked (>40 %)
*Number of cells per high powered field (400x)					

Appendix A. Metabolic profiling of cecal content

Putative Compound	**Relative abundance** (average peak area as % of total)	
	Un-infected	*S.* Tm infected
Butyric Acid	0.65	0.09
Lactic acid	0.005	0.38
L-Glutamic acid	0.33	0.055
Guanidine	0.18	0.005
3-Hydroxy-azetidine-1-carboxylic acid	0.005	0.14
Tartaric acid	0.11	0.005
L-Alanine	0.06	0.055
Glyceric acid	0.095	0.005
L-Lysine	0.045	0.055
Dimethyl 2-methoxyhexane-1,6-dioate	0.085	0.005
Pentanoic acid	0.08	0.005
3-amino-1,2,4-triazole	0.04	0.045
Propargyl alcohol	0.005	0.075
Piperidine	0.04	0.04
L-Leucine	0.03	0.05
L-Valine	0.025	0.04
L-Tyrosine	0.03	0.03
L-Serine	0.035	0.02
2-Hexanol	0.05	0.005
5-nitrobarbiturate	0.05	0.005
L-Phenylalanine	0.015	0.04
2-Hydroxy-4-(methylsulfonyl)isophthalic acid	0.04	0.01
Hypoxanthine	0.035	0.01
Cholesterol	0.005	0.04
N-Acetylaspartic acid	0.005	0.04
Citric acid	0.035	0.005
L-Methionine	0.02	0.02
L-Aspartic acid	0.02	0.015
Meglutol	0.03	0.005
Bisphenol A	0.03	0.005
2,8,10,12,18-Pentamethyl-3,7,13,17-tetraethyl-21H,23H-porphine	0.03	0.005
D-Pyroglutamic acid	0.03	0.005
cis-1,4-Cyclohexanedicarboxylic acid	0.005	0.03
Pentanedioic acid	0.005	0.03
Uric acid	0.005	0.03
Glycolic acid	0.025	0.005

2-Phenylquinoline-4-carboxylic acid N-oxide	0.02	0.01
L-Threonine	0.02	0.01
Dodecanoic acid	0.01	0.02
4,4-Dimethoxy-2-methyl-2-butanol	0.02	0.005
4-Hydroxybenzoic acid	0.02	0.005
Docosanoic acid	0.02	0.005
Glucuronic acid	0.02	0.005
Hexasiloxane	0.02	0.005
Isocitric acid lactone	0.02	0.005
Methyldiethanolamine	0.02	0.005
5-Aminovaleric acid	0.015	0.01
5-Bromoisatin-3-oxime	0.005	0.02
3,3-Dimethyl-2-butanol	0.005	0.02
L-Tryptophan	0.005	0.02
Glycerol	0.01	0.01
Ferulic acid	0.01	0.005
Alpha-ketoglutaric acid	0.01	0.005
3-Methoxy-5-prop-2-en-1-yl-2-[(trimethylsilyl)oxy]-N-(2-[(trimethylsilyl)oxy]ethyl)benzamide	0.005	0.01
4-Coumaric acid	0.005	0.01
Butanal	0.005	0.01
Dodecane	0.005	0.01
Hexanoic acid	0.005	0.01
Nonanoic acid	0.005	0.01
Tetrapentacontane	0.005	0.01
Urea	0.005	0.005
Sinapinic acid	0.005	0.005
Thymidine	0.005	0.005
Isosorbide	0.005	0.005
Hexadecanedioic acid	0.005	0.005
4'-(Salicylideneamino)acetanilide	0.005	0.005
9-methylheptadecane	0.005	0.005
Aconitic acid	0.005	0.005
Cyclooctasiloxane	0.005	0.005
Phenol	0.005	0.005

REFERENCES

1. Eckburg, P.B., et al., *Diversity of the human intestinal microbial flora.* Science, 2005. **308**(5728): p. 1635-8.

2. Ley, R.E., et al., *Obesity alters gut microbial ecology.* Proc Natl Acad Sci U S A, 2005. **102**(31): p. 11070-5.

3. Burkholder, P.R. and I. McVeigh, *Synthesis of Vitamins by Intestinal Bacteria.* Proc Natl Acad Sci U S A, 1942. **28**(7): p. 285-9.

4. Sorini, C., et al., *Commensal Bacteria-Specific CD4(+) T Cell Responses in Health and Disease.* Front Immunol, 2018. **9**: p. 2667.

5. Stecher, B., et al., *Salmonella enterica serovar typhimurium exploits inflammation to compete with the intestinal microbiota.* PLoS Biol, 2007. **5**(10): p. 2177-89.

6. Salyers, A.A., et al., *Fermentation of mucin and plant polysaccharides by strains of Bacteroides from the human colon.* Appl Environ Microbiol, 1977. **33**(2): p. 319-22.

7. Salyers, A.A., et al., *Fermentation of mucins and plant polysaccharides by anaerobic bacteria from the human colon.* Appl Environ Microbiol, 1977. **34**(5): p. 529-33.

8. Cantarel, B.L., et al., *The Carbohydrate-Active EnZymes database (CAZy): an expert resource for Glycogenomics.* Nucleic Acids Res, 2009. **37**(Database issue): p. D233-8.

9. Cantarel, B.L., V. Lombard, and B. Henrissat, *Complex carbohydrate utilization by the healthy human microbiome.* PLoS One, 2012. **7**(6): p. e28742.

10. Xu, J., et al., *A genomic view of the human-Bacteroides thetaiotaomicron symbiosis.* Science, 2003. **299**(5615): p. 2074-6.

11. Xu, J., et al., *Evolution of symbiotic bacteria in the distal human intestine.* PLoS Biol, 2007. **5**(7): p. e156.

12. Sonnenburg, J.L., et al., *Glycan foraging in vivo by an intestine-adapted bacterial symbiont.* Science, 2005. **307**(5717): p. 1955-9.

13. Martens, E.C., et al., *Recognition and degradation of plant cell wall polysaccharides by two human gut symbionts.* PLoS Biol, 2011. **9**(12): p. e1001221.

14. Martens, E.C., H.C. Chiang, and J.I. Gordon, *Mucosal glycan foraging enhances fitness and transmission of a saccharolytic human gut bacterial symbiont.* Cell Host Microbe, 2008. **4**(5): p. 447-57.

15. Ndeh, D., et al., *Complex pectin metabolism by gut bacteria reveals novel catalytic functions.* Nature, 2017. **544**(7648): p. 65-70.

16. Ze, X., et al., *Ruminococcus bromii is a keystone species for the degradation of resistant starch in the human colon.* ISME J, 2012. **6**(8): p. 1535-43.

17. Mahowald, M.A., et al., *Characterizing a model human gut microbiota composed of members of its two dominant bacterial phyla.* Proc Natl Acad Sci U S A, 2009. **106**(14): p. 5859-64.

18. El Kaoutari, A., et al., *The abundance and variety of carbohydrate-active enzymes in the human gut microbiota.* Nat Rev Microbiol, 2013. **11**(7): p. 497-504.

19. Cummings, J.H., et al., *Short chain fatty acids in human large intestine, portal, hepatic and venous blood.* Gut, 1987. **28**(10): p. 1221-7.

20. Bergman, E.N., *Energy contributions of volatile fatty acids from the gastrointestinal tract in various species.* Physiol Rev, 1990. **70**(2): p. 567-90.

21. Eilam, O., et al., *Glycan degradation (GlyDeR) analysis predicts mammalian gut microbiota abundance and host diet-specific adaptations.* MBio, 2014. **5**(4).

22. Sonnenburg, E.D., et al., *Specificity of polysaccharide use in intestinal bacteroides species determines diet-induced microbiota alterations.* Cell, 2010. **141**(7): p. 1241-52.

23. Giaffer, M.H., C.D. Holdsworth, and B.I. Duerden, *The assessment of faecal flora in patients with inflammatory bowel disease by a simplified bacteriological technique.* J Med Microbiol, 1991. **35**(4): p. 238-43.

24. Baumgart, M., et al., *Culture independent analysis of ileal mucosa reveals a selective increase in invasive Escherichia coli of novel phylogeny relative to depletion of Clostridiales in Crohn's disease involving the ileum.* ISME J, 2007. **1**(5): p. 403-18.

25. Frank, D.N., et al., *Molecular-phylogenetic characterization of microbial community imbalances in human inflammatory bowel diseases.* Proc Natl Acad Sci U S A, 2007. **104**(34): p. 13780-5.

26. Seksik, P., et al., *Alterations of the dominant faecal bacterial groups in patients with Crohn's disease of the colon.* Gut, 2003. **52**(2): p. 237-42.

27. Miyoshi, J. and E.B. Chang, *The gut microbiota and inflammatory bowel diseases.* Transl Res, 2017. **179**: p. 38-48.

28. Vujkovic-Cvijin, I., et al., *Dysbiosis of the gut microbiota is associated with HIV disease progression and tryptophan catabolism.* Sci Transl Med, 2013. **5**(193): p. 193ra91.

29. Okayasu, I., et al., *A novel method in the induction of reliable experimental acute and chronic ulcerative colitis in mice.* Gastroenterology, 1990. **98**(3): p. 694-702.

30. Lupp, C., et al., *Host-mediated inflammation disrupts the intestinal microbiota and promotes the overgrowth of Enterobacteriaceae.* Cell Host Microbe, 2007. **2**(2): p. 119-29.

31. Kuhn, R., et al., *Interleukin-10-deficient mice develop chronic enterocolitis.* Cell, 1993. **75**(2): p. 263-74.

32. Garrett, W.S., et al., *Communicable ulcerative colitis induced by T-bet deficiency in the innate immune system.* Cell, 2007. **131**(1): p. 33-45.

33. Garrett, W.S., et al., *Enterobacteriaceae act in concert with the gut microbiota to induce spontaneous and maternally transmitted colitis.* Cell Host Microbe, 2010. **8**(3): p. 292-300.

34. Unden, G., P.A. Steinmetz, and P. Degreif-Dunnwald, *The Aerobic and Anaerobic Respiratory Chain of Escherichia coli and Salmonella enterica: Enzymes and Energetics.* EcoSal Plus, 2014. **6**(1).

35. Lundberg, J.O., et al., *Greatly increased luminal nitric oxide in ulcerative colitis.* Lancet, 1994. **344**(8938): p. 1673-4.

36. Boughton-Smith, N.K., et al., *Nitric oxide synthase activity in ulcerative colitis and Crohn's disease.* Lancet, 1993. **342**(8867): p. 338-40.

37. Singer, II, et al., *Expression of inducible nitric oxide synthase and nitrotyrosine in colonic epithelium in inflammatory bowel disease.* Gastroenterology, 1996. **111**(4): p. 871-85.

38. Szabo, C., H. Ischiropoulos, and R. Radi, *Peroxynitrite: biochemistry, pathophysiology and development of therapeutics.* Nat Rev Drug Discov, 2007. **6**(8): p. 662-80.

39. Winter, S.E., et al., *Host-derived nitrate boosts growth of E. coli in the inflamed gut.* Science, 2013. **339**(6120): p. 708-11.

40. Hughes, E.R., et al., *Microbial Respiration and Formate Oxidation as Metabolic Signatures of Inflammation-Associated Dysbiosis.* Cell Host Microbe, 2017. **21**(2): p. 208-219.

41. Johnson, M.K., D.C. Rees, and M.W. Adams, *Tungstoenzymes.* Chem Rev, 1996. **96**(7): p. 2817-2840.

42. Gates, A.J., et al., *Properties of the periplasmic nitrate reductases from Paracoccus pantotrophus and Escherichia coli after growth in tungsten-supplemented media.* FEMS Microbiol Lett, 2003. **220**(2): p. 261-9.

43. Zhu, W., et al., *Precision editing of the gut microbiota ameliorates colitis.* Nature, 2018. **553**(7687): p. 208-211.

44. Barman, M., et al., *Enteric salmonellosis disrupts the microbial ecology of the murine gastrointestinal tract.* Infect Immun, 2008. **76**(3): p. 907-15.

45. Sekirov, I., et al., *Salmonella SPI-1-mediated neutrophil recruitment during enteric colitis is associated with reduction and alteration in intestinal microbiota.* Gut Microbes, 2010. **1**(1): p. 30-41.

46. Garcia-del Portillo, F., J.W. Foster, and B.B. Finlay, *Role of acid tolerance response genes in Salmonella typhimurium virulence.* Infect Immun, 1993. **61**(10): p. 4489-92.

47. Stecher, B., et al., *Flagella and chemotaxis are required for efficient induction of Salmonella enterica serovar Typhimurium colitis in streptomycin-pretreated mice.* Infect Immun, 2004. **72**(7): p. 4138-50.

48. Jones, B.D., N. Ghori, and S. Falkow, *Salmonella typhimurium initiates murine infection by penetrating and destroying the specialized epithelial M cells of the Peyer's patches.* J Exp Med, 1994. **180**(1): p. 15-23.

49. Galan, J.E. and R. Curtiss, 3rd, *Cloning and molecular characterization of genes whose products allow Salmonella typhimurium to penetrate tissue culture cells.* Proc Natl Acad Sci U S A, 1989. **86**(16): p. 6383-7.

50. Santos, R.L., et al., *Morphologic and molecular characterization of Salmonella typhimurium infection in neonatal calves.* Vet Pathol, 2002. **39**(2): p. 200-15.

51. Mills, D.M., V. Bajaj, and C.A. Lee, *A 40 kb chromosomal fragment encoding Salmonella typhimurium invasion genes is absent from the corresponding region of the Escherichia coli K-12 chromosome.* Mol Microbiol, 1995. **15**(4): p. 749-59.

52. Kubori, T., et al., *Supramolecular structure of the Salmonella typhimurium type III protein secretion system.* Science, 1998. **280**(5363): p. 602-5.

53. Zhou, D. and J. Galan, *Salmonella entry into host cells: the work in concert of type III secreted effector proteins.* Microbes Infect, 2001. **3**(14-15): p. 1293-8.

54. Shea, J.E., et al., *Identification of a virulence locus encoding a second type III secretion system in Salmonella typhimurium.* Proc Natl Acad Sci U S A, 1996. **93**(6): p. 2593-7.

55. Abrahams, G.L. and M. Hensel, *Manipulating cellular transport and immune responses: dynamic interactions between intracellular Salmonella enterica and its host cells.* Cell Microbiol, 2006. **8**(5): p. 728-37.

56. Coombes, B.K., et al., *Analysis of the contribution of Salmonella pathogenicity islands 1 and 2 to enteric disease progression using a novel bovine ileal loop model and a murine model of infectious enterocolitis.* Infect Immun, 2005. **73**(11): p. 7161-9.

57. Coburn, B., et al., *Salmonella enterica serovar Typhimurium pathogenicity island 2 is necessary for complete virulence in a mouse model of infectious enterocolitis.* Infect Immun, 2005. **73**(6): p. 3219-27.

58. Hapfelmeier, S., et al., *Microbe sampling by mucosal dendritic cells is a discrete, MyD88-independent step in DeltainvG S. Typhimurium colitis.* J Exp Med, 2008. **205**(2): p. 437-50.

59. Hapfelmeier, S., et al., *The Salmonella pathogenicity island (SPI)-2 and SPI-1 type III secretion systems allow Salmonella serovar typhimurium to trigger colitis via MyD88-dependent and MyD88-independent mechanisms.* J Immunol, 2005. **174**(3): p. 1675-85.

60. Harris, J.C., H.L. Dupont, and R.B. Hornick, *Fecal leukocytes in diarrheal illness.* Ann Intern Med, 1972. **76**(5): p. 697-703.

61. Ackermann, M., et al., *Self-destructive cooperation mediated by phenotypic noise.* Nature, 2008. **454**(7207): p. 987-90.

62. Lawley, T.D., et al., *Host transmission of Salmonella enterica serovar Typhimurium is controlled by virulence factors and indigenous intestinal microbiota.* Infect Immun, 2008. **76**(1): p. 403-16.

63. Winter, S.E., et al., *Gut inflammation provides a respiratory electron acceptor for Salmonella.* Nature, 2010. **467**(7314): p. 426-9.

64. Suarez, F., et al., *Production and elimination of sulfur-containing gases in the rat colon.* Am J Physiol, 1998. **274**(4 Pt 1): p. G727-33.

65. Roediger, W.E., et al., *Reducing sulfur compounds of the colon impair colonocyte nutrition: implications for ulcerative colitis.* Gastroenterology, 1993. **104**(3): p. 802-9.

66. Levitt, M.D., et al., *Detoxification of hydrogen sulfide and methanethiol in the cecal mucosa.* J Clin Invest, 1999. **104**(8): p. 1107-14.

67. Furne, J., et al., *Oxidation of hydrogen sulfide and methanethiol to thiosulfate by rat tissues: a specialized function of the colonic mucosa.* Biochem Pharmacol, 2001. **62**(2): p. 255-9.

68. Hensel, M., et al., *The genetic basis of tetrathionate respiration in Salmonella typhimurium.* Mol Microbiol, 1999. **32**(2): p. 275-87.

69. Hinsley, A.P. and B.C. Berks, *Specificity of respiratory pathways involved in the reduction of sulfur compounds by Salmonella enterica.* Microbiology, 2002. **148**(Pt 11): p. 3631-8.

70. Lopez, C.A., et al., *The Periplasmic Nitrate Reductase NapABC Supports Luminal Growth of Salmonella enterica Serovar Typhimurium during Colitis.* Infect Immun, 2015. **83**(9): p. 3470-8.

71. Lopez, C.A., et al., *Phage-mediated acquisition of a type III secreted effector protein boosts growth of salmonella by nitrate respiration.* MBio, 2012. **3**(3).

72. Faber, F., et al., *Host-mediated sugar oxidation promotes post-antibiotic pathogen expansion.* Nature, 2016. **534**(7609): p. 697-9.

73. Spiga, L., et al., *An Oxidative Central Metabolism Enables Salmonella to Utilize Microbiota-Derived Succinate.* Cell Host Microbe, 2017. **22**(3): p. 291-301 e6.

74. Amarasingham, C.R. and B.D. Davis, *Regulation of alpha-ketoglutarate dehydrogenase formation in Escherichia coli.* J Biol Chem, 1965. **240**(9): p. 3664-8.

75. Iuchi, S. and E.C. Lin, *arcA (dye), a global regulatory gene in Escherichia coli mediating repression of enzymes in aerobic pathways.* Proc Natl Acad Sci U S A, 1988. **85**(6): p. 1888-92.

76. Cronan, J.E., Jr. and D. Laporte, *Tricarboxylic Acid Cycle and Glyoxylate Bypass.* EcoSal Plus, 2005. **1**(2).

77. Thiennimitr, P., et al., *Intestinal inflammation allows Salmonella to use ethanolamine to compete with the microbiota.* Proc Natl Acad Sci U S A, 2011. **108**(42): p. 17480-5.

78. Ali, M.M., et al., *Fructose-asparagine is a primary nutrient during growth of Salmonella in the inflamed intestine.* PLoS Pathog, 2014. **10**(6): p. e1004209.

79. Faber, F., et al., *Respiration of Microbiota-Derived 1,2-propanediol Drives Salmonella Expansion during Colitis.* PLoS Pathog, 2017. **13**(1): p. e1006129.

80. Barcenilla, A., et al., *Phylogenetic relationships of butyrate-producing bacteria from the human gut.* Appl Environ Microbiol, 2000. **66**(4): p. 1654-61.

81. Vital, M., A.C. Howe, and J.M. Tiedje, *Revealing the bacterial butyrate synthesis pathways by analyzing (meta)genomic data.* MBio, 2014. **5**(2): p. e00889.

82. Duncan, S.H., et al., *Roseburia intestinalis sp. nov., a novel saccharolytic, butyrate-producing bacterium from human faeces.* Int J Syst Evol Microbiol, 2002. **52**(Pt 5): p. 1615-20.

83. Duncan, S.H., et al., *Growth requirements and fermentation products of Fusobacterium prausnitzii, and a proposal to reclassify it as Faecalibacterium prausnitzii gen. nov., comb. nov.* Int J Syst Evol Microbiol, 2002. **52**(Pt 6): p. 2141-6.

84. Byndloss, M.X., et al., *Microbiota-activated PPAR-gamma signaling inhibits dysbiotic Enterobacteriaceae expansion.* Science, 2017. **357**(6351): p. 570-575.

85. Rivera-Chavez, F., et al., *Depletion of Butyrate-Producing Clostridia from the Gut Microbiota Drives an Aerobic Luminal Expansion of Salmonella.* Cell Host Microbe, 2016. **19**(4): p. 443-54.

86. Gill, N., et al., *Neutrophil elastase alters the murine gut microbiota resulting in enhanced Salmonella colonization.* PLoS One, 2012. **7**(11): p. e49646.

87. Roediger, W.E., *Role of anaerobic bacteria in the metabolic welfare of the colonic mucosa in man.* Gut, 1980. **21**(9): p. 793-8.

88. Donohoe, D.R., et al., *The microbiome and butyrate regulate energy metabolism and autophagy in the mammalian colon.* Cell Metab, 2011. **13**(5): p. 517-26.

89. Donohoe, D.R., et al., *Microbial Regulation of Glucose Metabolism and Cell-Cycle Progression in Mammalian Colonocytes.* PLoS ONE, 2012. **7**(9): p. e46589.

90. Ahmad, M.S., et al., *Butyrate and glucose metabolism by colonocytes in experimental colitis in mice.* Gut, 2000. **46**(4): p. 493-9.

91. Kelly, C.J., et al., *Crosstalk between Microbiota-Derived Short-Chain Fatty Acids and Intestinal Epithelial HIF Augments Tissue Barrier Function.* Cell Host Microbe, 2015. **17**(5): p. 662-71.

92. Alex, S., et al., *Short-chain fatty acids stimulate angiopoietin-like 4 synthesis in human colon adenocarcinoma cells by activating peroxisome proliferator-activated receptor gamma.* Mol Cell Biol, 2013. **33**(7): p. 1303-16.

93. Lefebvre, M., et al., *Peroxisome proliferator-activated receptor gamma is induced during differentiation of colon epithelium cells.* J Endocrinol, 1999. **162**(3): p. 331-40.

94. Wachtershauser, A., S.M. Loitsch, and J. Stein, *PPAR-gamma is selectively upregulated in Caco-2 cells by butyrate.* Biochem Biophys Res Commun, 2000. **272**(2): p. 380-5.

95. Byndloss, M.X., S.R. Pernitzsch, and A.J. Baumler, *Healthy hosts rule within: ecological forces shaping the gut microbiota.* Mucosal Immunol, 2018. **11**(5): p. 1299-1305.

96. Adachi, M., et al., *Peroxisome proliferator activated receptor gamma in colonic epithelial cells protects against experimental inflammatory bowel disease.* Gut, 2006. **55**(8): p. 1104-13.

97. Atarashi, K., et al., *Induction of colonic regulatory T cells by indigenous Clostridium species.* Science, 2011. **331**(6015): p. 337-41.

98. Arpaia, N., et al., *Metabolites produced by commensal bacteria promote peripheral regulatory T-cell generation.* Nature, 2013. **504**(7480): p. 451-5.

99. Riggs, M.G., et al., *n-Butyrate causes histone modification in HeLa and Friend erythroleukaemia cells.* Nature, 1977. **268**(5619): p. 462-4.

100. Boffa, L.C., et al., *Suppression of histone deacetylation in vivo and in vitro by sodium butyrate.* J Biol Chem, 1978. **253**(10): p. 3364-6.

101. Furusawa, Y., et al., *Commensal microbe-derived butyrate induces the differentiation of colonic regulatory T cells.* Nature, 2013. **504**(7480): p. 446-50.

102. Singh, N., et al., *Activation of Gpr109a, receptor for niacin and the commensal metabolite butyrate, suppresses colonic inflammation and carcinogenesis.* Immunity, 2014. **40**(1): p. 128-39.

103. Smith, P.M., et al., *The microbial metabolites, short-chain fatty acids, regulate colonic Treg cell homeostasis.* Science, 2013. **341**(6145): p. 569-73.

104. Antunes, L.C., et al., *Impact of salmonella infection on host hormone metabolism revealed by metabolomics.* Infect Immun, 2011. **79**(4): p. 1759-69.

105. Noriega, C.E., et al., *Asymmetric cross-regulation between the nitrate-responsive NarX-NarL and NarQ-NarP two-component regulatory systems from Escherichia coli K-12.* Mol Microbiol, 2010. **75**(2): p. 394-412.

106. Darwin, A.J., et al., *Fnr, NarP, and NarL regulation of Escherichia coli K-12 napF (periplasmic nitrate reductase) operon transcription in vitro.* J Bacteriol, 1998. **180**(16): p. 4192-8.

107. Schmittgen, T.D. and K.J. Livak, *Analyzing real-time PCR data by the comparative C(T) method.* Nat Protoc, 2008. **3**(6): p. 1101-8.

108. Bustin, S.A., et al., *The MIQE guidelines: minimum information for publication of quantitative real-time PCR experiments.* Clin Chem, 2009. **55**(4): p. 611-22.

109. Caporaso, J.G., et al., *QIIME allows analysis of high-throughput community sequencing data.* Nat Methods, 2010. **7**(5): p. 335-6.

110. Quast, C., et al., *The SILVA ribosomal RNA gene database project: improved data processing and web-based tools.* Nucleic Acids Res, 2013. **41**(Database issue): p. D590-6.

111. Vazquez-Baeza, Y., et al., *EMPeror: a tool for visualizing high-throughput microbial community data.* Gigascience, 2013. **2**(1): p. 16.

112. Miller, J.H., *Experiments in molecular genetics*. 1972, Cold Spring Harbor, N.Y.: Cold Spring Harbor Laboratory. xvi, 466 p.

113. Berkowitz, D., et al., *Procedure for identifying nonsense mutations.* J Bacteriol, 1968. **96**(1): p. 215-20.

114. Vogel, H.J. and D.M. Bonner, *Acetylornithinase of Escherichia coli: partial purification and some properties.* J Biol Chem, 1956. **218**(1): p. 97-106.

115. Santos, R.L., *Pathobiology of salmonella, intestinal microbiota, and the host innate immune response.* Front Immunol, 2014. **5**: p. 252.

116. Rivera-Chavez, F. and A.J. Baumler, *The Pyromaniac Inside You: Salmonella Metabolism in the Host Gut.* Annu Rev Microbiol, 2015. **69**: p. 31-48.

117. Monack, D.M., *Helicobacter and salmonella persistent infection strategies.* Cold Spring Harb Perspect Med, 2013. **3**(12): p. a010348.

118. Hensel, M., et al., *Simultaneous identification of bacterial virulence genes by negative selection.* Science, 1995. **269**(5222): p. 400-3.

119. Tsolis, R.M., et al., *Contribution of Salmonella typhimurium virulence factors to diarrheal disease in calves.* Infect Immun, 1999. **67**(9): p. 4879-85.

120. Zhang, S., et al., *The Salmonella enterica serotype typhimurium effector proteins SipA, SopA, SopB, SopD, and SopE2 act in concert to induce diarrhea in calves.* Infect Immun, 2002. **70**(7): p. 3843-55.

121. Gutnick, D., et al., *Compounds which serve as the sole source of carbon or nitrogen for Salmonella typhimurium LT-2.* J Bacteriol, 1969. **100**(1): p. 215-9.

122. Becker, D., et al., *Robust Salmonella metabolism limits possibilities for new antimicrobials.* Nature, 2006. **440**(7082): p. 303-7.

123. Steeb, B., et al., *Parallel exploitation of diverse host nutrients enhances Salmonella virulence.* PLoS Pathog, 2013. **9**(4): p. e1003301.

124. McClelland, M., et al., *Complete genome sequence of Salmonella enterica serovar Typhimurium LT2.* Nature, 2001. **413**(6858): p. 852-6.

125. Belenguer, A., et al., *Impact of pH on lactate formation and utilization by human fecal microbial communities.* Appl Environ Microbiol, 2007. **73**(20): p. 6526-33.

126. Augoff, K., A. Hryniewicz-Jankowska, and R. Tabola, *Lactate dehydrogenase 5: an old friend and a new hope in the war on cancer.* Cancer Lett, 2015. **358**(1): p. 1-7.

127. Pryde, S.E., et al., *The microbiology of butyrate formation in the human colon.* FEMS Microbiol Lett, 2002. **217**(2): p. 133-9.

128. Pavia, A.T., et al., *Epidemiologic evidence that prior antimicrobial exposure decreases resistance to infection by antimicrobial-sensitive Salmonella.* J Infect Dis, 1990. **161**(2): p. 255-60.

129. Macdonald, R.H. and M. Beck, *Neomycin: a review with particular reference to dermatological usage.* Clin Exp Dermatol, 1983. **8**(3): p. 249-58.

130. Ferreyra, J.A., et al., *Gut microbiota-produced succinate promotes C. difficile infection after antibiotic treatment or motility disturbance.* Cell Host Microbe, 2014. **16**(6): p. 770-7.

131. Ng, K.M., et al., *Microbiota-liberated host sugars facilitate post-antibiotic expansion of enteric pathogens.* Nature, 2013. **502**(7469): p. 96-9.

132. Eisele, N.A., et al., *Salmonella require the fatty acid regulator PPARdelta for the establishment of a metabolic environment essential for long-term persistence.* Cell Host Microbe, 2013. **14**(2): p. 171-82.

133. McCoy, M.W., S.M. Moreland, and C.S. Detweiler, *Hemophagocytic macrophages in murine typhoid fever have an anti-inflammatory phenotype.* Infect Immun, 2012. **80**(10): p. 3642-9.

134. Nix, R.N., et al., *Hemophagocytic macrophages harbor Salmonella enterica during persistent infection.* PLoS Pathog, 2007. **3**(12): p. e193.

135. Bjerrum, J.T., et al., *Metabolomics of human fecal extracts characterize ulcerative colitis, Crohn's disease and healthy individuals.* Metabolomics, 2015. **11**: p. 122-133.

136. Hove, H., et al., *Butyrate absorption and lactate secretion in ulcerative colitis.* Dis Colon Rectum, 1995. **38**(5): p. 519-25.

137. Hove, H. and P.B. Mortensen, *Influence of intestinal inflammation (IBD) and small and large bowel length on fecal short-chain fatty acids and lactate.* Dig Dis Sci, 1995. **40**(6): p. 1372-80.

138. Montgomery, R.D., et al., *Studies of intestinal fermentation in ulcerative colitis.* Gut, 1968. **9**(5): p. 521-6.

139. Vernia, P., et al., *Fecal lactate and ulcerative colitis.* Gastroenterology, 1988. **95**(6): p. 1564-8.

140. Vernia, P., et al., *Organic anions and the diarrhea of inflammatory bowel disease.* Dig Dis Sci, 1988. **33**(11): p. 1353-8.

141. Santos, R.L., et al., *Life in the inflamed intestine, Salmonella style.* Trends Microbiol, 2009. **17**(11): p. 498-506.

142. Vazquez-Torres, A., et al., *Salmonella pathogenicity island 2-dependent evasion of the phagocyte NADPH oxidase.* Science, 2000. **287**(5458): p. 1655-8.

143. Gillis, C.C., et al., *Dysbiosis-Associated Change in Host Metabolism Generates Lactate to Support Salmonella Growth.* Cell Host Microbe, 2018. **23**(1): p. 54-64 e6.

144. Aguilera, L., et al., *Dual role of LldR in regulation of the lldPRD operon, involved in L-lactate metabolism in Escherichia coli.* J Bacteriol, 2008. **190**(8): p. 2997-3005.

145. Dong, J.M., et al., *Three overlapping lct genes involved in L-lactate utilization by Escherichia coli.* J Bacteriol, 1993. **175**(20): p. 6671-8.

146. Iuchi, S., et al., *Effects of nitrate respiration on expression of the Arc-controlled operons encoding succinate dehydrogenase and flavin-linked L-lactate dehydrogenase.* J Bacteriol, 1994. **176**(6): p. 1695-701.

147. Hong, J.S. and H.R. Kaback, *Mutants of Salmonella typhimurium and Escherichia coli pleiotropically defective in active transport.* Proc Natl Acad Sci U S A, 1972. **69**(11): p. 3336-40.

148. Evans, M.R., et al., *Analysis of the ArcA regulon in anaerobically grown Salmonella enterica sv. Typhimurium.* BMC Microbiol, 2011. **11**: p. 58.

149. Lynch, A.S. and E.C. Lin, *Transcriptional control mediated by the ArcA two-component response regulator protein of Escherichia coli: characterization of DNA binding at target promoters.* J Bacteriol, 1996. **178**(21): p. 6238-49.

150. Georgellis, D., O. Kwon, and E.C. Lin, *Quinones as the redox signal for the arc two-component system of bacteria.* Science, 2001. **292**(5525): p. 2314-6.

151. Day, D.W., B.K. Mandal, and B.C. Morson, *The rectal biopsy appearances in Salmonella colitis.* Histopathology, 1978. **2**(2): p. 117-31.

152. McGovern, V.J. and L.J. Slavutin, *Pathology of salmonella colitis.* Am J Surg Pathol, 1979. **3**(6): p. 483-90.

153. Alvarado, T., *Faecal leucocytes in patients with infectious diarrhoea.* Trans R Soc Trop Med Hyg, 1983. **77**(3): p. 316-20.

154. Barthel, M., et al., *Pretreatment of mice with streptomycin provides a Salmonella enterica serovar Typhimurium colitis model that allows analysis of both pathogen and host.* Infect Immun, 2003. **71**(5): p. 2839-58.

155. Nuccio, S.P. and A.J. Baumler, *Comparative analysis of Salmonella genomes identifies a metabolic network for escalating growth in the inflamed gut.* MBio, 2014. **5**(2): p. e00929-14.

156. McClelland, M., et al., *Comparison of genome degradation in Paratyphi A and Typhi, human-restricted serovars of Salmonella enterica that cause typhoid.* Nat Genet, 2004. **36**(12): p. 1268-74.

157. Tanner, J.R. and R.A. Kingsley, *Evolution of Salmonella within Hosts.* Trends Microbiol, 2018. **26**(12): p. 986-998.

158. Thomson, N.R., et al., *Comparative genome analysis of Salmonella Enteritidis PT4 and Salmonella Gallinarum 287/91 provides insights into evolutionary and host adaptation pathways.* Genome Res, 2008. **18**(10): p. 1624-37.

159. Chiu, C.H., et al., *The genome sequence of Salmonella enterica serovar Choleraesuis, a highly invasive and resistant zoonotic pathogen.* Nucleic Acids Res, 2005. **33**(5): p. 1690-8.

160. Adeva-Andany, M., et al., *Comprehensive review on lactate metabolism in human health.* Mitochondrion, 2014. **17**: p. 76-100.

161. Futai, M. and H. Kimura, *Inducible membrane-bound L-lactate dehydrogenase from Escherichia coli. Purification and properties.* Journal of Biological Chemistry, 1977. **252**(16): p. 5820-5827.

162. Shin, N.R., T.W. Whon, and J.W. Bae, *Proteobacteria: microbial signature of dysbiosis in gut microbiota.* Trends Biotechnol, 2015. **33**(9): p. 496-503.

163. Eaves-Pyles, T., et al., *Escherichia coli isolated from a Crohn's disease patient adheres, invades, and induces inflammatory responses in polarized intestinal epithelial cells.* Int J Med Microbiol, 2008. **298**(5-6): p. 397-409.

164. Nash, J.H., et al., *Genome sequence of adherent-invasive Escherichia coli and comparative genomic analysis with other E. coli pathotypes.* BMC Genomics, 2010. **11**: p. 667.

165. Pinchuk, G.E., et al., *Genomic reconstruction of Shewanella oneidensis MR-1 metabolism reveals a previously uncharacterized machinery for lactate utilization.* Proc Natl Acad Sci U S A, 2009. **106**(8): p. 2874-9.

166. Sweeney, J., C.D. Murphy, and K. McDonnell, *Towards an effective biosensor for monitoring AD leachate: a knockout E. coli mutant that cannot catabolise lactate.* Appl Microbiol Biotechnol, 2015. **99**(23): p. 10209-14.

167. Belenguer, A., et al., *Rates of production and utilization of lactate by microbial communities from the human colon.* FEMS Microbiol Ecol, 2011. **77**(1): p. 107-19.

168. Bourriaud, C., et al., *Lactate is mainly fermented to butyrate by human intestinal microfloras but inter-individual variation is evident.* J Appl Microbiol, 2005. **99**(1): p. 201-12.

169. Duncan, S.H., P. Louis, and H.J. Flint, *Lactate-utilizing bacteria, isolated from human feces, that produce butyrate as a major fermentation product.* Appl Environ Microbiol, 2004. **70**(10): p. 5810-7.

170. Franzosa, E.A., et al., *Gut microbiome structure and metabolic activity in inflammatory bowel disease.* Nat Microbiol, 2019. **4**(2): p. 293-305.

171. Raffatellu, M., et al., *Lipocalin-2 resistance confers an advantage to Salmonella enterica serotype Typhimurium for growth and survival in the inflamed intestine.* Cell Host Microbe, 2009. **5**(5): p. 476-86.

172. Raymond, K.N., E.A. Dertz, and S.S. Kim, *Enterobactin: an archetype for microbial iron transport.* Proc Natl Acad Sci U S A, 2003. **100**(7): p. 3584-8.

173. Goetz, D.H., et al., *The neutrophil lipocalin NGAL is a bacteriostatic agent that interferes with siderophore-mediated iron acquisition.* Mol Cell, 2002. **10**(5): p. 1033-43.

174. Flo, T.H., et al., *Lipocalin 2 mediates an innate immune response to bacterial infection by sequestrating iron.* Nature, 2004. **432**(7019): p. 917-21.

175. Deriu, E., et al., *Probiotic bacteria reduce salmonella typhimurium intestinal colonization by competing for iron.* Cell Host Microbe, 2013. **14**(1): p. 26-37.

176. Grozdanov, L., et al., *Analysis of the genome structure of the nonpathogenic probiotic Escherichia coli strain Nissle 1917.* J Bacteriol, 2004. **186**(16): p. 5432-41.

177. Vaishnava, S., et al., *The antibacterial lectin RegIIIgamma promotes the spatial segregation of microbiota and host in the intestine.* Science, 2011. **334**(6053): p. 255-8.

178. Pan, N. and J.A. Imlay, *How does oxygen inhibit central metabolism in the obligate anaerobe Bacteroides thetaiotaomicron.* Mol Microbiol, 2001. **39**(6): p. 1562-71.

179. Johnson, E. and S.W. Barthold, *The ultrastructure of transmissible murine colonic hyperplasia.* Am J Pathol, 1979. **97**(2): p. 291-313.

180. Lopez, C.A., et al., *Virulence factors enhance Citrobacter rodentium expansion through aerobic respiration.* Science, 2016. **353**(6305): p. 1249-53.

181. Petty, N.K., et al., *The Citrobacter rodentium genome sequence reveals convergent evolution with human pathogenic Escherichia coli.* J Bacteriol, 2010. **192**(2): p. 525-38.

182. Richardson, A.R., S.J. Libby, and F.C. Fang, *A nitric oxide-inducible lactate dehydrogenase enables Staphylococcus aureus to resist innate immunity.* Science, 2008. **319**(5870): p. 1672-6.

183. Vitko, N.P., N.A. Spahich, and A.R. Richardson, *Glycolytic dependency of high-level nitric oxide resistance and virulence in Staphylococcus aureus.* MBio, 2015. **6**(2).

184. Spahich, N.A., et al., *Staphylococcus aureus lactate- and malate-quinone oxidoreductases contribute to nitric oxide resistance and virulence.* Mol Microbiol, 2016. **100**(5): p. 759-73.

185. Xavier, M.N., et al., *PPARgamma-mediated increase in glucose availability sustains chronic Brucella abortus infection in alternatively activated macrophages.* Cell Host Microbe, 2013. **14**(2): p. 159-70.

186. Thurlow, L.R., G.S. Joshi, and A.R. Richardson, *Peroxisome Proliferator-Activated Receptor gamma Is Essential for the Resolution of Staphylococcus aureus Skin Infections.* Cell Host Microbe, 2018. **24**(2): p. 261-270 e4.

187. Gantois, I., et al., *Butyrate specifically down-regulates salmonella pathogenicity island 1 gene expression.* Appl Environ Microbiol, 2006. **72**(1): p. 946-9.

188. Bronner, D.N., et al., *Genetic Ablation of Butyrate Utilization Attenuates Gastrointestinal Salmonella Disease.* Cell Host Microbe, 2018. **23**(2): p. 266-273 e4.

189. Virlogeux, I., et al., *Role of the viaB locus in synthesis, transport and expression of Salmonella typhi Vi antigen.* Microbiology, 1995. **141 (Pt 12)**: p. 3039-47.

190. Haneda, T., et al., *The capsule-encoding viaB locus reduces intestinal inflammation by a Salmonella pathogenicity island 1-independent mechanism.* Infect Immun, 2009. **77**(7): p. 2932-42.

191. Parkhill, J., et al., *Complete genome sequence of a multiple drug resistant Salmonella enterica serovar Typhi CT18.* Nature, 2001. **413**(6858): p. 848-52.

192. Crawford, R.W., et al., *Loss of very-long O-antigen chains optimizes capsule-mediated immune evasion by Salmonella enterica serovar Typhi.* MBio, 2013. **4**(4).

193. Riley, L.W., et al., *Hemorrhagic colitis associated with a rare Escherichia coli serotype.* N Engl J Med, 1983. **308**(12): p. 681-5.

194. Tzipori, S., et al., *The pathogenesis of hemorrhagic colitis caused by Escherichia coli O157:H7 in gnotobiotic piglets.* J Infect Dis, 1986. **154**(4): p. 712-6.

195. McDaniel, T.K., et al., *A genetic locus of enterocyte effacement conserved among diverse enterobacterial pathogens.* Proc Natl Acad Sci U S A, 1995. **92**(5): p. 1664-8.

196. Cameron, E.A. and V. Sperandio, *Frenemies: Signaling and Nutritional Integration in Pathogen-Microbiota-Host Interactions.* Cell Host Microbe, 2015. **18**(3): p. 275-84.

197. Bertin, Y., et al., *Enterohaemorrhagic Escherichia coli gains a competitive advantage by using ethanolamine as a nitrogen source in the bovine intestinal content.* Environ Microbiol, 2011. **13**(2): p. 365-77.

198. Kendall, M.M., et al., *Ethanolamine controls expression of genes encoding components involved in interkingdom signaling and virulence in enterohemorrhagic Escherichia coli O157:H7.* MBio, 2012. **3**(3).

199. Anderson, C.J., et al., *Ethanolamine Signaling Promotes Salmonella Niche Recognition and Adaptation during Infection.* PLoS Pathog, 2015. **11**(11): p. e1005278.

200. Bank, S., et al., *Polymorphisms in the inflammatory pathway genes TLR2, TLR4, TLR9, LY96, NFKBIA, NFKB1, TNFA, TNFRSF1A, IL6R, IL10, IL23R, PTPN22, and PPARG are associated with susceptibility of inflammatory bowel disease in a Danish cohort.* PLoS One, 2014. **9**(6): p. e98815.

201. Andersen, V., et al., *Polymorphisms in NF-kappaB, PXR, LXR, PPARgamma and risk of inflammatory bowel disease.* World J Gastroenterol, 2011. **17**(2): p. 197-206.

202. Rousseaux, C., et al., *Intestinal antiinflammatory effect of 5-aminosalicylic acid is dependent on peroxisome proliferator-activated receptor-gamma.* J Exp Med, 2005. **201**(8): p. 1205-15.

203. Niess, J.H., et al., *CX3CR1-mediated dendritic cell access to the intestinal lumen and bacterial clearance.* Science, 2005. **307**(5707): p. 254-8.

204. Morita, N., et al., *GPR31-dependent dendrite protrusion of intestinal CX3CR1(+) cells by bacterial metabolites.* Nature, 2019. **566**(7742): p. 110-114.

205. Lee, Y.S., et al., *Microbiota-Derived Lactate Accelerates Intestinal Stem-Cell-Mediated Epithelial Development.* Cell Host Microbe, 2018. **24**(6): p. 833-846 e6.

206. Chitapanarux, I., et al., *Randomized controlled trial of live lactobacillus acidophilus plus bifidobacterium bifidum in prophylaxis of diarrhea during radiotherapy in cervical cancer patients.* Radiat Oncol, 2010. **5**: p. 31.

207. Rodriguez-Colman, M.J., et al., *Interplay between metabolic identities in the intestinal crypt supports stem cell function.* Nature, 2017. **543**(7645): p. 424-427.

208. Luethy, P.M., et al., *Microbiota-Derived Short-Chain Fatty Acids Modulate Expression of Campylobacter jejuni Determinants Required for Commensalism and Virulence.* MBio, 2017. **8**(3).

209. Altekruse, S.F., et al., *Campylobacter jejuni--an emerging foodborne pathogen.* Emerg Infect Dis, 1999. **5**(1): p. 28-35.

210. Beery, J.T., M.B. Hugdahl, and M.P. Doyle, *Colonization of gastrointestinal tracts of chicks by Campylobacter jejuni.* Appl Environ Microbiol, 1988. **54**(10): p. 2365-70.

211. Gu, S., et al., *Bacterial community mapping of the mouse gastrointestinal tract.* PLoS One, 2013. **8**(10): p. e74957.

212. Donaldson, G.P., S.M. Lee, and S.K. Mazmanian, *Gut biogeography of the bacterial microbiota.* Nat Rev Microbiol, 2016. **14**(1): p. 20-32.

213. Shi, L., et al., *Infection with Mycobacterium tuberculosis induces the Warburg effect in mouse lungs.* Sci Rep, 2015. **5**: p. 18176.

214. Billig, S., et al., *Lactate oxidation facilitates growth of Mycobacterium tuberculosis in human macrophages.* Sci Rep, 2017. **7**(1): p. 6484.

215. Czyz, D.M., J.W. Willett, and S. Crosson, *Brucella abortus Induces a Warburg Shift in Host Metabolism That Is Linked to Enhanced Intracellular Survival of the Pathogen.* J Bacteriol, 2017. **199**(15).

216. Kingsley, R.A., et al., *Molecular and phenotypic analysis of the CS54 island of Salmonella enterica serotype typhimurium: identification of intestinal colonization and persistence determinants.* Infect Immun, 2003. **71**(2): p. 629-40.

217. Gillis, C.C., et al., *Host-derived metabolites modulate transcription of Salmonella genes involved in l-lactate utilization during gut colonization.* Infect Immun, 2019.

218. Pal, D., et al., *Multipartite regulation of rctB, the replication initiator gene of Vibrio cholerae chromosome II.* J Bacteriol, 2005. **187**(21): p. 7167-75.

219. Stojiljkovic, I., A.J. Baumler, and F. Heffron, *Ethanolamine utilization in Salmonella typhimurium: nucleotide sequence, protein expression, and mutational analysis of the cchA cchB eutE eutJ eutG eutH gene cluster.* J Bacteriol, 1995. **177**(5): p. 1357-66.

220. Simon, R., Priefer, U., Puhler, A. , *A broad host range mobilization system for in vivo genetic engineering: transposon mutagenesis in gram negative bacteria.* Nat Biotechnol, 1983. **1**: p. **pp. 784–791**.

221. Rivera-Chavez, F., et al., *Salmonella uses energy taxis to benefit from intestinal inflammation.* PLoS Pathog, 2013. **9**(4): p. e1003267.

222. Winter, S.E., et al., *The TviA auxiliary protein renders the Salmonella enterica serotype Typhi RcsB regulon responsive to changes in osmolarity.* Mol Microbiol, 2009. **74**(1): p. 175-93.

223. Baumler, A.J., et al., *Identification of a new iron regulated locus of Salmonella typhi.* Gene, 1996. **183**(1-2): p. 207-13.

224. Miller, V.L. and J.J. Mekalanos, *A novel suicide vector and its use in construction of insertion mutations: osmoregulation of outer membrane proteins and virulence determinants in Vibrio cholerae requires toxR.* J Bacteriol, 1988. **170**(6): p. 2575-83.

225. Kingsley, R.A., et al., *Ferrioxamine-mediated Iron(III) utilization by Salmonella enterica.* Appl Environ Microbiol, 1999. **65**(4): p. 1610-8.

226. Overbergh, L., et al., *The use of real-time reverse transcriptase PCR for the quantification of cytokine gene expression.* J Biomol Tech, 2003. **14**(1): p. 33-43.

227. Godinez, I., et al., *T cells help to amplify inflammatory responses induced by Salmonella enterica serotype Typhimurium in the intestinal mucosa.* Infect Immun, 2008. **76**(5): p. 2008-17.

228. Bohez, L., et al., *Salmonella enterica serovar Enteritidis colonization of the chicken caecum requires the HilA regulatory protein.* Vet Microbiol, 2006. **116**(1-3): p. 202-10.